Accepted Manuscript

Gold mineralization and orogenic metamorphism in the Lena Province of Siberia as assessed from Chertovo Koryto and Sukhoi Log deposits

Marina A. Yudovskaya, Vadim V. Distler, Vsevolod Yu. Prokofiev, Nickolay N. Akinfiev

PII: S1674-9871(15)00090-0

DOI: 10.1016/j.gsf.2015.07.010

Reference: GSF 379

To appear in: *Geoscience Frontiers*

Received Date: 30 May 2015

Revised Date: 30 July 2015

Accepted Date: 31 July 2015

Please cite this article as: Yudovskaya, M.A., Distler, V.V., Prokofiev, V.Y., Akinfiev, N.N., Gold mineralization and orogenic metamorphism in the Lena Province of Siberia as assessed from Chertovo Koryto and Sukhoi Log deposits, *Geoscience Frontiers* (2015), doi: 10.1016/j.gsf.2015.07.010.

Proterozoic
metamorphism &
granitoid magmatism
2000-1800 Ma

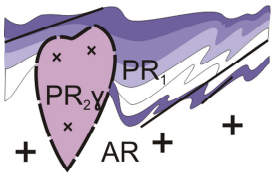

Sedimentation
on
passive margin
1000-600 Ma

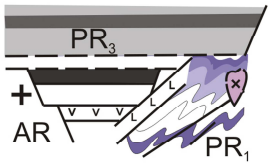

Orogenic metamorphism,
deformation &
gold mineralisation
460-440 Ma

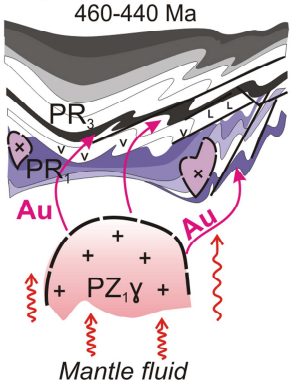

Tectono-magmatic
activation
320-270 Ma

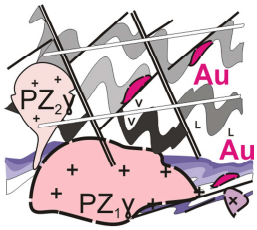

Gold mineralization and orogenic metamorphism in the Lena Province of Siberia as assessed from Chertovo Koryto and Sukhoi Log deposits

Marina A. Yudovskaya[a,b,*], Vadim V. Distler[a], Vsevolod Yu. Prokofiev[a], Nickolay N. Akinfiev[a]

[a] *Institute of Geology of Ore Deposits, Petrography, Mineralogy and Geochemistry RAS, 35 Staromonetny, Moscow 119017, Russia*

[b] *EGRI, University of the Witwatersrand, Private Bag 3, Wits 2050, South Africa*

* Corresponding author. E-mail address: marina.yudovskaya@wits.ac.za; maiya@igem.ru

Abstract

The Chertovo Koryto gold deposit (80 t Au at 1.84 g/t) in the Lena gold province, Siberia, is hosted in a metamorphosed sequence of the Paleoproterozoic Mikhailovsk Formation that comprises the oldest black shale strata of the Baikal-Patom region. The mineralisation is confined to the thrust zone complicated with a conjugate anticline fold, zones of shearing and dislocation. The structural position of the mineralisation is similar to that at the giant Sukhoi Log deposit in the neighboring Mama-Bodaibo zone. In the latter, the isotope age data suggest that Khomolkho black shales, hosts to Sukhoi Log mineralisation, are of Ediacaran age and underwent prograde metamorphism during early Paleozoic. The geochemical composition of the terrigenous rocks that host Sukhoi Log, Chertovo Koryto, and a number of other deposits at the various stratigraphic levels throughout the Proterozoic sequence have much in common. They do not show elevated metal contents above the common black shale abundances, except for Au and As, which is at variance with the accepted view on diagenetic enrichment of black shales in the Lena Province. The occurrence of sagenitic rutile in quartz and chlorite pseudomophs after biotite and other petrographic observations provide evidence on a retrograde nature of the metamorphic mineral assemblages in the Mikhailovsk rocks. The sulphides are pyrrhotite and arsenopyrite with very minor pyrite at Chertovo Koryto, whereas pyrite is the predominant sulphide in the Sukhoi Log ore. Fluid inclusion data on both deposits emphasise a high-temperature nature of the mineralisation albeit revealing great contrast in the fluid composition. Sukhoi Log mineralisation was formed at mixing between low-salinity aqueous solutions and dense

gaseous carbonic fluids, which facilitated effective gold scavenging and precipitation, as was demonstrated by thermodynamic simulation. The precursory devolatalisation of the Mikhailovsk sediments at the prograde stage results in the paucity of gaseous carbonic fluid during retrograde metamorphism and mineralisation. The similarity in the styles and chemical parameters of mineralisation, and the predominant structural control of ore localisation within the same Precambrian regional tectonic unit support an idea that orogenic gold mineralisation in the Lena Pprovince was produced during a single early Paleozoic event.

Key words: Gold; Black shales; Orogenic metamorphism; Orogenic fluid; Sukhoi Log; Chertovo Koryto

1. Introduction

The Lena gold province is known for richness of its gold placers, which have been exploited since the mid-19th century to endow more than 2000 tons Au (Buryak and Khmelevskaya, 1997). The unique placer wealth corresponds to a high potential of lode deposits that include the giant Sukhoi Log deposit along with three large (Vysochaishee, Verninskoe and Chertovo Koryto) and a few dozen smaller deposits and occurrences. Most of these lode resources remain unexploited as of yet, with the only three mines currently operating in the region. The Vysochaishee Mine developed by the GV Gold Company, the Pervenets-Verninskoe Mine by Polyus Gold, and the Nevskoe Mine by Druza Company produced 5.2, 4.7 and 0.62 t Au, respectively, in 2014 according to the company's records, whereas the total annual production in the province reached 22 t Au, with half of this amount provided by the placer gold fields.

New economic conditions with a lower cutoff led to the substantial reappraisal of proved and probable reserves at the Sukhoi Log deposit, which are currently estimated at 2956 t Au and 1541 t Ag (Migachev et al., 2008). The reserve was increased twice with respect to previous evaluation that totaled 1040 t at an average grade of 2.73 g/t Au approved by the USSR State Reserves Committee in 1977. According to a Polyus Gold press release, the proved and probable reserves of the Verninskoe deposit are close to 179 t at an average 2.7 g/t Au or within 240 t Au of measured and indicated resources, i.e. three times higher than the previous estimation during the Soviet period. The proved and probable reserves of the Chertovo Koryto deposit appeared to be close to 80 t Au at an average 1.84 g/t, which is slightly lower than the previous Soviet assessment. The reserves of the Vysochaishee deposit

were estimated at around 90 t Au, although these reserves are now almost depleted. In addition, recent exploration works were targeted at and confirmed several medium-sized deposits whose resources range between 10 and 50 t Au, such as the Nevskoe, Ugakhan, Khodokan, Krasnoe and Kopylovskoe deposits.

The genesis of the gold lodes and relationships between mineralisation, metamorphism and granitoid magmatic events are debatable since the discovery of the Sukhoi Log gold-quartz-sulphide disseminated ore in 1961 (Buryak, 1982). The metamorphic–hydrothermal–sedimentary model suggests a Precambrian age of the gold mineralisation, assuming that ore zones were formed through metamorphic redistribution of metal, which was primarily accumulated at sedimentary or exhalative-sedimentary processes (Nemerov, 1989; Buryak and Khmelevskaya, 1997; Large et al., 2007). According to this model, the mineralisation and metamorphism predate the Paleozoic granite intrusions. The distribution of the gold deposits is believed to be controlled by their confinement to weakly metamorphosed rocks, as the model envisages gold migration from anatectic and high-grade metamorphic zones on the periphery of the province towards the central parts metamorphosed under greenschist facies conditions. An alternative model relates mineralisation to the Paleozoic granitoids and orogenic metamorphism (Sher, 1972, Rundqvist et al., 1992; Distler et al., 1996; Kucherenko et al., 2011). Both of these extreme views have their weak and strong points that give rise to a number of intermediate hypotheses, which try to account for the complex multi-stage geological history of the region (Meffre et al., 2008; Kryazhev et al., 2009). An ultimate source of gold, whether it was primarily deposited together with other black shale components or derived by high-temperature fluids from a depth, is one of the keystones to elucidate the gold provenance. The timing of mineralisation relative to the metamorphic events, whether it predates or postdates the metamorphic peaks, is another key evidence for the genetic type of gold mineralisation in the province.

Two outstanding monographs summarized geological knowledge on the Lena Province in due course. The two-volume review *Lena Gold-bearing Region* (Kazakevich et al., 1971) is based on the research output obtained at TSNIGRI in 1952–1964. *The Precambrian of the Patom Highlands* (Ivanov et al., 1995) compiled and interpreted data of geological mapping and geochronological dating under the leadership of Irkutskgeologia in the 1980s and early 1990s. Both books extensively referred to the published and unpublished results of the other research teams, such as the Institute of Precambrian Geology, VSEGEI, Geological Institute (GIN) and Lenzoloto. New data were obtained during the past two decades under the Program of State Geological Mapping or academic studies (Mitrofanov,

2006) and also involved the results obtained in exploration, prospecting and reassessment projects of various mining companies (Migachev et al., 2008; Ivanov, 2014).

Here we report newly obtained data on the geological setting, metamorphism and mineralisation of the little known and unexploited Chertovo Koryto deposit in the north of the Patom Highlands in comparison to the Sukhoi Log giant deposit. The Chertovo Koryto deposit is hosted in the lower Proterozoic black shale strata of the Mikhailovsk Formation that are intruded by 1.85–1.95 Ga Chuya-Nechera granite in the vicinity of the deposit. The age of the mineralisation is not constrained because its host rocks are the oldest black shale succession in the region, but mineralisation was believed to be confined to a thrust zone of supposedly late Riphean age (Ivanov et al., 1995). It should be admitted that the age of Sukhoi Log mineralisation hosted by ca. 1 Ga younger Ediacaran (Russian Vendian) black shales is still also highly disputable (Meffre et al., 2008; Yudovskaya et al., 2011; Yakubchuk et al., 2014).

Our fluid inclusion data indicate that Sukhoi Log and Chertovo Koryto gold ores were formed under high-temperature conditions, while modeling shows that physical mixing of gaseous and aqueous fluids could be an important factor controlling effective gold deposition. Similarity of the styles and chemical parameters of the mineralisation, the predominant structural control of emplacement as well as the localization within the same Precambrian regional structure (Fig. 1) allows speculating upon a common endogenous event that triggered gold mineralisation throughout the province.

We use the subdivisions of the International Stratigraphic Scale through the paper whereas the equivalents of the Russian Stratigraphic scales are given in Fig. 2 and shown in brackets when relevant.

2. Geological setting of the Lena gold province

2.1. Sedimentation and regional metamorphism

The Lena Province is located in the Patom Highlands of the Baikal orogen separated from the Angara block of the Siberian Platform by the Akitkan-Zherba Suture (Mitrofanov, 2006). The Archean basement of the craton extends beneath the Baikal orogen for 80–100 km according to geophysical data (Ivanov et al., 1995). The Baikal orogen together with the Enisei and the Eastern Sayan Ranges form the complex Sayan-Baikal Fold Belt which rims the southern margins of the platform (Fig. 1). The Sayan-Baikal fold belt was initially founded on the reworked basement of the Siberian craton, although its later evolution was related to the higher-level Central Asian Orogenic Belt, one of the Earth's largest accretionary

orogens, existing from about 1000 Ma (Kröner et al., 2014). The voluminous Neoproterozoic terranes adjacent to the Siberian craton were generated during an early phase of CAOB evolution through continuous subduction–accretion within the long-lived Palaeo-Asian Ocean (e.g., Yarmolyuk et al., 2006, Rytsk et al., 2011). The upper Proterozoic carbonate terrigenous sequences of the Baikal orogen were recognised as a regional stratigraphic standard of so-called Baikalides in Siberia although their stratigraphic age is currently appeared to be revisited (Kuznetsov et al., 2013).

The Baikal orogen is subdivided into two structural megazones: the outer Baikal-Patom and inner Baikal-Vitim-Barguzin (Mitrofanov, 2006). The Proterozoic black shale deposition spreads over the whole Baikal-Patom megazone and margins of the adjacent Aldan Shield (Fig. 1). The Patom and Mama-Bodaibo synclinoriums separated by the Tonoda-Chuya-Nechera Uplift are the major structural units of the Baikal-Patom megazone (Fig. 3).

The basement of the Baikal-Patom megazone is composed of metaterrigenous rocks of the Kevakta Group (Figs. 2 and 3), which includes metamorphosed siltstone, sandstone and black shale of the Albazinsk and Mikhailovsk formations and the coeval Khodokan Formation, which are exposed within the Tonoda and Nechera uplifts, respectively. The sediments are transformed into a zoned green schists–amphibolite–migmatite assemblage; the U–Pb isotope dating of newly-formed zircon from the migmatitised metasandstone and local granite–gneisses yields ages of 2010 ± 50 and 2020 ± 50 Ma, respectively (Makar'ev and Chukhonin, 1992). These values are consistent with dating of detrital zircon from the overlying strata (Landa et al., 2006). High-alumina and high-silica sediments of the Mesoproterozoic Purpol Formation uncomformably overlie the Mikhailovsk rocks. The composition of Purpol quartzite and diasporite indicates sub-continental sedimentation and re-deposition of weathering crust material after a significant hiatus (Ivanov et al., 1995). The chemical-sedimentary Purpol Formation and the volcanogenic-sedimentary Medvezhevsk Formation are combined into the Teptorgo Group (Fig. 2), which filled rift-related trough-like depressions and narrowed towards basement highs in the Mesoproterozoic. The Medvezhevsk Formation is characterised by a local accumulation of banded iron formation (BIF) that can be correlated with the Superior-type BIF (Beukes and Gutzmer, 2008). The further widening of these troughs led to the formation of a vast long-lived sea basin, in which Neoproterozoic carbonaceous carbonate-terrigenous sediments were accumulating. The Neoproterozoic sequence of the Mama-Bodaibo zone is subdivided into the Ballaganakh and the Nygri groups, with the latter being coeval to the Dal'nyaya Taiga Group. The Cryogenian

Ballaganakh Group up to 2500 m thick consists mainly of terrigenous gravel-sand-siltstone sediments (Fig. 2) replaced upwards by calcareous sandstone and limestone. The Ediacaran (Russian Vendian) sedimentary rocks of the Nygri Group are divided into the Bujuikhta, Ugakhan, Khomolkho and Imnyakh formations (Fig. 2), up to 1500 m in total thickness, although intense ductile deformations commonly result in lesser thicknesses. The sequence includes basal diamictites as important marker horizons, which were reported in the Dzhemkukan Formation of the Dal'nyaya Taiga Group (Chumakov et al., 2011). Up to 2500 m of rhythmically interbedded sandstones, shales, carbonaceous shales, limestones and sandstones comprise the Ediacaran Bodaibo Group, which is subdivided into the Aunakit, Vacha, Anangr, Dogaldyn and Iligir formations (Fig. 2). The deposition of carbon-bearing sediments (black shale) reached a maximum in the Ediacaran, as it follows from the elevated proportions of carbonaceous and carbon-rich shales in the Khomolkho, Aunakit and Vacha formations (Nemerov, 1989) (Fig. 2).

Geochronological data indicate that deposition of the Nygri Group started in the early Ediacaran (Fig. 2). A wide range of K–Ar isotope ages from 633 to 520 Ma was obtained for gabbro-dolerite sills at the base of the Barakun Formation of the Dal'nyaya Taiga Group (Oleinikov et al., 1983) The K–Ar and Rb–Sr whole rock isochrons on Dal'nyaya Taiga sedimentary rocks suggest epigenetic alteration at 530–450 Ma (Vinogradov et al., 1996). The Ediacaran, rather than Cryogenian, age of the upper strata of the Bodaibo Group was inferred by Sovetov (2002) from correlation with other sedimentary formations of southern Siberia. Meffre et al. (2008) found youngest detrital zircon population with an isotope age of 600 ± 10 Ma in metasediments of the Khomolkho and Aunakit formations and interpreted this as evidence of a substantial contribution of syndiagenetic juvenile (volcanic or exhalative) material during the deposition of the black shales. This age appeared to be rather close to the weighted average metamorphic monazite age of 573 ± 12 Ma of the same rock (Meffre et al., 2008). Yudovskaya et al. (2011) found hydrothermal overgrowths on detrital zircon from Khomolkho carbonate-bearing carbonaceous shale and argued that this might indicate a high-temperature process causing the partial resetting of the U–Pb isotope system and rejuvenation of the zircon isotope age. These researchers estimated the age of the regional metamorphic event at 630 Ma (Yudovskaya et al., 2011), which was in agreement with the Rb–Sr isochron age of 625 ± 60 Ma determined for chlorite mineral assemblage in the Bodaibo region (Vilor et al., 1991). Recently, more overwhelming evidence testifies that the age of Nygry Group sediments is younger than it was thought earlier. This is supported by an U–Pb age of 646.9±3.4 Ma (1σ, n=8, MSWD=0.0077) for the youngest detrital zircon

population from basal sandstone of the Nikolsk Formation, which is coeval with the Imnyakh Formation that overlies the Khomolkho Formation (Chumakov et al., 2011). Sr isotope stratigraphy of the Baikal Group in the Lake Baikal area, which served as the basis for upper Precambrian stratigraphy of the whole Baikal–Sayan Fold Belt, and the Pb–Pb isochron age of 560±30 Ma for the Uluntui Formation, which can be correlative of the upper part of the Nygri Group, demonstrate that entire siliciclastic–carbonate succession of the Baikal Group was most likely deposited during the Ediacaran (Kuznetsov et al., 2013).

2.2. Magmatism

Paleoproterozoic intrusions are mostly exposed in the Chuya-Tonoda-Nechera Plateau (Fig. 3). The oldest known intrusions belong to the Teprokan mafic complex. Paleoproterozoic granitoids of the Chuya-Nechera batholith intruded the Paleoproterozoic Mikhailovsk Formation and are uncomformably overlain by Purpol sediments with weathering crusts at the contact. The wide range of isotopic ages of 1850–2000 Ma (Makar'ev and Chukhonin, 1992; Ivanov et al., 1995) obtained for these granitoids is explained by multiple intrusions and widespread overprinted metasomatic and metamorphic alteration. The Chuya-Nechera Complex comprises bodies of leucocratic gneisses and pegmatoidal granite that are commonly surrounded by zones of migmatites and porphyroblastic recrystallisation in the host sedimentary rocks. Various mafic sill and dyke complexes were emplaced in the area in the Neoproterozoic, but their ages are still locally uncertain. One of them is the Yazovsk granitoid complex at the Tonoda Uplift, whose U–Pb zircon age is 730 ± 97 Ma, as determined by A.M. Larin and A.L. Neimark (Ivanov et al., 1995).

The next significant magmatic event in the area was the empalcement of Paleozoic granites. The subdivision of the Paleozoic granite complexes was revised many times, and now the major Mama-Oron, Konkuder-Mamakan and Synnyr complexes are distinguished. The Mama-Oron Complex dated at ca. 420 Ma (Ivanov et al., 1995) occurs mostly in the southern part of the region. Along with massive granite, it comprises granite pegmatite, famous for large muscovite deposits of the Mama mica-bearing region. The Konkuder-Mamakan Complex includes bodies of compositionally variable sub-alkaline and alkaline granite, quartz syenite, quartz monzonite and leucogranite. The massifs of the Konkuder-Mamakan Complex, such as the Dzhegdokar, Telmam, Konkuder, Bryzgun, Synn, Dovgakit massifs, crosscut the folded strata and form contact-metamorphic aureoles, varying from tens metres to 1–3 km wide in host Proterozoic rocks. The mineral assemblages of the contact metamorphism are strongly dependant on conditions of regional metamorphism during

emplacement: endocontact aureoles abundant in xenoliths and assimilated host-rock material where the granite intruded high-grade amphibolite-facies rock. In cases if the granite intruded greenschist-facies rocks, the massifs usually have fine-grained endocontact rims and are surrounded by fine-grained granite veins in the host hornfels (Ivanov et al., 1995). It was approved earlier that the age of the Konkuder-Mamakan multiphase complex is ca. 320 Ma based on U–Pb dating on titanite and on Sm–Nd mineral isochron dating, although the U–Pb zircon age was in the range of 600–500 Ma and suggested zircon inheritance (Rundqvist et al., 1992; Neimark et al., 1993a, b). Other recently obtained U–Pb zircon and Rb–Sr mica data suggest an older age of ca. 420 Ma for the main phase of the complex (Gerasimov et al., 2007). In the light of the new data, the insignificant portion of the massifs that was previously assigned to the Konkuder-Mamamkan Complex may be of late Paleozoic age, whereas the largest massifs such as Telmam and Dzhegdokar are of early Paleosoic age and have thus to be assigned to the Mama-Oron Complex. The vein-dyke phases and small bodies, such as the Konstantinovskiy stock, are proved to be of late Paleosoic age and are correlative to a phase of the Angara-Vitim batholith. The polychronous Angara-Vitim batholith was emplaced mostly in Barguzin zone as the early (340–320 Ma) and late (310–270 Ma) magmatic phases that were accompanied by regional-contact metamorphism and extensive assimilation and re-working of the previous crustal complexes (Bukharov et al., 1992; Neimark et al., 1993b; Tsygankov et al., 2007).

The massifs of the 320 Ma Synnyr syenite and alkaline granite complex are rare in the area but are abundant in the Baikal-Vitim-Barguzin zone. The Kadali-Butuin diorite-lamprophyre dykes with a similar age of 320 Ma are widespread. They crosscut Konkuder-Mamakan granites. Small bodies of late Paleozoic REE-Nb carbonatite (Biraya), together with the Murun alkaline-carbonatite complex, occur within a zone trending towards the boundary with the Aldan Shield of the Siberian craton.

2.3. Mineralisation

The two types of lode gold mineralisation traditionally distinguished in the Lena Province are the veinlet-disseminated and quartz vein types (Kazakevich et al., 1971). The veinlet-disseminated gold-quartz-sulphide (Sukhoi Log-type) mineralisation is the most important economic type which occurs at the Sukhoi Log, Vysochaishee, Verninskoe, Chertovo Koryto and Nevskoe deposits. This mineralisation is controlled by linear and overturned anticlines, and fault zones in their axial parts and flanks. The largest deposits are hosted in rocks metamorphosed to the sericite-chlorite greenschist facies. A few deposits

(Ozherel'e, Ykan) occur in rocks metamorphosed to the epidote-amphibolite and amphibolite facies, although they are confined to a zone of retrograde metamorphism (Ivanov, 2014).

The quartz vein type (Kazakevich et al., 1971) or gold-sulphide-quartz mineralisation (Ivanov et al., 1995) is confined to sublatitudinal linear vein clusiters in the axial parts of anticlines, tectonic faults, shear zones and tension fractures, including those concordant to the bedding plane (Pervenets, Dogaldyn, Krasnoe deposits) and those of cross-cutting setting (Kavkaz). The largest vein cluster is Centralnoe in the Sukhoi Log camp and Dogaldyn in the Artemovskiy camp.

2.4. Age data

A Rb–Sr whole-rock isochron age of 447 ± 6 Ma for Sukhoi Log was interpreted as the crystallisation age of muscovite coeval with gold-quartz-sulphide mineralisation (Laverov et al., 2007). The Rb–Sr isotopic dates for barren rocks of the Valyukhta Formation coeval to the Khomolkho Formation in the outer part of the Patom Highlands substantially deviate from the isochron. The U–Th–Pb isotopic data on newly-formed crystalline monazite and hydrothermal zircon overgrowths from Khomolkho shales at Sukhoi Log correspond to an age of 440–460 Ma for the high-temperature event occurring within the mineralised zone, specifically in gold-rich intervals (Yudovskaya et al., 2011). These dates are similar to the age of the 441 ± 57 Ma of an event that disturbed the U–Pb system of detrital zircon from the Khodokan gold deposit in the Nechera Plateau. The whole rock Rb–Sr isochron age of metasomatised rocks of the Khodokan deposit hosted in the Mesoproterozoic Purpol Formation was estimated at 492 ± 70 Ma (Landa et al., 2006). The recently obtained pilot Re–Os isotope dates of sulphides from Sukhoi Log suggest that the mineralisation was formed between 470 and 508 Ma, assuming that the Re–Os systematics in sulphides was preserved throughout metamorphism (Yakubchuk et al., 2014).

The Rb–Sr isotopic age of 321 ± 14 Ma for quartz from the late hydrothermal veins (Laverov et al., 2007) and isotopic ages of 375 ± 20 and 288 ± 22 Ma for hydrothermal monazite (Meffre et al., 2008) coincide with the age of the intrusive phases of the Konkuder–Mamakan Complex, which was produced by the plume-related multiphase Angara-Vitim magmatic event.

Comparison of available Pb–Pb isotopic data on sulphides from gold deposits in the Lena Province and whole-rock samples of late Paleozoic igneous rocks exposed in the Bodaibo district show that the late Paleozoic granitoids cannot be regarded as a potential source of Pb for the ores (Rundqvist et al., 1992; Landa et al., 2006; Meffre et al., 2008; Chernyshev et al., 2009; Chugaev et al., 2010, 2014). With Pb isotope data progressively

amassing over the past decade, the heterogeneity of the Pb isotope compositions becomes more obvious and indicates that Pb was extracted from multiple sources of variable age. However, the regional heterogeneity is not accompanied by notable heterogeneity on the scale of individual ore deposits because each of them exhibits a certain range of variations, and larger-scale mineralisation is likely characterised by a narrower variations in the Pb isotope composition. On the diagram (Fig. 4), the array of the Pb isotope compositions of galena and pyrite from Sukhoi Log is constrained between 600 and 200 Ma model age values according to the Stacey-Kramers model (μ=9.74), and this does not contradict the age of the host rocks and may imply Pb inheritance from the host shales. The Pb isotope compositions from Chertovo Koryto mineralisation do not reveal any input of the ancient sedimentary source material comparable to the 2.0 Ga old host rocks (Chugaev et al., 2014). Within this model, it could be only correlated with 0.7 Ga Yazovsk granitoids, although this hypothesis cannot be validated due to an absence of Pb isotope data on the Proterozoic granite complexes.

3. Methods and samples

The Sukhoi Log drillhole samples (SRK6 and SRK8 boreholes) used in this study were collected by the authors in the course of the 1995–1997 fieldwork and were subject to previous comprehensive mineralogical, geochemical, and isotopic studies (Distler et al., 1996, 2004; Distler and Yudovskaya, 2005; Laverov et al., 2006, 2007; Rusinov et al., 2008; Chernyshev et al., 2009; Yudovskaya et al., 2011). A new rock collection was sampled from the Zapadnoe open pit and exploration holes in 2006–2007. Samples from the Chertovo Koryto and Vysochaishee deposits were collected in 2006 from exploration boreholes (ChK51, ChK82 and ChK85) that were drilled through the central part of the orebody. The numbers of samples in the text include borehole number and depth in meters.

Morphology of mineral grains and intergrowths was studied on a JEOL-5610 scanning electron microscope (SEM), with minerals analysed on an energy-dispersive spectrometer (EDS) at the Institute of Geology of Ore Deposits, Petrography, Mineralogy, and Geochemistry (IGEM RAS). Major oxides and trace elements in rocks were determined with X-ray fluorescent (XRF) and instrumental neutron activation analysis (INNA, Supplementary Tables 1 and 2) at IGEM RAS (analysts A. Yakushev and A. Kerzin). The deviations from the recommended standard values were less than 0.7% for all major elements and 10% for trace elements.

The study summarizes microthermometric data on more than 1000 fluid inclusions in quartz from the Sukhoi Log and Chertovo Koryto deposits which were partly published earlier (Laverov et al., 2000; Distler et al., 2004). These data were obtained using a THMSG-600 Linkam stage at IGEM RAS. Fluid inclusion salinities were estimated from ice melting temperatures (Bodnar and Vityk, 1994). The salinities of fluid inclusions containing dense CO_2–CH_4-rich fluid could not be determined on the basis of clathrate melting temperature (Collins, 1979; Darling, 1991) because the clathrate melting temperature was higher than +10 °C due to the high methane content. The salinity was assessed from the ice melting temperature, and corrected in terms of the volumetric proportions of CO_2 and H_2O with the subsequent calculation of the carbonic acid concentrations in the solution. Methane concentration was estimated on the basis of volumetric proportions and methane density deduced from its partial pressure, which is determined from the methane clathrate melting temperature (Claypool and Kaplan, 1974). On the basis of these data, the necessary corrections for the amount of gas hydrate water were used to estimate the salinity of the CO_2–CH_4–H_2O-rich fluid. Pressure of the heterogeneous fluid was derived as the sum of vapour pressure and the pressure of dense gases (CO_2, CH_4 and N_2) in vapour-rich and vapour–liquid inclusions. The salinity, densities of CO_2–CH_4 mixtures and N_2, and their pressures were evaluated using the FLINCOR program (Brown, 1989; Brown and Lamb, 1989). The isochores were constructed and the pressure in CO_2–CH_4-rich inclusions was estimated using data of Kerkhof (1988) and Thiery et al. (1994).

Aqueous extracts from inclusions were analysed by several methods, including gas and ion chromatography and ICP-MS, in extracts from 0.5 g charges of the 0.50- to 0.25-mm quartz fraction at the Central Institute of Geological Exploration for Base and Precious Metals (TSNIGRI, analyst Yu.V. Vasyuta) according to the procedure described by Kryazhev et al. (2006). The amount of water in inclusions of the same charge was determined to calculate concentrations of elements in the hydrothermal solution. Carbon dioxide and methane were also analysed. Gas composition was checked beside microthermometry by Raman analysis at the Nancy University, using a spectrometer Dilor RTI-30 (analyst J. Dubessy).

4. Geology of the deposits

4.1. Geological setting of Sukhoi Log

The geology of Sukhoi Log was described in much details elsewhere (e.g. Distler et al., 1996, 2004; Buryak and Khmelevskaya, 1997; Wood and Popov, 2006 and references therein). Here we summarise some features relevant to the further comparison with the Chertovo Koryto deposit. The Sukhoi Log is located in the Mama-Bodaibo Synclinorium, which consists of alternating synclines and anticlines trending nearly west-east (Fig. 3). Thrust faults in the Mama-Bodaibo Synclinorium commonly strike north-northwestward, conformably with the orientation of the bedding (Ivanov et al., 1995). The Sukhoi Log deposit is confined to the Sukhoi Log overturned anticline that complicates the larger Marakan–Tunguska syncline with conjugate thrusts in both of its limbs (Fig. 5). It is hosted in sedimentary rocks of the Khomolkho Formation and partially in the overlying dolomite-dominated Imnyakh Formation. Igneous rocks in the vicinity of the deposit are confined within the small Konstantinovskiy granitoid stock, 6 km south of the deposit. The larger Dzhegdakar granitic pluton of the Konkuder–Mamakan Complex is situated at a distance of 35 km. The interpretation of a gravity anomaly in the area suggests that the so-called Ugakhan granitic pluton occurs at a depth of about 3 km beneath the deposit (Lishnevsky and Distler, 2004).

The Sukhoi Log deposit is a tabular lode, striking northwestward. The largest orebody, which has the same name, is about 4 km^2 in area and is composed of stringer–disseminated gold-quartz-sulphide mineralisation and gold–quartz veins. The gold-quartz-sulphide stockwork-type mineralisation is confined to the core of the anticline and is surrounded by a wider aureole of barren sulphides.

The deposit is hosted mostly in carbonaceous quartz–sericite–carbonate shales to sandstones metamorphosed to the sericite and locally sericite–chlorite subfacies of the greenschist facies. The shales consist of (vol.%) quartz (30–35), sericite (35–40), graphite-like carbonaceous matter (up to 5, mostly ranging 0.5–1.0), and carbonates (5–30). Chlorite is uncommon in the ore zone and becomes more abundant with depth. Biotite, rutile, hematite, tourmaline, zircon, apatite and monazite are accessory. The sandstone is a quartz-rich rock with rare clastic feldspar grains and mica-graphite stringers.

The degree of deformation depends on the structural setting. Rock fabrics in the highly deformed anticline core (such as flexures, isoclinal folding, crenulation cleavage, segregation and metamorphic banding, boudinage of competent sandstone within shales, offset of earlier folds along foliation, crosscutting relationships between quartz–sulphide veinlets and later quartz veins) provide evidence of multiple predominantly ductile deformation (Fig. 6).

4.2. Geological setting of Chertovo Koryto

The geochemistry and mineralisation in Chertovo Koryto were partly presented in a few papers (Kucherenko et al., 2008; Vagina, 2012); and its geological setting is described herein based on unpublished data by V.G. Martynenko and A.V. Verkhozin (Verkhozin et al., 2007). The state geological map is borrowed from the same unpublished reports and shown simplified (Fig. 7).

Alluvial gold was mined in the local rivers in the central part of the Tonoda Uplift starting in the mid-19th century. The lode mineralisation of the Chertovo Koryto (can be translated as the Devil's Trough Pan) was discovered in 1963. A gently dipping orebody, up to 80 m thick, was traced for 950 m along its strike and 250 m downdip at a 1 g/t Au cutoff as a result of new drilling and reassessment of older data obtained in the 1960s and 1980s. The Kevakta ore camp was found to contain several other gold occurrences of the same style which are underexplored.

The deposit is located within the limits of the Tonoda Uplift, which is part of the extended Chuya-Tonoda Uplift (Fig. 3). The major ancient regional tectonic structures are latitudinal and sublatitudinal faults with accompanying shearing. The deposit is hosted by Mezoproterozoic metasediments of the Mikhailovsk Formation that form the second-order latitudinal Mikhailovsk broad syncline, whose flanks gently dip at 10º–20º (Fig. 7). The eastern flank of the Mikhailovsk syncline is complicated by a sub-longitudinal overthrust dipping at 5°–40º westward. The ore zone is controlled by a gently dipping dislocation zone that accompanies the thrust and comprises multiple thrusts, a low-order conjugate anticline fold and zones of shearing, folding, microfolding, fracturing and boudinage (Verkhozin et al., 2007). The orientation of the quartz and quartz-sulphide veins is generally sub-concordant to the orientation of the dislocations and cross-cutting to the bedding.

5. Whole-rock geochemistry of ore-bearing sequences

5.1. Major oxide compositions

The ore-bearing sequence of the Mikhailovsk Formation is composed of rhythmically intercalating carbonaceous schists (metamorphosed black shale), metasiltstone, metasandstone and metamarl (metamorphosed argillaceous dolomite).

Mikhailovsk carbonaceous schist and metasandstone are compositionally within a range of the major-oxide compositions of the sub-platform sediments, such as the North American Shale Composite (NASC) (Taylor and McLennan, 1985), sediments at the Russian platform (Ronov and Migdisov, 1971) and sedimentary rocks at the Yangtze Craton (Gao et

al., 1998). Their major oxide compositions are also similar to the other carbonaceous shales and sandstone in the Lena region, regardless of presence or absence of mineralisation (Table 1). According to data of Kucherenko et al. (2008), the carbon content of Mikhailovsk rocks varies within 0.07–1.9 wt.% C, which is lower than that of Khomolkho shales (0.2–2.7 wt.% C according to Distler et al. (2004)). Figure 8 shows similarities between the compositions of rocks from five formations: the Mesoproterozoic Mikhailovsk and Neoproterozoic Dzhemkukan and Khomolkho formations, which host ore deposits, and the overlaying barren Vacha and Anangr formations, which display indications of a sedimentation regime that did not vary with the time. The Na_2O and K_2O variations mostly reflect the variable proportions of sandy fraction, rich in Na due to petrogenic or ash-derived plagioclase, and a shaly fraction, rich in sericite-muscovite that replaced clay precursors. However, it was shown earlier that the K_2O content in the Sukhoi Log ore zone (3.1 wt.% K_2O on average) is generally higher than the average K_2O content in barren Khomolkho shales, whereas the ore zone is depleted in Na_2O compared to the underlying and overlying zones (Distler et al., 2004). This suggests an influx of potassium into the zone of ore deposition (Distler et al., 2004), with sodium enrichment interpreted as a diagenetic geochemical signature, based on the predominant development of Na-rich mica in the barren rocks and muscovite prevailing in the ore zone (Rusinov et al., 2008). The K_2O vs. SiO_2 plot (Fig. 8) shows that the K_2O content of mineralised Khomolkho and Mikhailovsk rocks is generally higher than that of barren shales of other formations, whereas the range of the Na_2O variations is the same supporting the link between potassic metasomatism and mineralisation.

Mikhailovsk metamarl has a distinct chemical composition with low SiO_2, K_2O, Na_2O and high MgO, Fe_2O_3 and CaO contents, as is typical of dolomite sedimentation. The high Ti content in the metamarl (Fig. 8) is uncommon in rocks of the region. Hence, to deduce the provenance of the Mikhailovsk sediments, we used geochemical indexes introduced by Yudovich and Ketris (2000). The Alumina Index AI = $(Al_2O_3+TiO_2+Fe_2O_3+FeO+MnO)/SiO_2$ serves as an indicator of the chemical maturity of sediments, because silica and potassium contents decrease and alumina increases during weathering. Mikhailovsk metamarl, as well as one of the Khomolkho shales, have AI higher than 0.55, which likely indicates a hydrolysate provenance. The Titanium Index TI = TiO_2/Al_2O_3 helps differentiating between sandy and shaly fractions, because it is higher in sandstone (typically within 0.055–0.075) than in finer-grained lithologies (0.03–0.06). This is a result of the partial separation of Ti-bearing accessories and lighter clay matter during sedimentation according to the so-called Migdisov rule (Yudovich and Ketris, 2000). A correlation between a high TI and elevated

proportions of Mg and Fe oxides commonly suggests that the potential source consisted of mafic rocks or volcanic ash. The TI = 0.34 of Mikhailovsk metamarl is much higher than that of other lithologies in the region and, when considered together with the high AI and enrichment in Mg and Fe, suggests an input of tuffaceous mafic material or mafic hydrolysates during the deposition of the marl layers.

5.2. Trace elements

The trace element contents in the Mikhailovsk mineralised rocks are assessed mostly from 91 INAA analyses with a minor addition of XRF trace element data on elements that were not analysed by INAA (Supplementary Table 2). These are compared with the trace element compositions of Khomolkho mineralised rocks at Sukhoi Log (85 analyses, Supplementary Table 1, partly published earlier in Distler and Yudovskaya, 2004), and Vysochaishee (20 analyses). The average values, the element abundances (clarke) in black shales worldwide (after Yudovich and Ketris, 1988) and the rock compositions referred to are shown in Table 2.

The trace element patterns of Sukhoi Log, Chertovo Koryto and Vysochaishee mineralised rocks are broadly similar to the pattern of typical sub-platform sediments exemplified by the Yangtze sediments (Gao et al., 1998). It shows strong, by two to three orders of magnitude, enrichment in gold and arsenic among all ore elements (Fig. 9a), with slightly elevated lead and copper contents compared to the Yangtze values. Figure 9b shows these values normalised to the average element abundances in black shales worldwide. It is well known that some black shales are anomalously enriched in the redox-sensitive ore elements (Yudovich and Ketris, 1988; Coveney et al., 1992; Pašava, 1993; Mao et al., 2002), which may result from: (1) primary enrichment of the source of clastic material; (2) enrichment on a reduced geochemical barrier under euxinic conditions; and (3) syn-depositional exhalative process deriving ore components from a deep source. It was repeatedly stated that black shales of the Lena Province are anomalously enriched in Pb, Zn, Cu, Mo, Ag, Au and some other elements, although these conclusions were derived mostly from semi-quantitative spectroscopic data that were obtained well before precise and fast analytics become widely available (Buryak and Khmelevskaya, 1997). The Fig. 9b shows that even mineralised Khomolkho and Mikhailovsk rocks are not enriched in any metals with respect to their background values in the average black shales, except for the strong Au and As and slight Pb anomalies. For comparison, the trace element abundances in black shales of the Niutitang Formation in China are shown in Fig. 9b. This famous strata-bound Ni–Mo–PGE–Au sulphide mineralisation occurs in the lower Cambrian black shale sequence of the

Niutitang Formation throughout China. Strata of this formation and its stratigraphic equivalents stratigraphically unconformably overlie the Neoproterozoic sequence comprising diamictite with an age of ca. 630 Ma (Mao et al., 2002; Jiang et al., 2006), implying that Niutitang and Khomolkho sediments were deposited broadly simultaneously in the basins of the Paleo-Asian Ocean. The geochemical and isotope data suggest that Niutitang mineralised black shales formed via submarine hydrothermal exhalation, and the trace element pattern correspondingly shows coupled enrichment in redox-sensitive elements and base metals and depletion in lithophile elements due to a limited detrital input.

The ore zone of the Chertovo Koryto deposit shows the irregular distribution of gold that does not correlate well with the As variations, as is also the case with the Sukhoi Log mineralisation (Figs. 10 and 11). The other element variations are related to changes in the lithology and to the occurrence of metamarl in particular. The coeval enrichment in Ca, Fe, REE, Co and Cr with the strong depletion in sodium is an unequivocal feature of the metamarl horizons (Figs. 10 and 11). The iron content does not correlate with either gold or arsenic contents. The occurrence of quartz stockwork veining and thicker (up to 10 cm) veinlets is not revealing in these variations due to the long sampling interval (1 m samples) comparing to the vein thicknesses (commonly 2–3 cm).

The trace elements in the metamarl reflect that its sedimentation environment was different from those of adjacent terrigenous rocks. The metamarl does not carry any gold grade but is twice richer in Fe, Mg, Co, Cr and REE than the neighbouring carbonate-poor sediments (Fig. 11 and Supplementary Table 1). However, the similar level of Co, Cr and REE enrichment is seen in rocks of the Vysochaishee deposit in the lower part of the Khomolkho Formation close to the boundary with underlying Ugakhan limestone (Fig. 11). Positive correlations between Cr, Co, Fe and REE (+Th) contents are typical of rock compositions of the region regardless their gold grades and arsenic contents. Elevated chromium in sediments is commonly indicative of two sources: (1) tuffs and mafic pyroclastics and (2) erosion and re-deposition of residual soils developing on mafic-ultramafic rocks (Yudovich and Ketris, 1988). The elevated REE, Zr and Th and the findings of syneruptive zircon in Khomolkho rocks (Meffre et al., 2008; Yudovskaya et al., 2011) support the first option implying the higher proportion of the pyroclastic material in Mikhailovsk metamarl and in lower Khomolkho sequence at Vysochaishee.

6. Mineral associations at Chertovo Koryto

The rocks are banded and schistose and show relic primary sedimentary bedding (Fig. 12). The bedding and schistosity may have the same orientation on the flanks of the low-order folds (Fig. 12a), although the cleavage invariantly cross-cuts the bedding in the axial parts of the folds and in flexures (Fig. 12b, c). Cleavage is clearly multi-staged in fine-grained shales and unobvious in coarser-grained sandstone (Fig. 12a, i). Rock textures are predominantly granoblastic, lepidogranoblastic, porphyroblastic and cataclastic (Fig. 13).

The micaceous schists (metamorphosed carbonaceous shales) consist of (in vol.%): quartz (20–35), sericite-muscovite (35–70), chlorite (10–20), graphite-like carbonaceous matter (up to 2, less than 0.5 on average), and carbonates (0–10). The quartz-feldspar metasandstone consists of (in vol.%): quartz (60–90), sericite-muscovite (5–10) and plagioclase (2–15) with minor chlorite, K-feldspar and carbonate. The metamarl or metamorphosed argillaceous dolomite consists of (in vol.%): carbonates (ankerite 30–50), quartz (30–35), muscovite (15–30), chlorite (10–15), epidote (2–10) and rutile (1–7). Biotite, hematite, titanite, tourmaline, zircon, epidote, apatite and allanite are accessory minerals.

The sulphide content reaches 5–8 vol.%, and the dominant sulphides are arsenopyrite and pyrrhotite. Pyrite, galena, sphalerite, chalcopyrite, cobaltite, gersdorffite and ullmannite are minor. Native lead, tellurobismuthite and valleriite were reported by Kucherenko et al. (2008). Secondary marcasite, pyrite and goethite replace the primary sulphides in the sub-surface oxidation zone and along fractures.

Three major stages of mineral formation can be distinguished based on observations in polished sections: metamorphic, hydrothermal and post-ore quartz veins.

6.1. Metamorphic stage

The only observable diagenetic feature is relict bedding that survives in weakly deformed domains (Fig. 13c). In highly-deformed domains primary bedding is blurred due to strong superimposed schistosity (Fig. 13b, d). The sedimentary textures are also deformed by re-distribution of shaly and sandy material into monomineralic micaceous, chlorite-rich and quartz-rich layers parallel to the schistosity due to their different competencies (Fig. 13a). Muscovite and chlorite foliation are draped around quartz porphyroblasts; the rocks show crenulation cleavage indicating multiple deformations (Fig. 13e, f). Single small biotite crystals were met within highly-deformed micaceous bands in flexures. Quartz in metamorphic quartz sandstone has interlobate contacts due to grain boundary migration and recrystallisation.

The metamorphic carbonates $(Fe_{0.02\text{-}0.12}Mg_{0.36\text{-}0.47}Ca_{0.51\text{-}0.61})CO_3$ are ankerite, which segregates into lenses and porphyroblasts in carbonate-poor rocks and forms massive

recrystallised bands after carbonate-rich matrix. The monomineralic quartz-rich and mica-rich bands commonly do not carry any carbonate impurity.

The observed mineral assemblage indicates conditions of the muscovite-chlorite sub-facies of the greenschist facies. However, the abundant needles of rutile in quartz and chlorite can be interpreted as products of biotite replacement during retrogression (Fig. 14). It cannot be ruled out that the replaced biotite was Ti-rich detrital biotite of primary igneous origin, but the size of quartz and chlorite pseudomorphs is much larger than the size of other detrital grains and matches better the size of the porphyroblasts. Crystallographically oriented aggregates of needle-like rutile are commonly observed in biotite or in chlorite produced by hydrothermal alteration of biotite (Shau et al., 1991). Therefore, the sagenitic texture of rutile in Mikhailovsk metasediments was likely formed during the retrograde stage at the replacement of metamorphic biotite grains that had crystallised during the prograde stage under conditions of the biotite-muscovite-chlorite sub-facies.

Coarse zoisite (Fig. 13f) and plagioclase porphyroblasts are found mostly in metamarl and carbonate-rich rock varieties in association with coarse metamorphic muscovite laths, which also suggests a higher metamorphic grade transitional to the zoisite-plagioclase subfacies. Rare grains of wollastonite were found in the metamarl in the course of the SEM study.

The metamorphic sulphides are pyrrhotite lenses and dissemination on schistosity planes.

6.2. Hydrothermal stage

Three major reactions control the formation of the hydrothermal metasomatic assemblages: silicification, sulfidation and minor carbonation (Fig. 15).

The carbonates of this stage are ankerite, which may contain small inclusions or exsolutions of younger pure calcite. The replacement of the retrograde metamorphic assemblages by carbonate is most widely spread in the metamarl (Fig. 14d). The quartz segregation and porphyroblasts are replaced along their margins and in central parts (Fig. 15 d); pseudomorphous quartz and chlorite after biotite were found to be partially or completely replaced by ankerite with sagenitic rutile remaining within the carbonate matrix (Fig. 14). The relationships between prevailed metamorphic and minor hydrothermal carbonates are obscure because both assemblages are superimposed on various precursor materials.

The hydrothermal quartz forms a stockwork ore zone with small concordant and mutually cross-cutting veinlets (Figs. 12 and 13e), thicker veins, quartz lenses, a zone of silicification, quartz overgrowths and pressure shadows around porphyroblasts. Undulose

extinction is common in large porphyroblastic quartz grains (Fig. 15a), showing that the rock underwent some ductile deformation postdating porphyroblastesis and veining. Tiny quartz veinlets fill fractures in cataclastic arsenopyrite where it associates with native gold (Fig. 15b, c).

Chlorite of the hydrothermal stage forms medium-grained segregations and coarser crystals in pressure shadows around ore minerals and quartz porphyroblasts (Fig. 15 b–f). Its composition differs from that of the metamorphic chlorite in higher Fe content, although both types belong to the chamosite-clinochlore series. The hydrothermal green chlorite has a $Mg^{\#}$=0.46–0.52 and contains 2.8–2.9 Al pfu, whereas metamorphic grey chlorite has a higher $Mg^{\#}$=0.67 and contains 2.4 Al pfu. The muscovite is a K-rich variety (10.1–10.4 wt.% K_2O), which contains 1.7–2.6 wt.% MgO, 1.5–2.8 wt.% FeO and 0.5–1 wt.% TiO_2. Chlorite and muscovite from the metamarl contain up to 0.4 and 1.8 wt.% Cr_2O_3, respectively. Chromium-bearing phillosilicates in the metamarl associate with Zn-bearing chromite, gersdorffite and REE-bearing minerals – allanite and monazite. Zn-rich chromite occurs as small grains with average contents (wt.%): 34.5 Cr, 24.8 Fe, 1.4 Ti, 5.1 Al and 4 Zn that corresponds to the formulae $(Fe_{0.86}Zn_{0.14})Cr_{1.45}Al_{0.41}Fe_{0.08}Ti_{0.06})O_4$.

The most prominent feature of the ore zone is the occurrence of sulphides and native gold.

Arsenopyrite is a major sulphide in association with gold. It forms disseminated euhedral crystals from 50 μm to 1 cm that are predominantly confined to coarser-grained sandstone domains and arranged concordantly to lithological boundaries. The lithological control on the sulphide distribution is more obvious for finer sulphide grains: fine-grained pyrrhotite is commonly confined to mica-rich bands whereas the neighboring quartz bands host fine-grained arsenopyrite (Fig. 16a, b). Arsenopyrite is superimposed on and replaces porous porphyroblasts of metamorphic titanate (Fig. 16c). In the sandstones, arsenopyrite is inevitably surrounded by symmetrical or assymetric pressure shadows of quartz and chlorite. The coarser crystals are commonly surrounded by wider quartz-chlorite shadows, which extend into larger lenses and segregated veins (Fig. 15f). Both arsenopyrite and host sandstone are more susceptible to brittle deformations compared to pyrrhotite and its micaceous matrix, which are subjected to ductile deformations. As a result of their different competency, arsenopyrite is often fractured and cataclastic (Fig. 16 d–g), whereas pyrrhotite reveals a granoblastic texture and is folded conformably to the schistosity.

The earlier metamorphic pyrrhotite is distributed along the foliation as small lenses and fine impregnation; its inclusions are common in the arsenopyrite and pyrite cores. The

hydrothermal pyrrhotite tends to fill the central part of thin quartz veinlets and cements, together with gold and galena, cataclastic arsenopyrite (Fig. 16e). The pyrite forms large euhedral crystals; some of them are gold-bearing and likely coeval to arsenopyrite but most of them are younger and do not associate with native gold.

Native gold is found predominantly in association with quartz as euhedral crystals and flattened particles in the selvages of quartz veins. Inclusions of native gold in arsenopyrite crystals are subhedral to anhedral and are accompanied by gold veinlets and disseminations along cataclastic fractures in arsenopyrite and neighboring minerals (Figs. 16e,f and 17). In these veinlets, native gold associates with galena and pyrrhotite (Fig. 16e, g).

Gersdorffite was found at Chertovo Koryto mostly in metamarl layers, in which it associates with Cr-bearing silicates, ullmannite, Zn-chromite, allanite and monazite (Fig. 19). It forms euhedral crystals, which show evidence of porphyroblastic growth and segregation of smaller nuclei to form larger crystals (Fig. 17 d–f). The perfect grain morphology of the gersdorffite is combined with its porous and imperfect internal texture, with numerous tiny inclusions of silicates similar to the textures of arsenopyrite and pyrite metacrysts (Fig. 17f). Gersdorffite and cobaltite are rare minerals in Sukhoi Log ore, although they associate with Au-rich mineralisation (Distler et al., 2004). Minerals of this group were found, together with millerite, pentlandite, violarite and ullmanite, in the gold ore of the Kopylovsk and Kavkaz deposits (Palenova et al., 2015) hosted in the Dogaldyn Formation (see in Fig. 3). The associations of Co-Ni minerals at Sukhoi Log, Kopylovsk and Kavkaz are strikingly similar, and their occurrence was not found out to be controlled by lithology, contrary to what is the case with Chertovo Koryto. It should be added that Vagina (2012) reported systematic relations between rare Co-Ni sulfoarsenides and native gold in Chertovo Koryto, supporting their crystallisation during the same stage.

6.3. Post-ore stages

The younger quartz veins are common in the ore zone and cross-cut zones of arsenopyrite dissemination and older quartz-sulphide veinlets. The relics of replaced minerals are locally seen in the selvages. Mineralisation in the quartz vein depends on the grade of the host matrix: the veins that cross gold-bearing intervals, as a rule, bear gold, otherwise, they are barren. The quartz veins contain mostly pyrite and galena, unless other sulphides were trapped and inherited from the host matrix. In the metamarl, the younger veins contain a significant proportion of Mg-rich siderite (Fig. 12e).

Later supergene alteration locally occurs as melnikovite, marcasite and goethite replacing sulphides, whereas native gold remains immobile (Fig. 16h).

6.4. Comparison of Sukhoi Log and Chertovo Koryto mineral assemblages

The Sukhoi Log mineral assemblages were forned during four stages: sedimentary process, prograde metamorphism, hydrothermal merasomathic mineralisation and post-ore veins (Buryak and Khmelevskaya, 1997; Distler et al., 2004; Rusinov et al., 2008). The degree of prograde contact-regional dynamothermal metamorphism of Sukhoi Log host rocks was lower than that of retrograde metamorphism at Chertovo Koryto in terms of the observed mineral associations. It becomes apparent from the paucity of chlorite and metamorphic pyrrhotite, the absence of phlogopite and more simple deformational fabrics. The Sukhoi Log metamorphic assemblage is composed of muscovite, paragonite, quartz, carbonate and minor pyrrhotite whereas hydrothermal-metasomatic ores consist of very diverse gangue and ore minerals includng hydrothermal pyrrhotite, Ni–Co sulphides, arsenides and sulphoarsenides, and platinum group minerals (Distler et al., 2004). The morphology of carbonate, quartz and monazite metamorphic porphyroblasts (Fig. 20a, b) at Sukhoi Log indicates their syn-kinematic origin whereas metacrystals of pyrite reveal both syn- and post-kinematic features (Fig. 20c). The high crystallinity of K-micas and the absence of their hydratation at Sukhoi Log points out that the lower temperature limit of their formation was at least 250 ^{o}C although it might reach 400 ^{o}C (Rusinov et al., 2008).

Gersdorffite and cobaltite are rare minerals in Sukhoi Log ore, although they associate with Au-rich mineralisation (Distler et al., 2004). Minerals of this group were found, together with millerite, pentlandite, violarite and ullmanite, in the gold ore of the Kopylovskoe and Kavkaz deposits (Palenova et al., 2015) hosted in the Dogaldyn Formation (see in Fig. 3). The associations of Co-Ni minerals at Sukhoi Log, Kopylovskoe and Kavkaz are strikingly similar, and their occurrence was not found out to be controlled by lithology, contrary to what is the case with Chertovo Koryto. It should be added that Vagina (2012) reported systematic relations between rare Co-Ni sulphoarsenides and native gold in Chertovo Koryto, supporting their coeval crystallisation during the same stage.

The association and morphology of native gold in Chertovo Koryto is in certain contrast with those in Sukhoi Log ores whose arsenopyrite is a minor mineral (Fig. 20d). The composition of native gold from Sukhoi Log varies from $Au_{75}Ag_{25}$ to $Au_{95}Ag_{5}$, and a predominant proportion of lower fineness gold occurs as small euhedral droplet-shaped crystals strongly linked to pyrite (Fig. 18 a–c) or to pyrite-quartz interfaces (Fig. 20e). Lower fineness gold may also occur in carbonate matrix of thin carbonate-quartz-sulphide veunlets in the ore zone (Fig. 20f). Native gold of higher fineness tends to form: (i) masses and veinlets of anhedral grains in fractured pyrite, arsenopyrite and along their grain boundaries

with quartz and silicates and (ii) coarser euhedral crystals and xenomorphic filling in late sulphide-poor quartz veins. As of now, the EDS data on gold composition ($Au_{75}Ag_{25}$ – $Au_{90}Ag_{10}$) are statistically insufficient to allow speculating as to whether these patterns are also typical of Chertovo Koryto. However, at Sukhoi Log, native gold in intergrowths with rare arsenopyrite has the same anhedral morphology penetrating and cementing cataclastic arsenopyrite (Fig. 18 d–f) as seen in Chertovo Koryto.

7. Ore-forming fluids and P-T conditions

7.1. Fluid inclusion in quartz from Sukhoi Log

Quartz and carbonate of veinlet-disseminated quartz-sulphide mineralisation and quartz veins host three types of fluid inclusions (Fig. 21): LLV-type is CO_2-H_2O inclusions which contain aqueous solution, liquid CO_2 and locally gaseous CO_2; G-type is gaseous inclusions; and LV-type is two-phase inclusions of salt-aqueous solutions. The gaseous inclusions are usually syngenetic to the LLV- or LV-types, thus indicating a heterogeneous state of the ore-forming fluid. When studying the inclusions, we selected two groups of the supposedly cogenetic inclusions (CO_2-H_2O and gaseous) with the similar phase relationships in each of the groups. Microthermometric statistics on the groups was used as representative for estimating the temperature and pressure of the fluid.

The LLV-type inclusions in minerals of Sukhoi Log **veinlet-disseminated ore** homogenise to liquid at 210–350 °C. They contain aqueous solution of Na chloride and hydrocarbonate, judging from eutectic temperatures of -34 to -31 °C. The estimated salinity ranges from 8.1 to 5.0 wt.% NaCl equiv., and the CO_2 content is from 7.6 to 1.8 mol/kg solution. Carbonic acid contains an admixture of other gases (methane and nitrogen), as follows from its melting temperature (-62.2 to -57.4 °C) and the temperature of gashydrate dissolution (which is lower than 12.4 °C). The syngenetic gaseous inclusions mainly consist of dense CO_2, which homogenises to liquid at -11.6 to 18.6 °C and to gas - at 23.8 to 6.5 °C. An admixture of other gases is also present, as seen from CO_2 melting temperature ranging from -60.8 to -57.0 °C. The density of CO_2 in the CO_2-CH_4-N_2 system is 0.90–0.14 g/cm^3, and the calculated trapping pressure varies greatly from 2370 to 190 bars at the temperature range from 350 to 210 °C. The presence of CO_2, methane and nitrogen in the gaseous inclusions is confirmed by Raman spectroscopy at the Henri Poincaré University, France. The Raman spectroscopic analysis of a gas inclusion in quartz (Fig. 21e–g) yields 83.4 mol.% N_2, 16.3 mol.% CO_2 and 0.3 mol.% CH_4, whereas nitrogen homogenisation to liquid was observed at -148 °C, and carbonic acid sublimated from solid to gas at -63 °C.

The LV-type inclusions contain low-salinity aqueous solution of Na chloride and hydrocarbonate with eutectic temperature of -34 to -25 °C and salinity of 9.5–3.7 wt.% NaCl equiv. This type is commonly in association with the syngenetic fluid inclusions whose temperature of homogenisation to gas is 385 to 205 °C. Carbonic acid and dense nitrogen (density of 0.57–0.003 g/cm^3) start condensing in these inclusions at cooling. The pressure is estimated to be within the range of 2290 to 210 bars at temperatures of 385–205 °C.

The LLV-type fluid inclusions in quartz of the gold-bearing **quartz veins** homogenise to liquid at 275–380 °C. They contain aqueous solution of Na chloride and hydrocarbonate with an eutectic temperature of -32 to -33 °C, salinity of 7.6–5.8 wt.% NaCl equiv. and CO_2 content ranging 7.0–2.1 mol/kg solution. The carbonic acid ubiquitously contains an admixture of other gases (methane and nitrogen), as is testified by the melting temperature of -60.9 to -57.1 °C and the gas-hydrate dissolution temperature of 11.6 °C. The syngenetic gaseous inclusions contain dense CO_2, which homogenises to liquid at 10.2 to 17.7 °C and to gas at 10.5 °C. The melting temperature of CO_2 varies from -60.7 to -57.3 °C, which confirms the presence of other gases. The density of CO_2 in the CO_2–CH_4–N_2 system ranges from 0.92 to 0.08 corresponding to a pressure of 2430 to 200 bars at 380–275 °C.

The LV-type inclusions contain aqueous solution of Na chloride and hydrocarbonate with an eutectic temperature of -22 °C and salinity in the range of 7.6–5.4 wt.% NaCl equiv.

The *T-P* diagram (Fig. 22) shows a wide range of pressure variations during the formation of Sukhoi Log ores, which was a possible result of two distinct processes that occurred at a relatively low pressure and at an elevated pressure. The gaseous fluid trapped in minerals from veinlet-disseminated ores is noted for a higher content of nitrogen and other gaseous admixtures that could be produced at the thermal decomposition of organic matter.

The bulk chemical composition of aqueous solutions in the inclusions is characterised by the predominance of Na over other cations and the hydrocarbonate ion over other anions (Table 4). Carbonic acid, methane, Cl, K, Ca and Mg are the minor components. Ore metals, including Au and Ag, are also detected leveling concentrations of tens of ppb (Fig. 23). Fluid inclusions in quartz from the quartz vein (SRK6-198.2) are enriched in CO_2, B, Br and some other elements with respect to the inclusions in quartz from the veinlet-disseminated ores (Fig. 23).

7.2. Fluid inclusion in quartz from Chertovo Koryto

Two types of fluid inclusions were found to be trapped in quartz from Chertovo Koryto mineralisation (Fig. 24): The LV-type comprises two-phase vapour-liquid inclusions and V-type is essentially vapour inclusions.

The primary vapour-liquid inclusions homogenise to liquid at 447 to 340 °C and contain aqueous solutions with salinity of 10.0–3.4 wt.% NaCl equiv. (Table 3). The eutectic temperature varies between –27 and –36 °C, suggesting the predominance of Na and Mg chlorides. The density is 0.66–0.52 g/cm^3.

The gaseous inclusions homogenise to gas within the temperature range of 453 to 388 °C and contain NaCl aqueous solution with salinity of 2.4 wt.% NaCl equiv. The calculated pressure ranges from 440 to 240 bars (44–24 MPa).

The ICP analysis of bulk solutions shows the predominance of Na and K over other cations and the hydrocarbonate-ion among the anions (Table 4). Subordinate amounts of CO_2, CH_4, Cl, K, Ca and Mg were detected, although the CO_2 concentration does not exceed 1.5 mol/kg solution in agreement with the absence of liquid CO_2 in the inclusions. Among metals, Pb and Cr concentrations are remarkably high compared to their concentrations in the solutions trapped at Sukhoi Log, and the measured Au concentration is as high as 1.1 ppm, i.e. two orders of magnitude higher than those in the Sukhoi Log solutions.

To represent variations of element contents in the fluid, we calculated the enrichment factors:

$$EF_i = (E_i/R)_{fluid} / (E_i/R)_{shale}$$

where E_i is an element content and R is the content of a reference element chosen to normalise both the fluid and the host rock compositions. Here, Na is chosen as the reference element because of its relatively persistent abundances and reliable determination in both rocks (Table 2) and fluids (Table 4). The relatively larger EF values for chalcophile elements and Au (Fig. 25) suggest that they were not borrowed from host rock but were rather derived by fluid from a source other than the host rocks. Elements with smaller EF values (Ba, U, Th, REE and Zr) were likely remobilised from host rocks by the high-temperature fluid.

7.3. Evidence of fluid mixing

Our fluid inclusion data indicate two types of ore-forming processes:

(1) A low-pressure (440–200 bars) hydrothermal process under conditions of relatively shallow depths, which produced Chertovo Koryto gold-bearing quartz veinlets and Sukhoi Log quartz veins;

(2.) A pneumatolitic-hydrothermal process under an elevated pressure (800–2400 bars) that involved aqueous fluid with dissolved gasses and immiscible gaseous high-density fluid.

The persistent co-existence of liquid-vapour and gaseous inclusions typical of the latter process can be explained by either coeval heterogeneous trapping of two distinct

hydrothermal fluids with their partial mixing or, alternatively, by phase separation (boiling) of an initially homogeneous H_2O–CO_2–NaCl fluid. Below, we argue that the mineralisation resulted from the mixing of CO_2-predominant and H_2O-predominant fluids at a significant depth.

The fluid pressure was estimated from the intersection of the isochore and isotherm (Roedder, 1984) for the associations of syngenetic of gaseous and CO_2–H_2O fluid inclusions. Most of the liquid-vapour inclusions are compositionally close to the H_2O–CO_2–NaCl system with a salinity no higher than 10 wt.% NaCl equiv. with NaCl as the dominant component (Table 2). The major component of the gaseous inclusions is CO_2, and the amount of other gases does not exceed 3 mol.% based on the CO_2 melting temperature of –58.5 to –56.6. Remarkable amounts of nitrogen and methane were found only in a few gaseous inclusions in lens-shaped quartz from the veinlet-disseminated ores. Figure 22 shows the parameters of those fluid inclusions, which chemically correspond to the H_2O–CO_2–NaCl system and do not contain any appreciable admixtures of other components. On the *P* vs. *T* plot, the fields of heterogeneous and homogeneous states of fluids for the H_2O–CO_2 and H_2O–CO_2–NaCl systems are shown according to Diamond (2003). The CO_2 concentrations in the model H_2O–CO_2 system (9.9 mol.% CO_2 and 90.1 mol.% H_2O) and the NaCl concentrations in the model H_2O–CO_2–NaCl system even exceed the highest CO_2 and NaCl concentrations established in H_2O–CO_2–NaCl fluids at Sukhoi Log. A significant number of Sukhoi Log inclusions lie within the field of a homogenous state of the H_2O–CO_2–NaCl fluid (Fig. 22), suggesting that the observed heterogeneity did not result from phase separation but rather from the mixing of gaseous fluid and aqueous solution. Similar explanations as the simplest one are commonly presented in interpretating associations of fluid inclusion with high-density CO_2 (Fedorovich et al., 1991; Klein and Fuzikava, 2010). Alternative assumptions of carbonic inclusion overfilling or “local heterogenization” in the field of homogeneous fluid (Baker et al., 2010) are inconsistent with the physical mechanism of heterogenization that is controlled by conditions regardless of the volume of fluid.

7.4. Thermodynamic simulation of gas-liquid interaction

Interaction between gas and aqueous solution is the most effective in the case of forced gas barbotage through liquid (Prokofiev and Selector, 2014). Gas barbotage results in numerous gas bubbles and, hence, in an increase in the surface areas of the phases. This facilitates chemical reactions and heat transfer following by the rapid establishment of chemical equilibrium between gas and liquid. This process is termed barbotage in processing technologies, and it cannot be comprehensively enough simulated with any of the currently

available software because of the complexity of the process. When simulating barbotage, one has to take into account the kinetic effects of heterogeneous fluid interaction and enhanced interaction on phase boundaries. Our model considers one aspect of interaction: the whole barbotage process is described as a sequence of consecutive partial equilibria between the gas and the liquid. The initial components are aqueous fluid with dissolved ore components and pure gas fluid at given temperature and pressure. At the beginning of the process, the state of the system is homogenous, and the gas should be completely dissolved in the liquid until solution achieves saturation with gas and an individual gas phase exsolves.

As gas bubbles through and reaches equilibrium with aqueous fluid, a certain proportion of the gas dissolves in the solution, and water vapour starts partitioning into the gas phase to become a component of the gas mixture. In the course of this process, the amount of water in the liquid systematically decreases as more gas percolates through the liquid. This process has the following geochemical implications:

(1) A decrease in the amount of liquid H_2O results to an increase in the concentrations of non-volatile ligands in the aqueous solution and, hence, an increase in the solubility of ore metals;

(2) At the same time, a decrease in the amount of liquid water results in a decrease in the absolute amount of the dissolved ore components in the fluid as a whole;

(3) Separation of water vapour and related volatile compounds (such as, H_2S and HCl) results in a loss of ligands and a corresponding decrease in the metal solubilities.

We developed a thermodynamic model of the 13-component Al–Au–C–Ca–Cl–Fe–H–K–Mg–Na–O–S–Si system that included 96 mineral phases, gaseous solution and aqueous solution of 98 dissolved components to quantitatively evaluate the chemical effects of gas-water mixing. The calculations were carried out with the use of HCh-4.5 software (Shvarov, 2008), which was designed to compute equilibria in multi-component systems. The software employed the extended DPRONS98 thermodynamic database (Shock et al., 1997; Sverjensky et al., 1997; Bastrakov et al., 2004). The behaviour of Au-bearing species in hydrothermal fluid was described according to the summaries of the thermodynamic data (Akinfiev and Zotov, 2001, 2010). The activity coefficients of species in solution were calculated by the Debye–Hückel equation in its second approximation (Helgeson et al., 1981). The initial gaseous solution was taken as non-ideal mixture of H_2O–CO_2–CH_4–H_2S–SO_2 gases. The calculation of non-ideality of gas phase was done by the methods installed in the HCh package (Shvarov, 2008) according to the Peng-Robinson formal approach (Stryjek and Vera,

1986) and using the “standard" model (Poling et al., 2001) with correction factors for inter-particle interaction $k_{ij} = 0$.

The aim of the simulations was to investigate the behaviour of gold initially dissolved in hydrothermal fluid as well as disseminated in the host rocks at a gradual increase in the amount of pure CO_2 gas percolating through the system. The calculation was done in the chemical system of mudstone similar to the average Khomolkho shale in composition. The fluid/rock ratio was assumed to be constant and equal to 1. The temperature and pressure were assumed to be constant: 350 °C and 50 MPa. The initial salinity of the aqueous solution was taken up to be as the average salinity of fluid inclusions in quartz from Sukhoi Log. The initial gold content was presumed to be as the Au content at saturation with native Au at the given *P*, *T* and fluid composition in equilibrium with the host shale, and was estimated at 2.82×10^{-7} mol/kg H_2O. The resulting solution is acidic with pH 4.3 and Au monohydrosulphide AuHS(aq) as the dominant solute Au species.

The proportion of precipitated gold (that is percent of the initial gold content in fluid) depending on the amount of CO_2 gas (mol/kg H_2O) in equilibrium with the host shale at 350 °C and 50 MPa is shown in Fig. 26. It can be seen that at the low CO_2 influx (less than 2.75 mol/kg H_2O), gas completely dissolves and the system remains homogenous. The negative value of precipitated gold (Fig. 26) stands for the dissolution of gold disseminated in the host rocks. An increase in the gold solubility is related to increasing acidity of the solution due to dissolution of CO_2. The turning point on the plot corresponds to the onset of separation of the gas phase. The main reason for the further decrease in the solubility and gold precipitation is the decrease in the amount of dense liquid fluid because of its outflux in the co-existing gas-vapour phase. Therefore, at the initial amount n_{CO_2} = 10 mol percolating through the initial aqueous solution n_{H_2O} = 1 kg, the total H_2O amount of water lost to the gas phase reaches 22 mol, whereas the total molecular gold content in the dense fluid changes insignificantly. The absolute amount of precipitated gold is not high because of the initially low gold solubility in fluid, although this mechanism is capable to recover 35–45% gold dissolved in the solution. The larger fluid amount passes through the system, the higher amount of gold precipitates.

8. Discussion

8.1. Timing of metamorphism and mineralisation

Gold deposits in the Lena Province occur at different stratigraphic levels throughout the terrigenous sequence, which is up to 15 km thick and was formed discontinuously in a time

span of more than 1 Ga in the Proterozoic. The rocks vary from conglomerate to fine-grained carbonate-bearing black shale and hydrolisates and reflect changes in the outlines of the huge Precambrian shallow marine basin. The synthesis of available dates testifies to Ediacaran rather than Cryogenian age of the Nygri and Bodaibo groups, whose deposition had terminated by the early Cambrian. Therefore, the U–Pb isotope age interval from 630 and 570 Ma obtained by dating porphyroblastic monazite from Khomolkho and Imnyakh black shale (Meffre et al., 2008; Yudovskaya et al., 2011) (Fig. 25) should be interpreted as the age of prograde catagenetic transformation of Nygri and Bodaibo Group sediments (Fig. 27)..

It is a great temptation to make a link between the second Great Oxidation event (Campbell and Squire, 2010) or the Marinoan Snowball event (Chumakov et al., 2011) (Fig. 2) and the higher productivity of contemporaneous sedimentary formations in terms of organic matter and some metals. However, our data show that the geochemical specialisation of carbonaceous sediments was relatively uniform through the Proterozoic stratigraphy, the compositions of ore hosted in the different formations are similar with a variable proportion of pyrrhotite and pyrite controlled by *PT* conditions of metamorphism, as well as the peak of organic carbon accumulation does not coincide with the larger numbers of ore deposits.

The timing of the high-temperature mineralisation is restricted to the age interval of 460–440 Ma (Fig. 27), as follows from the whole-rock Rb-Sr isotope isochron age (Laverov et al., 2007), hydrothermal monazite dates (Yudovskaya et al., 2011) and Re–Os isotope age of sulphides (Yakubchuk et al., 2014). Products of early Paleozoic granitoid magmatism of this age (Mama-Oron Complex) seems to be spread more widely in the region than it was thought earlier (Gerasimov et al., 2007), and the hidden Ugakhan pluton beneath the Sukhoi Log orefield could probably be assigned to this epoch. Orogenic metamorphism closely predated or was synchronous with the emplacement of the early Paleozoic granitic domes and formation of related zonal metamorphic aureoles (Fig. 27). The late Paleozoic tectono-magmatic reactivation, which was probably linked to the peripheral influence of the Angara-Vitim super-plume (Yarmolyuk et al., 2006; Tsygankov et al., 2007), resulted in post-ore veins with both local enrichment and depletion in gold.

8.2. Gold scavenging and deposition

Geochemical data show that carbonaceous metasediments at Sukhoi Log, Chertovo Koryto and Vysochaishee are not enriched in any metals other than gold, arsenic and, to a certain degree, lead above the common abundance levels in black shale. This conclusion is in agreement with the interpretation and data by Kucherenko et al. (2008) on the Chertovo Koryto surrounding wallrocks that show clarke abundances of all elements outside the ore

zone. These authors argue that the local elevated gold abundances in wallrocks outside the orefield are resulted from superimposed fluid circulation rather than primary diagenetic enrichment. The gold and arsenic anomalies at Chertovo Koryto and the outlines of the gold orebody and the sulphide-rich zone at Sukhoi Log overlap only partly, and this creates the impression that the gold mineralisation is superimposed onto substrate enriched in sulphides (arsenopyrite and pyrite, respectively). The same morphological types of sulphides (arsenopyrite and pyrite) do not associate with gold grade outside the ore-controlling structures, whereas different morphotypes are variably gold-bearing within the limit of the ore zone. The spatial separation of the gold and sulphide anomalies (Fig. 10) explains the absence of apparent positive correlation between the arsenic and gold contents (Fig. 11), as well as between the sulphide content and the gold grade (Distler et al., 1996, 2004 and this study).

The high metal content in some sulphides of the Sukhoi Log (Large et al., 2007) and Kopylovskoe and Kavkaz (Palenova et al. 2015) deposits support an idea of the primary diagenetic enrichment of black shales. The aforementioned authors favour the predominant role of the sedimentary-exhalative processes in gold accumulation, which was followed by a period of gold remobilization during metamorphism and deformation and resulted in that the Lena gold deposits are classed with sedimentary ones. It is seen from comparison with the well-known example of the Niutitang mineralisation that the geochemical signature of mineralisation in the Lena Province does not match geochemistry of syndiagenetic exhalation of auriferous fluids on the seafloor (Fig. 8); neither is exhalative origin consistent with the high-temperature character of fluids and the time constraints. In addition, it is widely approved (i.e. Ivanov, 2014) that the oldest sulphides at different deposits are either pyrite or pyrrhotite depending on the metamorphic grades. Metamorphic rocks of higher grades carry Au-free pyrrhotite (such as in Chertovo Koryto) that changes into pyrrhotite-pyrite association (as in the Sukhoi Log) and, finally, to pyrite alone in lower grade metamorphic rocks. The sulfur isotope composition of the metamorphic pyrrhotite is the same as that of pyrite (Kryazhev et al., 2009), and the pyrrhotite is thought to be formed in relation to metamorphic sulphidation. The pyrrhotite contains almost no gold (Large et al., 2007; Gavrilov and Kryazhev, 2008), that puts forth the problem of the source of gold for pyrite-poor deposits.

We did not find any criteria to subdivide pyrite of the hydrothermal stage into consequent generations, as was done by Large et al. (2007), while our conclusions are in agreement with the earlier observations by Distler et al. (1996, 2004), Gavrilov and Kryazhev (2008) and

Rusinov et al. (2008), who considered various morphological varieties of ore pyrite as growing coevally and continuously within the long-lasting hydrothermal process. Our viewpoint is partly supported by data on gold and arsenic abundances provided by Large et al. (2007). These authors reported widely overlapping ranges of gold and arsenic contents in subsequent pyrite types from earlier to later ones (ppm): 0.44–12 Au, 180–14000 As in pyrite 1; 0.02–13 Au, 2–18550 As in pyrite 2; 0.05–82 Au, 63–17743 As in pyrite 3; 0.02–1.3 Au, 400–5560 As in pyrite 4 and 0.01–0.22 Au, 980–10500 As in pyrite 5. Pyrite 3 (not pyrite 1) contains the highest gold, whereas the variable arsenic content does not allow distinguishing the types. Furthermore, the LA-ICP-MS data are not in good agreement with microprobe data of Gavrilov and Kryazhev (2008), who found broadly the same, although wider, range of arsenic contents in ore pyrite (0.01–2.5 wt.% As) but very low As contents in diagenetic fine-grained pyrite that corresponds to pyrite 1 as defined by Large et al. (2007).

It should be noted that the abovementioned studies of trace elements in sulphides were carried out using sulphides from mineralised zones and their vicinities. Large et al. (2007) showed that the fine-grained, sooty and concretionary sulphides are enriched in the whole spectrum of metals. However, the fact of the selective enrichment of the sulphide morphotype does not elucidate the time or process of enrichment whether it was diagenetic or superimposed. It is known from the experimental studies on hydrothermal sulphide synthesis and from natural observations that the defect-rich crystal lattice of both pyrite and arsenopyrite is capable of accommodating much more gold and other traces than the defect-free perfect lattice is. Simon et al. (1999) suggested that arsenic was preferrably incorporated into irregularly distributed marcasite- and arsenopyrite-like layers in the pyrite structure, which were also favourable for accommodating gold. Other studies suggested that chemosorption of Au–S and Au-As complexes at As-rich, Fe-deficient sites (Fleet and Mumin, 1997), or adsorption of $AuHS^{o}$ complexes (Widler and Seward, 2002), or deposition of Au nanoparticles on As-pyrite and arsenopyrite surfaces (Mikhlin et al., 2011) may be the major factors. The formation of a chemically-bound form of Au is proven to be valid at low- to moderate-temperature pyrite growth (Kozerenko et al., 2001; Laptev et al., 2006). Gold enrichment of porous, sooty, inclusion-rich or As-rich pyrite can be explained by its high capability to incorporate gold and other elements from infiltrating gold-bearing fluid, whereas higher-temperature more perfect crystals and domains would not be able to accommodate invisible gold and thus would facilitate free gold deposition.

Arsenopyrite plays the same role as pyrite in gold concentrating. Simultaneous gold and pyrite (±arsenopyrite) deposition can be enhanced by fluid cooling because of decomposition

of Au hydrosulphide complexes due to strong H_2S consumption by sulphides. As shown by our simulation, mixing of water-dominant and CO_2-dominant fluids favours gold scavenging and precipitation due to decreasing amount of aqueous fluid via its removal into co-existing vapour.

Late-stage deposition of native gold veins in cracks and intergranular space of pyrite and arsenopyrite can be facilitated by a change in the redox conditions at minor dissolution of arsenopyrite (Pokrovski et al., 2002).

8.3. Siderophile mineralisation

Our data on the routine metal abundances (except for gold and arsenic) in whole rocks suggest that the enrichment of sulphides in certain metals does not affect the geochemical background of black shales. At the same time, the common occurrence of accessory Ni–Co mineralisation is typical of Sukhoi Log ore and is now confirmed to be widespread at other deposits. Therefore, although the abundances of siderophile elements at gold deposits are not high, they give rise to certain Ni–Co mineral assemblages, which include pentlandite (mostly as exsolution in pyrrhotite), millerite, heazlewoodite, violarite, niccolite, cobaltite-gersdorffite, maucherite, rammelsbergite, ullmanite etc. (Distler et al., 2004; Vagina, 2012; Palenova et al., 2015).

The average Cr and Ni abundances in black shales worldwide are 81±5 ppm and 67±4 ppm respectively, according to Yudovich and Ketris (1988). Mikhailovsk metacarbonate rocks (metamarl) are enriched in these metals up to almost 500 ppm Cr and 200 ppm Ni (Table 1) that is 3–10 times higher than their abundance in neighbouring black shale and sandstone. The average Ni content in terrigenous rocks is around 50 ppm, which is lower than the black shale clarke abundance. The average Cr contents in Khomolkho sediments are 125 ppm at Sukhoi Log and 181 ppm in the carbonate-richer strata at Vysochaishee (Table 2, Fig. 10). The possible reason for this enrichment of carbonate-bearing layers in siderophile elements accompanied by elevated Ti is thought to be due to the tuffaceous mafic input during the period of ceasing sedimentation. The coupled accumulation of Cr and Ni (±Co) is an uncommon feature of mineralisation in black shales. Early Cambrian black shales in southern China (Mao et al., 2002; Jiang et al., 2006) and Devonian black shales in the Yukon (Hulbert et al., 1992) contain low chromium and very high nickel concentrations (more than 1 wt.%) in associations with high Zn, Mo and PGE contents, which are attributed either to coeval accumulation with organic matter or to exhalative-hydrothermal input. Significant nickel concentrations, up to an economic grade, is regularly present in U–Ni–Co–Cu deposits (such as Shinkolobwe) and in the newly discovered Enterprise nickel deposit in carbonate-

sedimentary (apo-black shale?) sequences of the Katangan Supergroup in Africa (Capistrant et al., 2015), in which it associates with minor Cu, Co, Au, Mo and PGE and forms diverse discrete sulphide minerals during the latest hydrothermal stages. The presence of various platinum minerals at Sukhoi Log (Distler et al., 2004) is suggestive of a similar process of the initial accumulation of siderophile elements.

8.4. Role of gaseous fluid

The model of metamorphic devolatilisation recently elaborated by Phillips and Powell (2010) to explain the origin of gold-only deposits suggests that aqueous-carbonic low-salinity fluid can efficiently dissolve gold in the form of a gold-sulphide complex, with subsequent precipitation, but is not effective to dissolve sufficient amounts of base metals (although transporting some other elements, including As, Sb, B, Se, Te, Hg, Bi, Mo and W). These authors emphasize the self-sufficient locally-penetrating character of devolatalisation initiated by the greenschist-to-amphibolite facies transition, in contrast to the flow-through-model that requires the external source for incoming fluid. Their model provides a good basis for the metamorphogenic-hydrothermal concept, which was first suggested for the Lena region by Buryak (1982), although Phillips and Powell (2010) do not assume any significant preliminary enrichment of the host rocks in gold. Taking into account the supporting isotope evidence on the low fluid/rock ratio (Dubinina et al., 2014) and the significant exchange between reduced and oxidised carbon (Kryazhev et al., 2009), the metamorphic devolatalisation is an undeniably important process responsible for CO_2-rich fluid generation at Sukhoi Log. However, some arguments show that this type of fluid was not the only one operating, and it did not provide gold endowment albeit promoting gold transport and deposition:

(1) Temperature and pressure of gold-bearing fluids exceed those for metamorphic facies conditions typical of Sukhoi Log and Chertovo Koryto rocks that require heat supply from an external (deep) source;

(2) Fluid inclusions indicate mixing of two different high-temperature fluids;

(3) Solutions in the fluid inclusions have higher gold and arsenic enrichment factors than in the surrounding rocks, indicating supply of these elements from an external source rather than scavenging from the host rocks;

(4) Metamorphic carbonation is a much more widely spread process over the every carbonate-bearing strata of the Proterozoic sequence in the Province, whereas hydrothermal assemblages are constrained to local ore-controlling structures;

(5) Mineralisation at Chertovo Koryto (as well as some other smaller deposits) occurs in the zone of retrograde metamorphism, in which devolatalisation (related to the earlier prograde metamorphic conversion) and mineralisation events were separated in time;

(6) Our simulation confirms that carbonic fluid can effectively facilitate gold deposition at mixing with aqueous fluid, given that the latter carries some gold in solution.

8.5. Genetic model

In the absence of reliable age estimates, it is not possible to correlate unambiguously the timing of ore-forming processes at Chertovo Koryto and in the central Bodaibo region. The occurrence of older regional-contact metamorphism simultaneous with the emplacement of Paleoproterozoic granites is reset by superimposed early Paleozoic retrograde metamorphism and late Paleozoic reactivation. We envisage that superposition of two (or multiple) metamorphic events is the main reason for the difference in the composition of ore-bearing fluids at Sukhoi Log and Chertovo Koryto. The ancient prograde metamorphism provided the preceding devolatalisation of Mikhalovsk sediments and the removal of much carbonic fluids, so that the retrograde metamorphic fluids had an essentially aqueous composition. The occurrence of wollastonite in the metamarl provides circumstantial evidence of a low CO_2 activity, emphasising that the mineral assemblages of the argillaceous dolostone reflect the metamorphic conditions more reliably than co-existing quartz-rich rocks do. Vagina (2012) reported five stages of mineralisation at Chertovo Koryto, with the consequent generations of quartz and carbonate deposited during every stage. Data of these authors on fluid inclusions revealed a continuous decrease in the temperature from 420 to 80 ^{o}C and in pressure from 300 to 40 MPa in the course of ore formation. The inconsistency between the results may be explained by the fact that our study was done exclusively on quartz from the ore zone (Fig. 12). Our fluid inclusion data indicate high-temperature (up to 450 ^{o}C) low-pressure (440–240 bars) conditions for gold precipitation, with no carbonic fluid involved at Chertovo Koryto. It is difficult to say whether the involvement of carbonic fluid was a crucial factor that determines the different scale of mineralisation at Chertovo Koryto and Sukhoi Log or the gold endowment was primarily controlled by the sizes of the favourable structural traps.

According to earlier Russian classifications, the Sukhoi Log deposit was considered a polygenetic metamorphic–plutonogenic deposit related to tectonomagmatic reactivation (Rundqvist, 1997; Safonov, 2006). It was proved that the Lena gold deposits belong to the mesothermal type in terms of the *PT* conditions (Sher, 1972; Laverov et al., 2007), i.e., epigenetic mineralisation hosted in deformed metamorphosed terrains and produced by the mixed metamorphic and magmatic fluids at relatively high temperature (200–400 ^{o}C) and

pressure (up to 3 kbar) (Bortnikov et al., 2007). At the same time, some authors regarded the deposit as orogenic (Sher, 1972; Groves et al., 1998; Goldfarb et al., 2005), based first of all on a generalised interpretation of regional geological setting rather than geochronological constraints (which were then not available). Typical orogenic deposits, as defined by Groves (1998), were formed simultaneously with or late in the course of orogenesis, during the main phase of crustal folding in compressional or transpressional environments. Orogenic gold deposits were typically generated in terranes that had been metamorphosed to the greenschist to amphibolite facies, with consequent generation of anatectic melts and flows of so-called orogenic (mainly aqueous-carbonic) fluids that had been broadly in equilibrium with the host rocks.

An environment of inverted pericontinental rifts was suggested by Hronsky et al. (2012) as the most important setting of orogenic deposits within accretionary orogens, and this closely matches the late Precambrian tectonic environment of the Baikal-Patom megazone. We believe that the main factors that predetermined the giant ore reserves in the province were as follows: (1) the high thickness of the primitive sedimentary sequences in the rift-related extensional basins and (2) a deep-seated lithosphere-scale heat source initiating the subsequent dynamothermal metamorphism with related crustal melting and high-temperature fluid flows. The mineralisation was settled in compressional structures regardless the original geochemical specialisation of the host rocks, while favouring distal facies remote from the centres of anatextic melt emplacement and high-grade metamorphism (Fig. 27). The timing of gold introduction was generally synchronous with or slightly postponed the peak of the dynamothermal metamorphism and compressional deformations, and its age correlates well with the ages of the early Paleozoic metamorphic events documented in other fragments of the southern surroundings of the Siberian craton (Mitrofanov, 2006; Rytsk et al., 2011; Yakubchuk et al., 2014).

9. Conclusions

The carbonate-black shale-terrigenous sequences of the Lena Province are characterised by similar geochemical signatures that reflect common source areas and inherited sedimentation regime over a time span from Mesoproterozoic through late Neoproterozoic. The gold deposits occur at different stratigraphic levels, but their mineralisation is invariably structurally controlled by the compressional deformations. Only gold and arsenic contents are highly anomalous in the mineralised sequences, and this narrow geochemical specialization does not fit in either the exhalative or the diagenetic model of

metal accumulation, in which other metals are expected to be also enriched by the same process.

Although the ultimate source of gold in the giant province remains unclear, it is plausible that gold was transported by high-temperature aqueous fluids, whereas its effective scavenging and precipitation were facilitated by the involvement of dense carbon-dominant gases. The process had to be initiated at a lithospheric scale to be able to maintain the scale of gold endowment in the province as a whole.

Acknowledgements

We thank Polyus Gold and personally the geologists A.V. Verkhozin, V.G. Martynenko, V.F. Benedyuk, and E.V. Evlanova of the Lena Gold Mining Company for assistance in the fieldwork and comments on the manuscript. We are grateful to M.V. Kuznetsova, S.F. Sluzhenikin, S.P. Korikovsky, A.V. Mokhov, I.B. Ignat'eva for the assistance and fruitful discussion during the study at IGEM RAS. E. Kurdyukov's help with English correction is appreciated. The paper was significantly improved due to constructive suggestions and revisions by Olga Plotinskaya and an anonymous reviewer. Authors thank M. Santosh and D.I. Groves for the invitation to submit the contribution to the special issue of the Geoscience Frontiers. This study is partly supported by the Russian Scientific Foundation (grant 14-17-00693).

References

Akinfiev, N.N., Zotov, A.V., 2001. Thermodynamic description of chloride, hydrosulphide, and hydroxide complexes of Ag(I), Cu(I), and Au(I) at temperatures of 25–500 ^{o}C and pressures of 1–2000 bar. Geochemistry International 39, 990–1006.

Akinfiev, N.N., Zotov, A.V., 2010. Thermodynamic description of aqueous species in the system Cu–Ag–Au–S–O–H at temperatures of 0–600 ^{o}C and pressures of 1–3000 bar. Geochemistry International 48, 714–720.

Baker, T., Bertelli, M., Blenkinsop, T., Creverley, J.S., Nugus, M., Gillen, D., 2010. P-T-X conditions of fluids in the Sunrise Dam gold deposit, Western Australia, and implications for the interplay between deformation and fluids. Economic Geology 105, 873–894.

Bastrakov, E., Shvarov, Y., Girvan, S., Creverley, J., McPhail, D, Wybom, I., 2004. FreeGs: web-enabled thermodynamic database for modeling of geochemical processes. Dynamic Earth: Past, present and future: Abstracts of the 17th Australian Geology Convention. Hobart (Tasmania), 52.

Beukes, N.J., Gutzmer, J., 2008. Origin and paleoenvironmental significance of major iron formations at the Archean-Paleoproterozoic boundary. Society of Economic Geologists SEG Reviews 15, 5–47.

Bodnar, R.J., Vityk, M.O., 1994. Interpretation of microthermometric data for H_2O–NaCl fluid inclusions. In: De Vivo, B., Frezzotti, M.L. (Eds.), Fluid inclusions in minerals: methods and applications. Pontignano-Siena, Lissabon, pp. 117– 130.

Bortnikov, N.S., Gamyanin, G.N., Vikent'eva, O.V., 2007. Fluid composition and origin in the hydrothermal system of the Nezhdaninsky gold deposit, Sakha (Yakutia). Geology of Ore Deposits 49, 97–128.

Brown, P., 1989. FLINCOR: a computer program for the reduction and investigation of fluid inclusion data. American Mineralogist 74, 1390–1393.

Brown, P.E., Lamb, W.M., 1989. P–V–T properties of fluids in the system H_2O-CO_2-NaCl: new graphical presentations and implications for fluid inclusion studies. Geochimica et Cosmochimica Acta 53, 1209-1222.

Bukharov, A.A., Khalilov, V.A., Strakhova, T.M., Chernikov, V.V., 1992. Geology of the Baikal–Patom Highland from new data on U–Pb dating of accessory zircon. Geology and Geophysics 33, 29–39.

Buryak, V.A., 1982. Metamorphism and Ore Formation. Nauka, Moscow, 256 pp (in Russian).

Buryak, V.A., Khmelevskaya, N.M., 1997. Sukhoi Log - one of the world's largest gold deposit: genesis, localization of ore, and forecasting criteria. Dal'nauka, Vladivostok, 156 pp (in Russian).

Campbell J.H., Squire, R.J., 2010. The mountains that triggered the Late Neoproterozoic increase in oxygen: The Second Great Oxidation Event. Geochimica et Cosmochimica Acta 74, 4187-4206.

Capistrant, P. L., Hitzman, M. W., Wood, D., Kelly, N. M., Williams, G., Zimba, M., Kuiper, Y., Jack, D., Stein, H., 2015. Geology of the Enterprise hydrothermal nickel deposit, North-Western Province, Zambia. Economic Geology 110, 9-38.

Chernyshev, I.V., Chugaev, A.V., Safonov, Yu.G., 2009. Lead isotopic composition from data of high-precession MC-ICP-MS and sources of matter in the Large-Scale Sukhoi Log noble metal deposit, Russia. Geology of Ore Deposits 51, 496–504.

Chugaev, A.V., Chernyshev, I.V., Safonov, Yu.G., Saroyan, M.R., 2010. Lead isotope characteristics of sulphides from large gold deposits of the Baikal-Patom Highland (Russia) from high-precision MC-ICP-MS Pb isotope analysis. Doklady Earth Sciences, 434, 677–680.

Chugaev, A.V., Plotinskaya, O.Yu., Chernyshev, I.V., Kotov A.A., 2014. Lead isotope heterogeneity in sulphides from different assemblages at the Verninskoe gold deposit (Baikal–Patom Highland, Russia). Doklady Earth Sciences 457, 887–892.

Chumakov, N.M., Pokrovsky, B.G., Melezhik, V.A., 2011. Glaciogenic Bol'shoy Patom Formation, Lena River, Middle Siberia. In: Arnaud, E., Halverson, G.P., Shields- Zhou, G.A. (Eds.), The geologic record of Neoproterozoic glaciations. Memoirs of the Geological Society of London 36, 309-316.

Claypool, G.M., Kaplan, J.R., 1974. The origin and distribution of methane in marine sediments. In: Kaplan, I.R. (Ed.), Natural gases in marine sediments. New York, Plenum 3, pp. 99-139.

Collins, P.L., 1979. Gas hydrates in CO_2-bearing fluid inclusions and the use of freezing data for estimation of salinity. Economic Geology 74, 1435-1444.

Coveney, R.M., Murowchick, Jr., Grauch, J.B., Glascock, R.I., Denison, M.D., 1992. Gold and platinum in shales with evidence against extraterrestrial sources of metals. Chemical Geology 99, 101-114.

Darling, R.S., 1991. An extended equation to calculate NaCl contents from final clathrate melting temperatures in H_2O-CO_2-NaCl fluid inclusions: Implications for P-T-isochore location. Geochimica et Cosmochimica Acta 55, 3869-3871.

Diamond, L.W., 2003. Introduction to gas-bearing, aqueous fluid inclusions. Fluid inclusions analysis and interpretation. Short Course Series of Mineralogical Association of Canada 32, pp. 101–158.

Distler, V.V., Yudovskaya, M.A., 2005. Polymetallic PGE–Au mineralization of the Sukhoi Log deposit. In: Mungall J. (Ed.), Exploration for deposits of platinum group elements. Short Course Series of Mineralogical Association of Canada 35, 457–485.

Distler, V.V., Mitrofanov, G.L., Nemerov, V.K., Kovalenker, V.A., Mokhov, A.V., Semeikina, L.K., Yudovskaya, M.A., 1996. Modes of occurrence of the platinum group elements and their origin in the Sukhoi Log Gold Deposit (Russia). Geology of Ore Deposits 38, 6, 413–428.

Distler, V.V., Yudovskaya, M.A., Mitrofanov, G.L., Prokof'ev, V.V., Lishnevsky, E.N., 2004. Geology, composition, and genesis of the Sukhoi Log noble metals deposit, Russia. Ore Geology Reviews 24, 7–44.

Dubinina, E. O., Chugaev, A. V., Ikonnikova, T. A., Avdeenko, A. S., Yakushev, A. I., 2014. Sources and fluid regime of quartz–carbonate veins at the Sukhoi Log gold deposit, Baikal–Patom Highland. Petrology 22, 329–358.

Fedorovich, J., Stauffer, M., Kerrich, R., 1991. Structural setting and fluid characteristics of the Proterozoic Tartan Lake Gold Deposit, Trans-Hudson Orogen, Northern Manitoba. Economic Geology 86, 1434-1467.

Fleet, M.E., Mumin, A.H., 1997. Gold-bearing arsenian pyrite and marcasite and arsenopyrite from Carlin Trend gold deposits and laboratory synthesis. American Mineralogist 82, 182–193.

Gao, S., Luo, T.C., Zhang, B.R., Zhang, H.F., Han, Y.W., Zhao, Z.D., Hu, Y.K., 1998. Chemical composition of the continental crust as revealed by studies in East China. Geochimica et Cosmochimica Acta 62, 1959–1975.

Gavrilov, A.M., Kryazhev, S.G., 2008. Mineralogy and geochemistry of ore at the Sukhoi Log deposit. Razvedka and Okhrana Nedr 8, 3–16 (in Russian).

Gerasimov, N.S., Grebenshikova, V.I., Noskov, D.A., Kalmychkova, T.N., Serebrennikov, L.M., 2007. On Early Paleozoic age of the Angara-Vitim batholith. Abstracts of All-Russian Scientific Meeting "Geodynamic evolution of lithosphere of the Central-Asian mobile belt (from ocean to continent)". Institute of the Earth's crust, Irkutsk 1, 49-51 (in Russian).

Goldfarb, R.J., Baker, T., Dube, B., Groves, D.I., Hart, C.J.R., Gosselin, P., 2005. Distribution, character, and genesis of gold deposits in metamorphic terranes. Economic Geology 100, 407–450.

Groves, D.I., Goldfarb, R.J., Gebre-Mariam, M., Hagemann, S.G., Robert, F., 1998. Orogenic gold deposits: A proposed classification in the context of their crustal distribution and relationship to other gold deposit types. Ore Geology Reviews 13, 7–27.

Helgeson, H.C., Kirkham, D.H., Flowers, G.C., 1981. Theoretical prediction of the thermodynamic behavior of aqueous electrolytes at high pressures and temperatures: IV. Calculation of activity coefficients, osmotic coefficients, and apparent molal and standard and relative partial molal properties to 600^{o}C and 5 kb. American Journal of Science 291, 1249–1516.

Hofmann, A.W., 1988. Chemical differentiation of the Earth: the relationship between mantle, continental crust, and oceanic crust. Earth and Planetary Science Letters 90, 297-314.

Hronsky, J.M.A., Groves, D.I., Loucks, R.R., Begg, G.C., 2012. A unified model for gold mineralisation in accretionary orogens and implications for regional scale targeting methods. Mineralium Deposita 47, 339-358.

Hulbert, L. J., Gregoire, C.D., Paktunc, D., Carne, R. C. 1992. Sedimentary nickel, zinc and platinum-group-element mineralisation in Devonian black shales at the Nick Property, Yukon, Canada: a new deposit type. Canadian Institute of Mining, Metallurgy and Petroleum, Exploration and Mining Geology 1, 39 - 62.

Ivanov, A.I., 2014. Gold of Baikal-Patom (geology, mineralisation, perspectives). TSNIGRI, Moscow, 215 pp (in Russian).

Ivanov, A.I., Lifshits, V.I., Perevalov, T.M., 1995. Precambrian of the Patom Highlands. Nedra, Moscow, 262 pp (in Russian).

Jiang, S.Y., Chen, Y.Q., Ling, H.F., Yang, J.H., Feng, H.Z., Ni, P., 2006. Trace- and rare-earth element geochemistry and Pb–Pb dating of black shales and intercalated Ni–Mo–PGE–Au sulphide ores in Lower Cambrian strata, Yangtze Platform, South China. Mineralium Deposita 41, 453–467.

Kazakevich, Yu.P., Sher, S.D., Zdanova, T.P., Storozhenko, A.A., Kondratenko, A.K., Nikolaeva, L.A., Aminev, V.B., 1971. Lena Gold-bearing Region. TSNIGRI, Moscow, Nedra, V. 2, 161 pp (in Russian).

Kerkhof, A.M., 1988. The system CO_2–CH_4–N_2 in Fluid Inclusions: Theoretical Modeling and Geological Applications. Free University Press, Amsterdam, 209 pp..

Klein, E.L., Fuzikawa, K., 2010. Origin of the CO_2-only fluid inclusions in the Palaeoproterozoic Carara vein-quartz gold deposit, Ipitinga auriferous district, SE-Guiana Shield, Brazil: Implications for orogenic gold mineralisation. Ore Geology Reviews 37, 31–40.

Kozerenko, S.V., Wagner, F.E., Friedl, J., Fadeev, V.V., 2001 Gold in pyrite formation process: 3. Mossbauer study of synthetic gold-bearing iron sulphides. Geochemistry International 39, S167-S172.

Kröner, A., Kovach, V.E. Belousova, E., Hegner, E., Armstrong, R., Dolgopolova, A., Seltmann, R., Alexeiev, D.V., Hoffmann, J.E., Wong, J., Sun, M., Cai, K., Wang, T., Tong, Y., Wilde, S.A., Degtyarev, K.E., Rytsk, E., 2014. Reassessment of continental growth during the accretionary history of the Central Asian orogenic Belt. Gondwana Research 25, 103–125.

Kryazhev, S.G., Prokofiev, V.Y., Vasyuta, Y.V., 2006. Application of ICPMS method to analysis of ore-forming fluid composition. Vestnik MGU 30–36 (in Russian).

Kryazhev, S.G., Ustinov, V.I., Grinenko, V.A., 2009. Fluid regime at the Sukhoi Log gold deposit: isotopic evidence. Geochemistry International 47, 1041–1049.

Kucherenko, I.V., Gavrilov, R.Yu., Martunenko, V.G., Verchozin, A.V., 2008. Petrological-geochemical features of wallrocks metasomatic aureole of the Chertovo Koryto gold deposit (Patom Highland). Proceedings of Tomsky Technical University 312(1), 11–20 (in Russian).

Kucherenko, I.V., Gavrilov, R.Yu., Martunenko, V.G., Verchozin, A.V., 2011. Petrological-geochemical features of wallrock metasomatizm in the Sukhoi Log gold deposit (Lena region). Part 2. Petrology of wallrock metasomatizm. Proceedings of Tomsky Technical University 320, 28–37 (in Russian).

Kuznetsov, A.B., Ovchinnikova, G.V., Gorokhov, I.M., Letnikova, E.F., Kaurova, O.K., and Konstantinova, G.V., 2013, Age constraints on the Neoproterozoic Baikal Group from combined Sr isotopes and

Pb-Pb dating of carbonates from the Baikal type section, southwestern Siberia: Journal of Asian Earth Sciences 62, 51–66.

Landa, E.A., Makar'ev, L.B., Bylinskaya, L.V., 2006. Isotope geochemistry and geochronology of the Khodokan gold deposit, East Siberia. Regional Geology and Metallogeny 28, 144–152 (in Russian).

Laptev, Yu V., Rozov, K B., 2006. Interaction of gold with sulphide surface as a factor of its concentration in hydrothermal ore formation. Doklady Earth Sciences 411, 1229-1232.

Large, R.R., Maslennikov, V.V., Robert, F., Danyushevsky, L., Chang, Z., 2007. Multi-stage sedimentary and metamorphic origin of pyrite and gold in the giant Sukhoi Log deposit, Lena Goldfield, Russia. Economic Geology 102, 1233–1267.

Laverov, N.P., Chernyshev, I.V., Chugaev, A.V., Bairova, E.D., Golzman, Yu.V., Distler, V.V., Yudovskaya, M.A., 2007. Formation stages of the large scale noble metal mineralisation in the Sukhoi Log deposit, East Siberia: results of isotope-geochronological study. Doklady Earth Science 415, 236–241.

Laverov, N.P., Prokof'ev, V.Yu., Distler, V.V., Yudovskaya, M.A., Spiridonov, A.M., Grebeshchikova, V.I., Matel, N.L., 2000. New data on conditions of ore deposition and composition of ore-forming fluids in the Sukhoi Log gold-platinum deposit. Doklady Earth Science 371, 357–361.

Lishnevsky, E.N., Distler, V.V., 2004. Deep structure of the earth's crust in the district of the Sukhoi Log gold-platinum deposit (Eastern Siberia, Russia) based on geological and geophysical data. Geology of Ore Deposits 46, 76–90.

Makar'ev, L.B., Chukhonin, A.P., 1992. Precambrian granitoids of the Nechera and Tonoda Uplifts of the Baikal fold region. Geology and Geophysics 9, 61-72 (in Russian).

Mao, J, Lehmann, B, Du, A, Zhang, G, Ma, D, Wang, Y, Zeng, M, Kerrich, R., 2002. Re-Os dating of polymetallic Ni-Mo-PGE-Au mineralisation in Lower Cambrian black shales of South China and its geologic significance. Economic Geology 97, 1051–1061.

Meffre, S., Large, R.R., Scott, R., Woodhead, J., Chang, Z., Gilbert, S.E., Danyushevsky, L.V., Maslennikov, V., Hergt, J.M., 2008. Age and pyrite Pb isotopic composition of the giant Sukhoi Log sediment-hosted gold deposit, Russia. Geochimica et Cosmochimica Acta 72, 2377–2391.

Migachev, I.F., Karpenko, I.A., Ivanov, A.I., 2008. The Sukhoi Log gold deposit: reappraisal and estimation of forecasing of ore field and district. Otechestvennaya Geologiya 2, 55–67 (in Russian).

Mikhlin, Y., Romanchenko, A., Likhatski, M., Karacharov, A., Erenburg, S., Trubina, S., 2011. Understanding the initial stages of precious metals precipitation: nanoscale metallic and sulphidic species of gold and silver on pyrite surfaces. Ore Geology Reviews 42, 47-54.

Mitrofanov, G.L., 2006. Tectonic basis of localization and formation of noble metal deposits in the southern framework of the Siberian Platform. Doctor of Science Dissertation of IGEM RAS, Moscow, 345 pp (in Russian).

Nemerov, V.K., 1989. Geochemical specialization of the late precambrian black shales of the Baikal-Patom Highlands. PhD dissertation of the Vinogradov Institute of Geochemistry RAS. Irkutsk, 144 pp (in Russian).

Neimark, L.A., Rytsk, E.Yu., Gorokhovsky, B.M., 1993a. Geochronology and isotope geochemistry of gold deposits in the Baikal Fold Region. In: Isotopic dating of endogenic rocks. Nauka, Moscow, pp. 124–146 (in Russian).

Neimark, L.A., Rytsk, E.Yu., Rizvanova, N.G., Gorokhovsky, B.M., 1993b. On polychronous genesis of Angara-Vitim batolith according to U-Pb data on zircon and sphene. Doklady Earth Science 333, 634-637.

Oleinikov, B.V., Tomshin, M.D., Kopylova, A.G., 1983. Mafic rocks of the Ura Uplift. In: Petrology and geochemistry of the late Precambrian intrusive mafic rocks at the Siberian Platform. Nauka, Novosibirsk, pp. 146–167 (in Russian).

Palenova, E.E., Belogub, E.V., Plotinskaya, O.Yu., Novoselov, K.A., Maslennikov, V.V., Kotlyarov, V.A., Blinov, I.A., Kuzmenko, A.A., Griboedova, I.G., 2015. Chemical evolution of pyrite at the Kopylovsk and Kavkaz black shale-hosted gold deposits, Bodaibo district, Russia: evidence from EPMA and LA-ICP-MS data. Geology of Ore Deposits 57, 64–84.

Palme, H., O'Neill, H.St.C., 2004. Cosmochemical estimates of mantle composition. In: Holland, H.D., Turrekian, K.K., (Eds.), Treatise on Geochemistry. Elsevier, Amsterdam, p. 1–38.

Pašava, J., 1993. Anoxic sediments – an important environment for PGE: An overview. Ore Geology Reviews 8, 425-445.

Phillips, G.N., Powell, R., 2010. Formation of gold deposits: a metamorphic devolatilization model. Journal Metamorphic Geology 28, 689–718.

Pokrovski, G. S., Kara, S., Roux, J. 2002. Stability and solubility of arsenopyrite, FeAsS, in crustal fluids. Geochimica et Cosmochimica Acta 66, 2361– 2378.

Poling, B.E., Prausnitz, J.M., O'Connell, J.P., 2001. The Properties of Gases and Liquids. Mc-Graw Hill, New York, pp. 1-802.

Prokofiev, V.Yu., Selector, S.L., 2014. Fluid inclusion evidence for barbotage and its role in gold deposition at the Darasun goldfield (eastern Transbaikalia, Russia). Central European Journal of Geosciences 6, 131-138.

Roedder, E., 1984. Fluid inclusions. In: Ribbe, P.H., (Ed.), Review in Mineralogy. Mineralogical Society of America 12, 644 pp.

Ronov, A.B., Migdisov, A.A., 1971. Geochemical history of the crystalline basement and the sedimentary cover of the Russian and North American Platforms. Sedimentology 16, 167-185 (in Russian).

Rundqvist, D.V., 1997. Time factor in the formation of hydrothermal deposits: periods, epochs, megastages, and stages of ore formation. Geology of Ore Deposits 39(1), 8–19 (in Russian).

Rundqvist, I.K., Bobrov, V.A., Smirnova, T.N, Cmirnov, M.Y., Danilova, M.Y., Ascheulov, A.A., 1992. Stages of formation of the Bodaibo Ore District. Geology of Ore Deposits 34, 3–15 (in Russian).

Rusinov, V.L., Rusinova, O.V., Kryazhev, S.G., Schegol'kov, Yu.V., Alusheva E.I., Borisovsky C.E., 2008. Wall-rock metasomatism of carbonaceous terrigenous rocks in the Lena gold district. Geology of Ore Deposits 50(1), 1–40.

Rytsk, E.Yu., Kovach, V.P., Yarmolyuk, V.V., Kovalenko, V.I., Bogomolov, E.S., Kotov, A.B., 2011. Isotopic structure and evolution of the continental crust in the East Transbaikalian segment of the Central Asian Fold belt. Geotectonics 45, 349–377.

Safonov, Yu.G., 2006. Geological–genetic types of gold and gold-bearing deposits. In: Large and Super-Large Ore Deposits. IGEM RAS, Moscow, 2, pp. 17–96 (in Russian).

Shau, Y.H., Yang, H.Yi, Peacor, D.R., l99I. On oriented titanite and rutile inclusions in sagenitic biotite. American Mineralogist 76, 1205-1217.

Sher, S.D., 1972. Metallogeny of gold. Nedra, Moscow, 256 pp. (in Russian).

Shock, E.L., Sassani, D.C., Willis, M., Sverjensky, D.A., 1997. Inorganic species in geologic fluids: correlation among standard molal thermodynamic properties of aqueous ions and hydroxide complexes. Geochimica et Cosmochimica Acta 61, 907–950.

Shvarov, Yu.V., 2008. HCh: new potentialities for the thermodynamic simulation of geochemical systems offered by Windows. Geochemistry International 46, 834–839.

Simon, G., Huang, H., Penner-Hahn, J. E., Kesler, S. E., Kao, L.-S. 1999. Oxidation state of gold and arsenic in gold-bearing arsenian pyrite. American Mineralogist 84, 1071–1079.

Sovetov, J.K., 2002. Vendian foreland basin of the Siberian cratonic margin: Paleopangean accretionary phases. Russian Journal of Earth Sciences 4, 363–387.

Stacey, J.S., Kramers, J.D., 1975. Approximation of terrestrial lead isotope evolution by a two stage model. Earth and Planetary Science Letters 26, 207-221.

Stryjek, R., Vera, J.H., 1986. PRSV2: A cubic equation of state for accurate vapour – liquid equilibria calculations. Canadian Journal of Chemical Engineering 64, 820–826.

Sverjensky, D.A., Shock, E.L., Helgeson, H.C., 1997. Prediction of the thermodynamic properties of aqueous metal complexes to 1000ºC and 5 kb. Geochimica et Cosmochimica Acta 61, 1359–1412.

Taylor, H.P., McLennan, S.M., 1985. The continental crust: Its composition and evolution. Blackwell, Oxford, 312 pp.

Thiery, R., Kerkhof, A.M, Dubessy, J., 1994. PTX properties of CH_4–CO_2 and CO_2–N_2 fluid inclusions: modeling for T<31^{o}C and P < 400 bars. European Journal of Mineralogy 6, 753– 771.

Tsygankov, A.A., Matukov, D.I., Berezhnaya, N.G., Larionov, A.N., Posokhov, V.E., Tsyrenov, B.Ts., Khromov, A.A., Sergeev, S.A., 2007. Magma sources and stages of emplacement of the Late Paleozoic granitoids in the West Transbaikal Region. Geology and Geophysics 48, 156–180.

Vagina, E.A., 2012. Mineral associations of ores and genesis of the Chertovo Koryto deposit (Patom Highland). Letters of Tomsky Technical University 321, 63-69 (in Russian).

Verkhozin, A.V., Martynenko, V.G., Benedyuk, V.F., Burakov, V.V., Leskov, V.V., Kolmakov, Yu.V., Kucherenko, I.V., 2007. Chertovo Koryto gold deposit. Unpublished report on exploration results and feasibility study 1996-2007. ZAO Tonoda Gold. Bodaibo (in Russian).

Vilor, N.V., Lepin, V.S., Stanevich, A.M., 1991, Radiological and paleophytological dating of sedimentation and metamorphism of rocks of the Baikal–Patom Highland. Doklady Akademii nauk SSSR 318(2), 396–400 (in Russian).

Vinogradov, V.I., Pichugin, L.P., Bykhover, V.N., 1996. Isotopic features and dating of epigenetic alterations of upper precambrian deposits isotopic features and dating of epigenetic alterations of upper precambrian deposits of the Ura Uplif. Lithology and Mineral Resources 31, 60–69 (in Russian).

Widler A.M., Seward, T.M., 1989. The adsorption of gold (I) hydrosulphide complexes by iron sulphide surfaces. Geochimica et Cosmochimica Acta 66, 383-402.

Wood, B.L., Popov, N.P., 2006. The giant Sukhoi Log gold deposit. Geology and Geophysics 47, 315–341.

Yakubchuk, A., Stein, H., Wilde, A., 2014. Results of pilot Re–Os dating of sulphides from the Sukhoi Log and Olympiada orogenic gold deposits, Russia. Ore Geology Reviews 59, 21–28.

Yarmolyuk, V.V., Kovalenko, V.I., Kovach, V.P., Rytsk, E.Yu., Kozakov, I.K., Kotov, A.B., Salnikova, E.B., 2006. Early stages of the Paleoasian ocean formation: results of geochronological, isotopic, and geochemical investigations of late Riphean and Vendian–Cambrian complexes in the Central Asian Fold belt. Doklady Earth Sciences 411, 1184–1189.

Yudovich, Ya.E., Ketris, M.P., 1988. Geochemistry of black shales, Nauka, Leningrad, 272 pp (in Russian).

Yudovich, Ya.E., Ketris, M.P., 2000. Basics of lithochemistry. Nauka, Moscow, 479 pp. (in Russian).

Yudovskaya, M.A., Distler, V.V., Rodionov, N.V., Mokhov, A.V., Antonov, A.V., Sergeev, S.A., 2011. Relationship between metamorphism and ore formation at the Sukhoi Log gold deposit hosted in black slates from the data of U–Th–Pb isotopic SHRIMP-dating of accessory minerals. Geology of Ore Deposits 53, 27–57.

Figure captions

Figure 1. Position of the Lena gold province in the Neoproterozoic orogens along the southern boundary of the Siberian Platform (after Safonov, 2006; Mitrofanov, 2006). Gold deposits: 1–Olimpiada, 2–Sovetskoe, 3–Eldorado, 4–Veduga, 5–Vasilevskoe, 6–Samsonovskoe, 8–Zun-Kholba, 9–Mukodek, 10–Sukhoi Log, 11–Vysochaishee, 12–Verninskoe, 13–Uryakh, 14–Irokinda, 15–Nazarovskoe.

Figure 2. Stratigraphic succession of the Lena region showing the stratigraphic position of the gold deposits and ore occurrences based on the stratigraphic schemes and data from Ivanov et al. (1995) and Ivanov (2014) with the changes discussed in the text.

Figure 3. Geological map of the Baikal–Patom Highlands, simplified after Kazakevich et al. (1971). Gold deposits and occurrences: 1–Sukhoi Log, 2–Vysochaishee, 3–Verninskoe, 4–Nevskoe, 5–Chertovo Koryto, 6–Ojerel'e, 7–Ykan, 8–Kopylovskoe, 9–Kavkaz, 10–Dogaldyn, 11–Krasnoe, 12–Svetlovskoe, 13–Verkhne-Ugakhan, 14–Khodokan, 15–Atyrkan.

Figure 4. Pb–Pb correlation diagrams for sulphides from the Sukhoi Log (Disler et al., 2004; Meffre et al., 2008; Chernyshev et al., 2009), Verninskoe (Chugaev et al., 2014), Chertovo Koryto (Chugaev et al., 2010) and Khodokan (Landa et al., 2006) deposits. The line corresponds to the evolution curve according to the model by Stacey and Kramers (1975).

Figure 5. Geological map of the Sukhoi Log deposit (simplified after data of Kropotkin Geological Exploration Party).

Figure 6. Textures of metamorphosed and mineralised intercalated shale and sandstone of the Khomolkho Formation from the Zapadnoe pit and exploration boreholes (Sukhoi Log). (a) Ductile deformation in shales (darker) along cleavage on contact with sandstone. Carbonate

porphyroblasts arranged along cleavage whereas thin quartz bands (at the top) cross it at acute angle (705-139); (b) different deformation styles in shale and sandstone (64-217); (c) isoclinal folding of syn-deformational quartz vein; (d) crenulation cleavage in shale saturated with quartz-carbonate veining (64-222); (e) deformed shale's relics in quartz-carbonate matrix after sandstone (151-29); (f) visible 2-mm native gold (Au) in pyrite (Py) –pyrrhotite (Po) segregation with quartz shadows. Elongated lenses of pyrrhotite follow cleavage in shale (65-7.6); (g) superimposed graphite stringers (black in the centre) along axial cleavage crosscut folded quartz-carbonate metasomatite after sandstone and foliated shale (64-203). Quartz is white, carbonate – light yellow, pyrite (Py) – bright yellow, pyrrhotite (Po) is rusted. Core samples 5 cm in diameter. Sample's selection courtesy of E. Evlanova.

Figure 7. Geological map of the Chertovo Koryto deposit and schematic geological section across the deposit (after unpublished work of A.V. Verkhozin and V.G. Martynenko).

Figure 8. Binary variation diagrams of SiO_2 vs. major oxides and geochemical indexes AI = $(Al_2O_3+TiO_2+Fe_2O_3+FeO+MnO)/SiO_2$ and TI = TiO_2/Al_2O_3 for rocks of the Anangr (Yudovich and Ketris, 2000), Vacha, Dzhemkukan (after Yudovich and Ketris, 1988), Khomolkho and Mikhailovsk Formations based on XRF data from Rusinov et al. (2008) and this study. Mikhailovsk metamarl is silica-poor rock with 30 wt.% SiO_2.

Figure 9. Trace element abundances in metasediments of the Khomolkho and Mikhailovsk formations which host Sukhoi Log and Chertovo Koryto mineralisation based on INAA and XRF data. (a) Primitive mantle-normalised values in comparison with those for sediments of the Yangtze Platform (Gao et al., 1998). Normalisation factors are from Hofmann (1988) except for As, Sb, Mo, V, Au and Cr, which are from Palme and O'Neill (2004); (b) element abundances normalised to the average abundances in black shales worldwide according to Yudovich and Ketris (1988). The pattern of Ni-Mo-PGE mineralisation in shales of the Niutitang Formation (Mao et al., 2002; Jiang et al., 2006) is shown as representative for hydrothermal-exhalative mineralisation in the Yangtze Platform. The sequence of elements is determined by decreasing concentrations in the continental crust.

Figure 10. Element distribution in the cross section along ChK85 drillhole through the orebody of the Chertovo Koryto deposit illustrating weak correlation between gold and arsenic and strong lithological control on coupled Fe, Co, Ni, Cr and REE variations based in INAA data. Apy–arsenopyrite, Po–pyrrhotite, Au–native gold, Q–quartz.

Figure 11. Binary variation diagrams of Au (a) and Cr (b) vs. Fe_2O_3, Co and As in mineralised rocks of the Sukhoi Log, Chertovo Koryto and Vysochaishee deposits based on

INAA data. Plots illustrate no correlation between gold and other elements as well as persistent co-variations between siderophile elements.

Figure 12. Textures of metamorphosed and mineralised shale and sandstone of the Mikhailovsk Formation at Chertovo Koryto and corresponded gold grade. (a) bedded texture of intercalated shales (darker) and sandstones (lighter) with superimposed cleavage expressed in cross-cutting graphite stringers in shales (ChK51-73.5); (b) lithological boundary (sub-vertical) between metamarl (greenish left) and shales (black right) is sheared by normal-oriented axial plain cleavage with quartz veining sub-parallel to schistosity (ChK51-167); (c) sheared lithological boundary between fine-grained sandstone (grey left) and shale (black right). Pyrrhotite is confined to the sheared contact and distributed along shearing; two crossing planes of quartz veining are seen in sandstone (ChK51-58); (d) deformed lenses and stringers of shaly relics (black) in sandstone (grey) with quartz vein (white) parallel to schistosity (ChK51-52); (e) late pyrite-quartz (white) vein cross-cuts earlier siderite veining (creamish) in metamarl (ChK51-159); (f) elongated lenses of pyrrhotite (cream-yellow) and rounded granular quartz “eyes” along cleavage in core of small fold. Later euhedral pyrite (yellow on the left) is not sheared (ChK51-94.5); (g) late irregular quartz vein (rusted white) and thinner quartz veinlets (white) with pyrrhotite lenses (yellow) crosscut original bedding and schistosity (ChK51-115); (h) boudinaged sandstone relics (grey) with quartz-chlorite segregations in shaly pyrrhotite-bearing matrix (black) (ChK51-96); (i) core of small fold composed of intercalated shales (black) and sandstones (grey). Fine arsenopyrite grains (white) are evenly distributed in sandstone and confined to lithological boundaries which are sheared by crosscutting axial plain cleavage. Coarser euhedral pyrite (yellow) occurs mostly in shales (ChK85-98.5); (j) disseminated arsenopyrite (white-grey crystals) in sandstone surviving in margin of thick quartz vein (rusted white) at replacement (ChK51-88); (k) quartz (white)-carbonate (yellowish) vein crosscuts relict bedding emphasised by arrangement of fine metasomatic arsenopyrite (white-grey) along lithological boundaries (ChK85-96); (l) quartz-carbonate (yellowish) and quartz (rusted white) veins arranged along bedding and schistosity in arsenopyrite-rich (grey crystals) schist (ChK51-84); (m) quartz-carbonate veinlets crosscut folded and foliated schists (black) and metasandstone (grey) rich in arsenopyrite crystals (ChK85-99). Gold content (ppm) is shown for 1-meter intervals. Half-core samples are 5 cm in diameter.

Figure 13. Typical textures of metamorphosed sedimentary rocks of the Mikhailovsk Formation at Chertovo Koryto in thin sections under XPL. (a) separation of granoblastic quartz and lepidoblastic mica layers in metasandstone (ChK51-52); (b) sheared bedding plane

between sandstone and shale with cleavage normal to original bedding (ChK51-52); (c) lenses and layers of granoblastic quartz after sandstone with schistosity parallel to bedding (ChK85-22). Opaque porphyroblast – arsenopyrite with quartz shadows; (d) lens-like quartz porphyroblasts in quartz-muscovite schist (ChK51-168) (e) quartz-muscovite veining crosscuts crenulation cleavage in sericite schist (ChK85-22); (f) zoisite porphyrobalsts in carbonate-chlorite schist after metamarl (ChK85-169).

Figure 14. Photomicrographs of sagenitic rutile formed at biotite replacement by chlorite and quartz in Mikhailovsk metasediments. (a) rutile-rich quartz and chlorite (Chl) pseudomorphs after biotite in quartz-ankerite (Ank) -chlorite schist, PPL (ChK51-169); (b) regularly-arranged rutile needles and stars in quartz (Q) pseudomorphs after biotite. Ankerite (Ank) substitutes high-Mg chlorite (Chl) and quartz, XPL (ChK51-169); (c) coupled quartz (Q) and chlorite (Chl) pseudomorphs after biotite with quartz colored by decomposed biotite under PPL. Ankerite (Ank) substitutes quartz along margins (ChK51-158); (d) the same as (c) under XPL.

Figure 15. Typical textures of hydrothermal metasomatic assemblages at Chertovo Koryto in transmitted light under XPL. (a) undulose extinction in deformed quartz (Q) porphyroblast in quartz-ankerite (Ank)-muscovite (Ms) vein (ChK51-84); (b) arsenopyrite (Apy) porphyroblast with quartz (Q) -chlorite (Chl) shadows intersecting foliation of mica (ChK85-64); (c) fractured arsenopyrite (Apy) with quartz filling coeval with quartz shadows (ChK85-64); (d) ankerite (Ank) substitutes quartz “eye” (Q) in carbonate-chlorite schist. Quartz and chlorite pseudomorphs after biotite have dark outlines saturated with rutile inclusions on the peripheries of quartz “eye” (ChK51-157.4); (e) quartz (Q) – chlorite (Chl) lenses around arsenopyrite (Apy) -pyrrhotite intergrowth (opaque) and crosscutting veining of granoblastic quartz (ChK82-84); (f) rotation of chlorite (Chl) –quartz (Q) pressure shadows around arsenopyrite (Apy) in accordance to foliation (ChK85-64).

Figure 16. Ore minerals of the Chertovo Koryto deposit in polished blocks under reflected light. (a) foliated intercalation of shaly (darker) and sandy (lighter) bands with concordant quartz veinlets. Schist is rich in pyrrhotite (Po, creamish elongated), sandy matrix contains arsenopyrite (Apy, anysotropic white isometric), XPL (ChK85-150); (b) arsenopyrite metacrysts (Apy) in thin sandy quartz (Q) bands neighbouring quartz-mica-pyrrhotite (Po, cremish) vein developed in shaly matrix, XPL (ChK85-44); (c) arsenopyrite (Apy) metacrysts superimposed on porphyrobalsts of metamorphic titanate (Ttn), XPL (ChK85-57.5); (d) cataclastic arsenopyrite (Apy) surrounded by quartz-chlorite-muscovite matrix, XPL (ChK85-54); (e) gold (Au), quartz and pyrrhotite (Po) in interstitial space and inside

arsenopyrite (Apy) crystals, XPL (ChK85-94); (f) the same generation of gold (Au) as in (e) included in arsenopyrite (Apy) metacryst partly recrystallised along margins, XPL (ChK85-94); (g) galena (Gn) cements cataclastic arsenopyrite (Apy) in quartz (Q) vein, XPL (ChK85-52); (h) native gold (Au) in goethite (Gt) with relics of replaced arsenopyrite (Apy), PPL (ChK85-85).

Figure 17. Arsenopyrite + native gold assemblage in Chertovo Koryto mineralisation. BSE images of unpolished grains. (a) euhedral non-fractured arsenopyrite (Apy) metacrysts (ChK85-84); (b) cataclastic arsenopyrite (Apy) saturated with native gold (Au), darker particles – muscovite and carbonate (ChK85-94); (c) jointing gold veinlets (Au) recovered from arsenopyrite (Ars); (d) flatten gold (Au) aggregates along arsenopyrite's face (Apy) comparing to gold veinlets (Au) inside arsenopyrite, dark particles – carbonate (Cbt) (ChK85-94); (e) prints of phillosilicates on surface of native gold (Au) (ChK85-94); (f) native gold emulsion (Au) in arsenopyrite (Apy) with particles less than 0.5 μm (ChK85-94).

Figure 18. Native gold assemblages in Sukhoi Log ores illustrating the dissimilar and similar features with respect to Chertovo Koryto gold mineralisation. BSE images of unpolished grains recovered from samples from the Zapadnoe open pit. (a) intergrowing euhedral cubic crystals of pyrite (Py) and $Au_{56}Ag_{44}$ alloy (Au); (b) xenomorphic gold (Au) connecting small pyrite (Py) metacrysts and growing inside pyrite skeletal crystals; (c) euhedral cubic crystals of gold $Au_{75}Ag_{25}$ (slightly darker) among xenomorphic massive gold $Au_{90}Ag_{10}$; (d) small cubic gold crystals in interstitial gold $Au_{80}Ag_{20}$ in association with pyrite (Py) and ankerite (Ank); (e) cataclastic arsenopyrite (Apy) in massive gold (Au); (f) cataclastic arsenopyrite (Apy) cemented with native gold (Au).

Figure 19. Accessory minerals in chlorite-carbonate schist after argillaceous dolostone (metamarl) of the Mikhailovsk Formation at Chertovo Koryto. (a) intergrowth of allanite (Aln) with Cr-bearing muscovite (Ms). Bright mineral is REE-rich Ca-Ti silicate (ChK51-157); (b) intergrowth of apatite (Ap) and allanite (Aln) which contains fine inclusions of monazite (bright along fractures), Mg-Fe carbonate, quartz and muscovite (ChK51-158); (c) euhedral crystal of ullmannite (Ulm) (ChK51-157); (d) euhedral gersdorffite (Gdf) metacryst with small grains of galena (bright) on its surface (ChK51-157); (e) complex metacryst of gersdorffite (Gdf) (ChK51-158); (f) porous metacryst of gersdorffite (Gdf) in chlorite-ankerite (Ank) schist with abundant rutile along carbonate interfaces (ChK85-167). (a–e) – BSE images of polished blocks (a, b) and unpolished grains (c–e), f – under reflected XPL.

Figure 20. Mineral assemblages at Sukhoi Log. (a) undeformed ankerite (Ank) porphyroblasts selectively enriched in disseminated chalcopyrite (Ccp) (8-239); (b) deformed

ankerite (Ank) and ankerite-quartz (Q) -pyrite (Py) porphyroblasts in folded mica-graphite shaly matrix. Note oriented inclusions in ankerite core (112-62); (c) relics of foliated shale inside pyrite (Py) metacrystal (6-204); (d) brecciated pyrite (Py) and arsenopyrite (Apy) in gold-bearing quartz veinlet. Quartz (Q) associates with chalcopyrite, carbonate and pyrrhotite (Po) (112-141); (e) native gold (Au) as inclusions inside pyrite (Py) and along contacts with quartz (Q) (112-141); (f) inclusions of native gold (Au), galena (Gn), chalcopyrite (Ccp) and pyrrhotite (Po) inside ankerite (Ank). Note oriented galena (Gn) dissemination along cleavage in ankerite. Pyrrhotite is surrounded by magnetite rim (112-141). (a, c–f) – under reflected PPL; b – transmitted XPL.

Figure 21. Photomicrographs of fluid inclusions in quartz from Sukhoi Log gold ores. (a, b) carbonic-aqueous at +20 °C (a) and -12 °C (b); (c, d) – gaseous with dense CO_2 at +20 °C (c) and -15 °C (d); (e–g) – gaseous with carbonic-nitrogen mixture at +20 °C (e), -105 °C (f) and -170 °C(g); (h, i) – two-phase vapour-liquid inclusions. L – liquid phase, V – vapour, L CO_2 – liquid CO_2, V CO_2 – gaseous CO_2, S CO_2 – solid CO_2, L N_2 – liquid nitrogen, V N_2 – gaseous nitrogen.

Figure 22. Binary plots for fluid inclusions at Sukhoi Log and Chertovo Koryto. (a) salinity vs. homogenisation temperature showing no correlation; (b) pressure vs. homogenisation temperature showing a positive correlation at higher pressures. Phase boundaries between heterogeneous and homogeneous fluids in the H_2O-CO_2 and H_2O-CO_2-NaCl systems are shown after Diamond (2003).

Figure 23. Major species and trace element compositions of fluids trapped in quartz at Sukhoi Log (a) and Chertovo Koryto (b). The sequence of elements is determined by decreasing concentrations in fluids.

Figure 24. Photomicrographs of fluid inclusions in quartz from Chertovo Koryto gold ores taken at room temperature. (a) two-phase vapour-liquid; (b) vapour.

Figure 25. Calculated enrichment factors (log EF) for representative elements in fluid inclusions in quartz from Sukhoi Log and Chertovo Koryto mineralisation (Tables 2 and 4). $EF_i = (E_i/R)_{fluid}/(E_i/R)_{shale}$, where E_i is an element content and R is a content of a reference element in both fluid and host rock. Sodium is chosen for normalisation. Element abundances in shales are taken for barren supra-ore intervals with less than 0.1 ppm Au.

Figure 26. Amount of precipitated gold (wt.% of initial content) with increasing amount of CO_2 (mole per kg H_2O) at T = 350 °C and P = 500 bar at chemical equilibrium with shale.

Figure 27. Genetic model for gold mineralisation of the Lena Province.

Table Captions

Table 1

Chemical compositions of sedimentary rocks of the Mikhailovsk Formation at Chertovo Koryto by XRF method.

Table 2

Average trace element abundances in mineralised sequences at Sukhoi Log (Upper Khomolkho F.), Chertovo Koryto (Mikhailovsk F.), Vysochaishee (Lower Khomolkho F.) and Khodokan (Purpol F., after Landa et al., 2006) with respect to the representative data on unmineralised black shales worldwide (Yudovich and Ketris, 1988), unmineralised Yangtze sediments (Gao et al., 1998) and mineralised Ni-Mo-PGE-Au layers of Niutitang F. in the Yangtze Platform (averaging after Mao et al., 2002; Jiang et al., 2006).

Table 3

Summary of microthermometric data on fluid inclusions in quartz from Sukhoi Log and Chertovo Koryto mineralisation.

Table 4

Chemical composition of ore-forming fluids in the Sukhoi Log and Chertovo Koryto gold deposits by ICP-MS analysis of fluid inclusion bulk solutions

Table 1

Chemical compositions of sedimentary rocks of the Mikhailovsk Formation at Chertovo Koryto by XRF.

Borehole	51	51	51	51	51	85	85	85
Depth (m)	157.2	27.5	52	85	88.6	22.5	27	98.5
Major elements (wt.%)								
SiO_2	30.21	73.37	64.01	72.21	59.90	57.21	67.72	60.20
TiO_2	2.26	0.46	0.71	0.51	0.64	1.16	0.71	1.11
Al_2O_3	6.70	11.69	15.79	11.61	16.75	18.93	13.62	18.10
Fe_2O_3	9.62	5.62	8.11	5.81	6.21	8.25	6.27	5.77
FeO								
MnO	0.50	0.04	0.05	0.02	0.03	0.04	0.07	0.02
MgO	10.98	1.45	2.45	1.69	2.39	2.70	1.88	2.39
CaO	15.21	0.46	0.26	0.16	0.25	0.22	1.09	0.19
Na_2O	0.04	2.01	1.18	1.68	1.00	1.59	1.51	1.29
K_2O	0.62	2.28	3.58	2.28	4.02	4.48	3.07	4.43
LOI	22.1	2.00	3.29	2.83	6.02	4.63	3.30	5.16
P_2O_5	1.36	0.12	0.12	0.13	0.15	0.15	0.13	0.14
S	0.02	0.30	0.16	0.26	0.42	0.21	0.36	0.17
Trace elements (ppm)								
Cr	486	118	160	128	184	145	158	154
V	86	95	158	100	125	158	107	147
Co	39	10	18	6	8	9	12	5
Ni	205	41	29	28	31	31	24	19
Cu	18	59	50	36	26	62	55	33
Zn	148	111	196	98	71	124	144	109
Rb	17	77	138	87	87	198	110	177
Sr	665	50	45	30	34	51	81	66
Zr	268	194	180	155	455	143	236	153
Ba	185	532	694	510	630	914	628	1106
Y	39	22	24	22	29	32	26	30
Nb	121	13	16	12	11	23	22	20
Pb	36	12	8	9	4	8	10	9
As	283	178	661	4864	15360	1371	422	5727
Cl	35	26	33	33	46	40	33	29

Table 2

Average trace element abundances in mineralised sequences at Sukhoi Log (Upper Khomolkho F.), Chertovo Koryto (Mikhailovsk F.), Vysochaishee (Lower Khomolkho F.) and Khodokan (Purpol F., after Landa et al. (2006) with respect to the representative data on unmineralised black shales worldwide (after Yudovich and Ketris, 1994), unmineralised Yangtze sediments (Gao et al., 1998) and mineralized Ni-Mo-PGE-Au layers of Niutitang F. in the Yangtze Platform (averaging after Mao et al., 2002; Jiang et al., 2006).

	Sukhoi Log	Chertovo Koryto	Vysochaishee	Khodokan	Black shales	Yangtze Platform	Nuititang F.
Pb	31	12		12	25	16	31
Ba	375	541	452	653	590	633	106
Th	7.17	11.4	11.3		7	8.70	0.47
As	49	3274		28	30	3	10000
U	1.27	2.78	3.79		8	1.38	38.8
La	29.4	32.3	43.0	27.4	37.3	37.3	9.72
Sb	2.14	0.56	0.27	0.49	6	0.26	
Ce	50.0	65.0	82.1	50.9	68.5	68.5	13.3
Nd	33.6	27.0	38.3	22.2	30.6	30.6	7.79
Zr	201	223		304	130	191	4.7
Hf	4.50	4.14	5.80		3.50	5.31	0.11
Mo		6.03	7.29	5.34	20	0.68	4518
Sm	5.01	4.78	8.28	5.52	5.04	5.04	1.48
Tb	0.68	0.33	0.68	0.88	0.85	0.85	0.28
Eu	1.26	1.22	1.74	1.25	1.21	1.21	0.50
Lu	0.37	0.22	0.54	0.40	0.34	0.34	0.07
Yb	2.50	1.52	3.93	2.37	2.24	2.24	0.57
V	146	122		91	205	94	110
Zn	109	125		95	140	69	398
Cu	56	42		234	87	36	202
Au	2.80	0.88	4.96		0.01	0.0013	0.33
Co	21	17	31	15	14	16	10
Cr	125	113	181	83	81	65	14
Ni	47	51		16	67	36	3336

Note: Abundances of Pb, Zr, V, Zn, Cu are average results of XRF analysis (*n*=20 for Sukhoi Log and *n*=8 for Chertovo Koryto), other elements – of INAA data (n=117 for Sukhoi Log, *n*=91 for Chertovo Koryto and *n*=20 for Vysochaishee).

Table 3

Summary of microthermometric data on fluid inclusions in quartz from Sukhoi log and Chertovo Koryto mineralisation.

Incl. Type*	**n****	***T*h** (ºC)	***T*eut** (ºC)	***T*m ice** (ºC)	***T*m CO_2** (ºC)	***T*h CO_2 or gases** (ºC)	**Hom. mode CO_2 or gases** (ºC)	***T*m clat-rate** (ºC)	**Sal.** (wt.% NaCl eq.)	**C_{CO2}** (mol/kg solu-tion)	***D*** (g/cm^3)	***P*** (bar)
Sukhoi Log deposit												
Veinlet-disseminated ores												
1	134	350–210	-34/ -31	-7.5/-4.6	-62.2/ -57.4	-16.7 /12.9	L	12.4–6.2	8.1–5.0	7.6–1.8	1.09–0.82	2370-190
2	53	–	–	–	-60.8/-57.0	-11.9/6.5	L-V	–	–	–	0.90–0.14	
3	361	385–130	-34/-25	-6.2/-2.2	–	–	–	–	9.5–3.7	–	0.97–0.65	–
2	252	385–205 V	–	–	-62.3/ -83.5	-156.5/-158.6	L-V	–	–	–	0.57–0.003	2290–210
Quartz veins												
1	149	380–275	-32/-30	-7.2/-5.4	-57.1/-60.9	-19.9/10.5	L	11.6–8.2	7.6–5.8	7.0–2.1	0.93	2430–200
2	63	–	–	–	-57.3/-60.7	-10.2/17.7	L-V	–	–	–	0.92–0.08	
3	42	210–185	-28	-4.8/-3.3	–	–	–	–	7.6–5.4	–	0.92	–
Chertovo Koryto deposit												
1	33	447–340	-36/-27	-6.6/-2.0	–	–	–	–	10.0–3.3	–	0.52–0.66	440–240
2	11	453–388 V	-22	-1.4	–	–	–	–	2.4	–	–	

Note: * Inclusions Type: 1 – aqueous solution + CO_2; 2 – water vapor ±CO_2±CH_4±N_2; 3 – dilute aqueous solution. ** – number of inclusions.

Table 4

Chemical composition of ore-forming fluids in the Sukhoi Log and Chertovo Koryto gold deposits by ICP-MS analysis of fluid inclusion bulk solutions.

Deposit	Sukhoi Log		Chertovo Koryto	
Sample	SRK6-198.2	SRK8-202.3	ChK51-84.5	ChK85-35.5
	Vein	Veinlet	Veinlet	Veinlet
Major components (g/kg solution)				
CO_2	91.72	46.52	49.6	34.32
CH_4	0.99	0.018	7.44	0.066
Cl^-	1.22	0.994	8.49	1.45
SO_4^{2-}	-	-	-	-
HCO_3^-	25.4	15.2	12.4	16.6
Na	9.48	5.55	7.53	2.36
K	0.38	0.62	1.15	5.27
Ca	0.73	0.15	1.28	1.00
Mg	-	0.16	0.32	0.34
Trace elements (ppm)				
Br	464	34.6	190	158
As	48.1	7.3	24.9	24.1
Li	57.4	11.4	7.5	32.0
B	2161	74.7	437	201
Rb	0.85	0.62	2.84	11.98
Cs	0.10	0.18	0.40	0.55
Sr	0.56	1.10	57.5	18.7
Mo	16.4	6.0	0.33	1.29
Ag	83.0	7.1	0.54	0.05
Sb	1.42	0.07	0.76	2.88
Cu	79.4	2.44	36.0	65.0
Zn	89.3	241	53.9	79.5
Cd	0.15	0.11	0.09	0.16
Pb	0.78	2.00	4.42	23.7
Bi	0.05	0.18	0.06	0.11
Th	0.02	0.004	0.04	0.06
U	-	0.004	0.04	0.09
Ga	-	-	0.09	0.56
Ge	3.43	0.84	1.01	2.33
Sc	26.4	8.27	51.2	57.3
Ti	1.47	1.57	6.55	12.6
Mn	-	-	18.5	21.6
Fe	-	-	67.1	205
Co	1.80	0.11	0.18	0.15
Ni	14.5	12.5	7.32	6.47
Cr	-	0.84	4.83	4.22
Y	-	-	5.80	9.33
Zr	0.15	0.22	0.04	0.04
Nb	-	-	0.30	0.24
In	-	-	0.01	0.04
Sn	-	0.29	0.14	0.91
Ba	2.82	0.51	5.75	9.78
W	4.16	1.68	0.38	7.13
Te	-	-	0.003	0.006
Au	0.049	0.020	0.159	1.151

Hg	0.71	0.36	0.24	3.38
Se	-	-	3.39	6.10
Tl	0.17	0.03	0.07	0.25
REE	0.25	0.08	0.77	0.15

Note: - below detection limit.

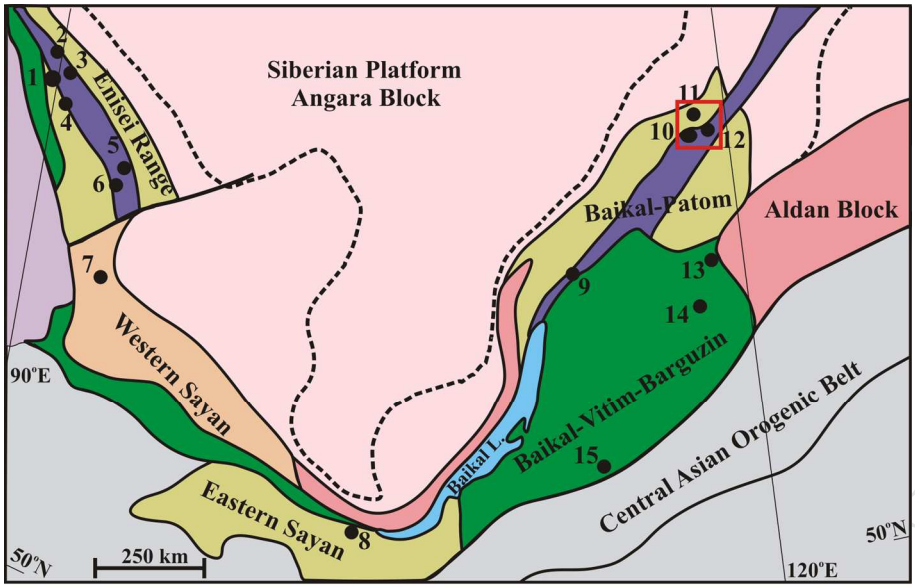

Siberian Platform cover
Siberian Platform basement
Western Siberian Platform
Neoproterozoic rift zones
Lena gold province (Fig. 3)
Precambrian basement of fold belts
Proterozoic passive margins
Neoproterozoic active margins
Central Asian Orogenic Belt
Boundary of Precambrian transgression
gold deposits
fault

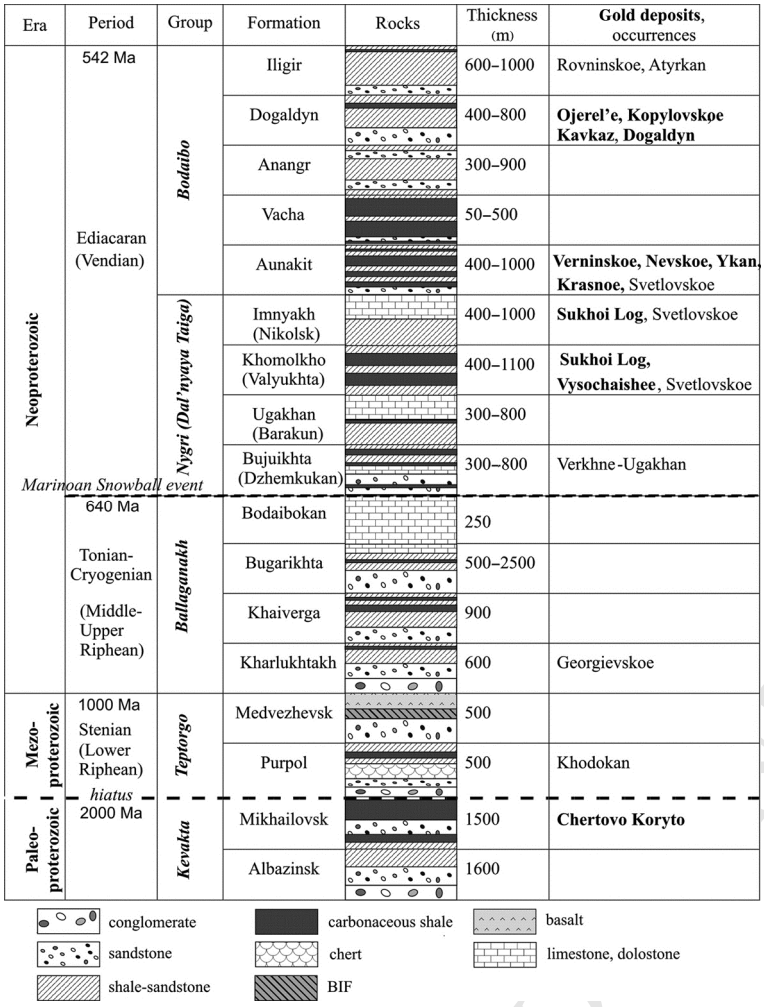

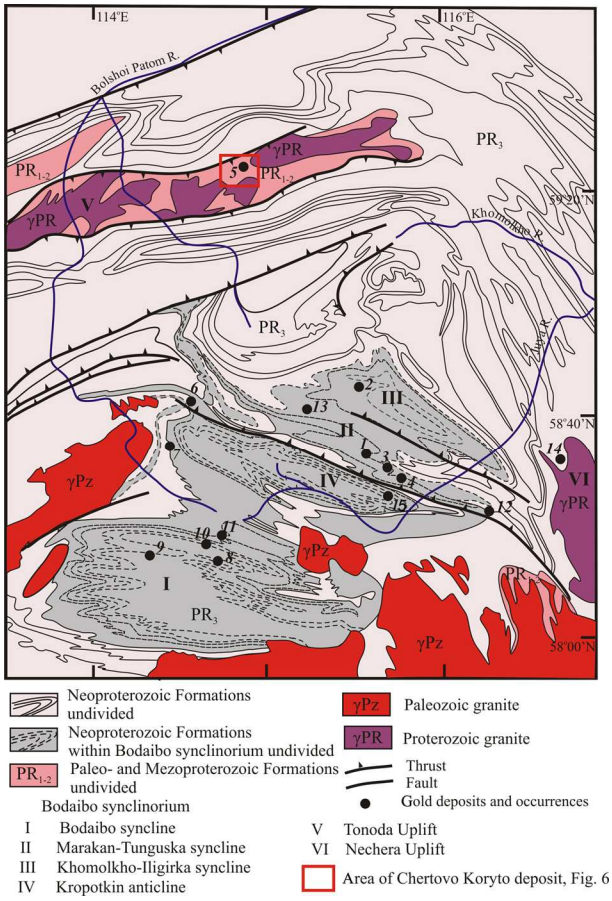

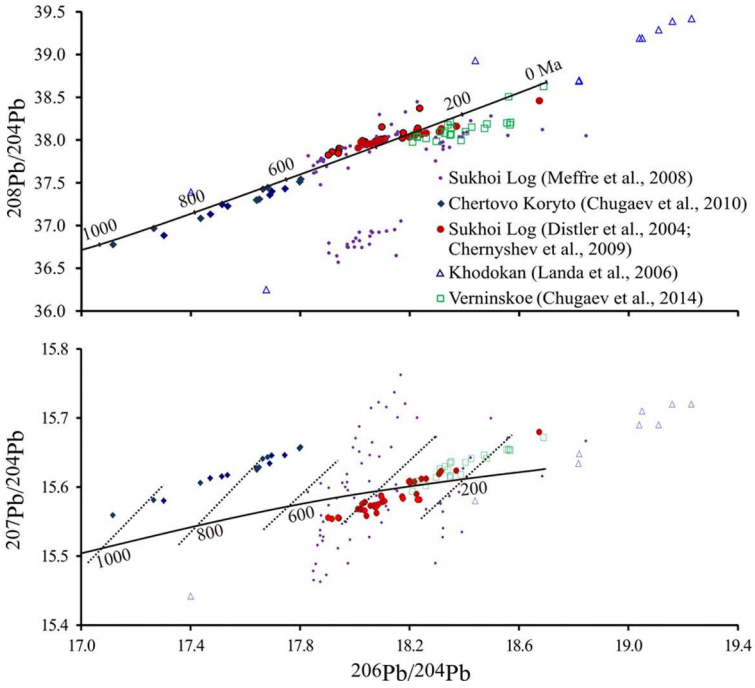

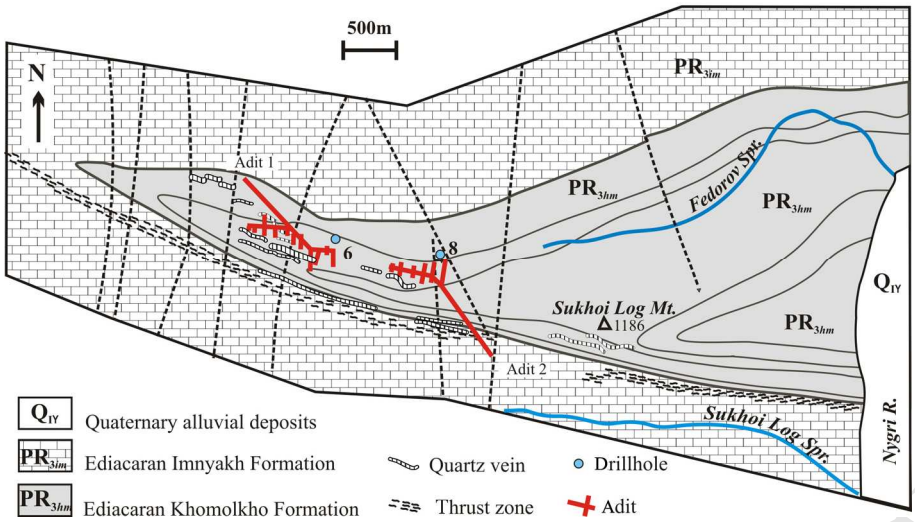

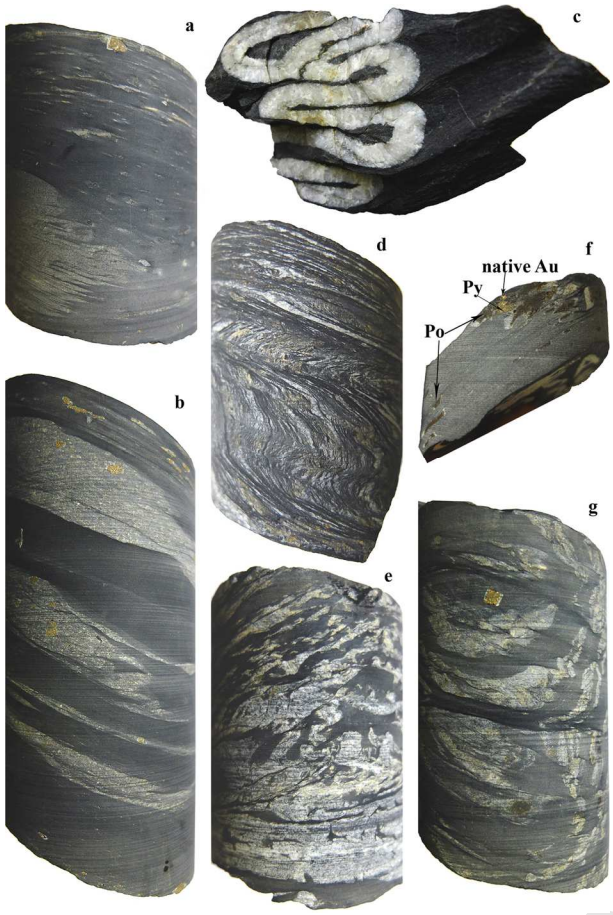

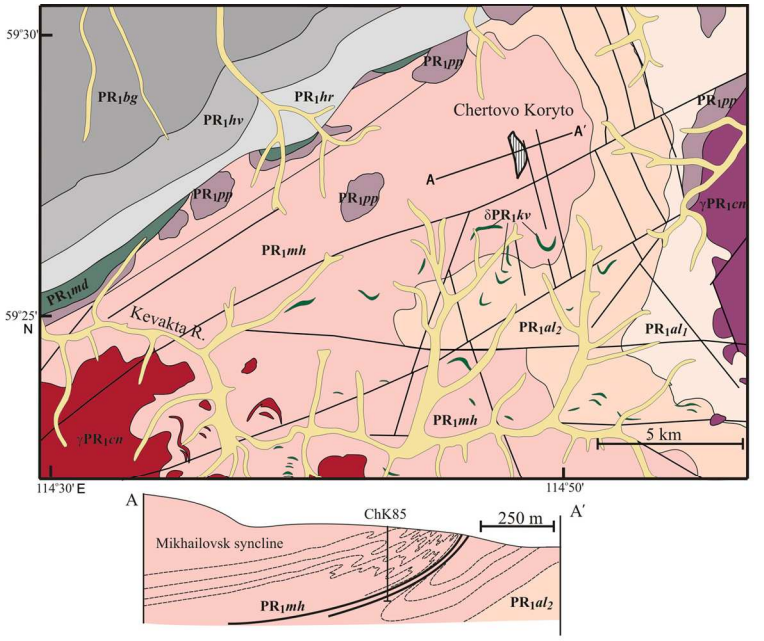

Quaternary alluvial sediments

Neoproterozoic Ballaganakh Group

PR_1bg Bugarikhta F. Terrigenous rocks

PR_1hv Khaiverga F. Terrigenous rocks

PR_1hr Kharlukhtakh F. Terrigenous rocks

Mezoproterozoic Teptorgo Group

PR_1md Medvezhevsk F. Sandstone, BIF

PR_1pp Purpol F. Quartzite, sandstone, shale

a - bedding; b - geological boundary

Drillhole

Paleoproterozoic Kevakta Group

PR_1mh Mikhailovsk F. Carbonaceous shale, sandstone

PR_1al_2 Upper Albazinsk F. Terrigenous rocks

PR_1al_1 Lower Albazinsk F. Terrigenous rocks

Paleoproterozoic Magmatic Complexes

δPR_1kv Kevakta Complex. Diabase sills

γPR_1cn Chuya-Nechera Complex. Muscovite granite

γPR_1cn Chuya-Nechera Complex. Biotite granite

Fault

Area of deposit

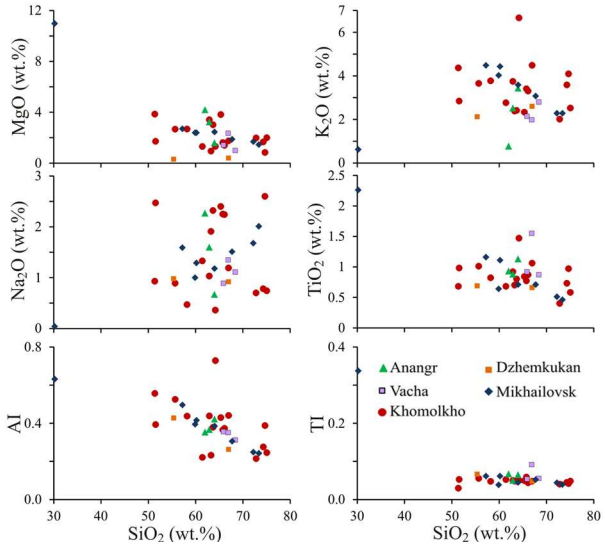

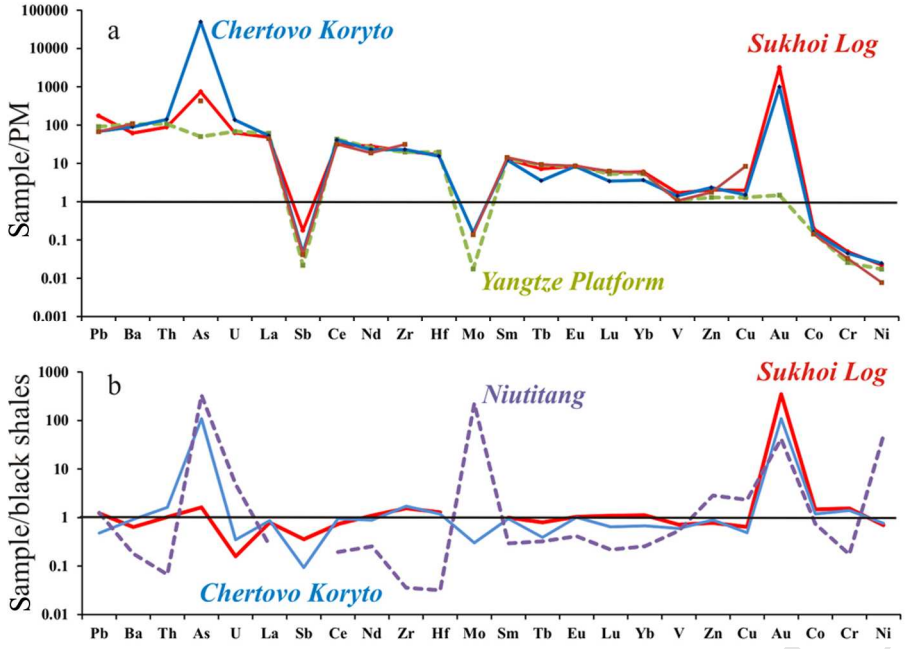

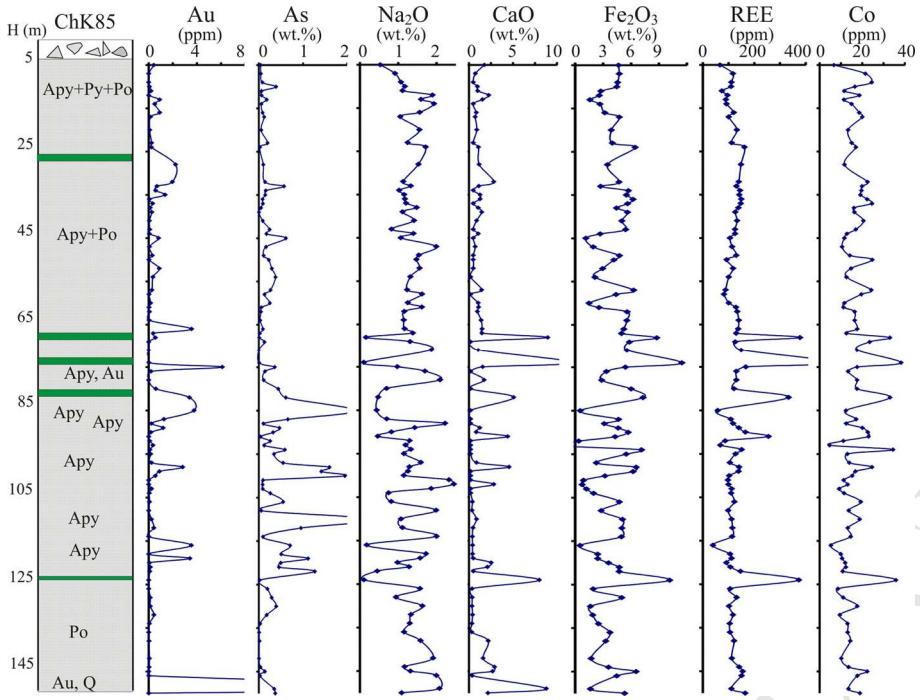

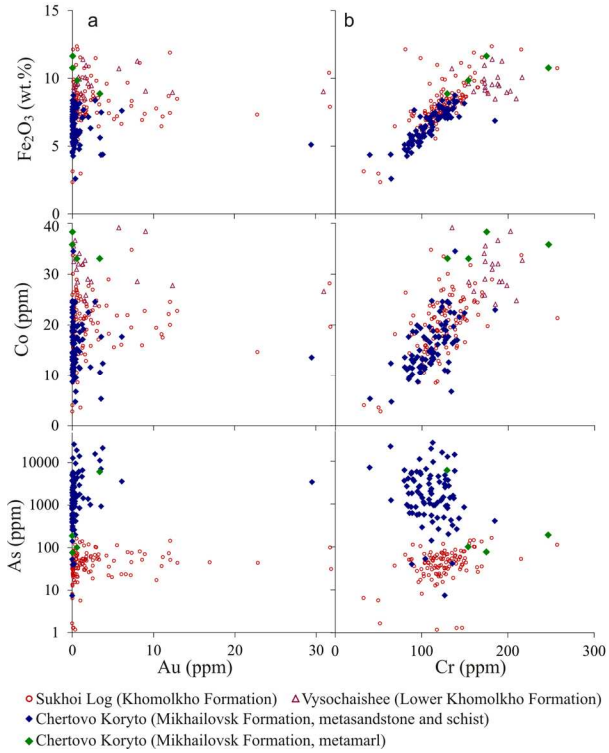

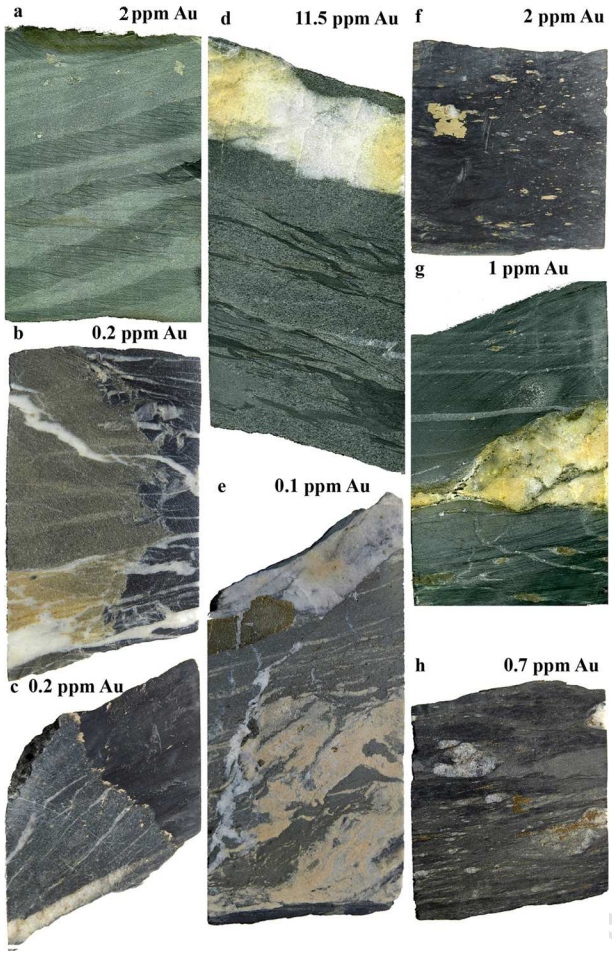

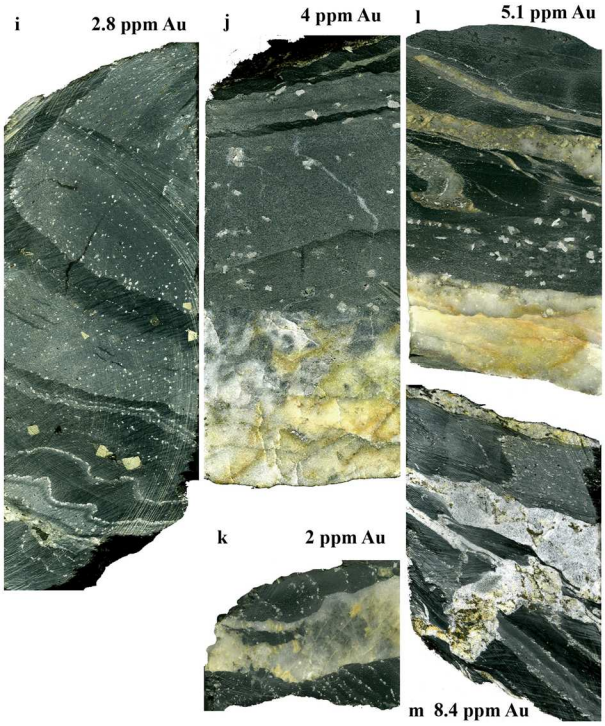

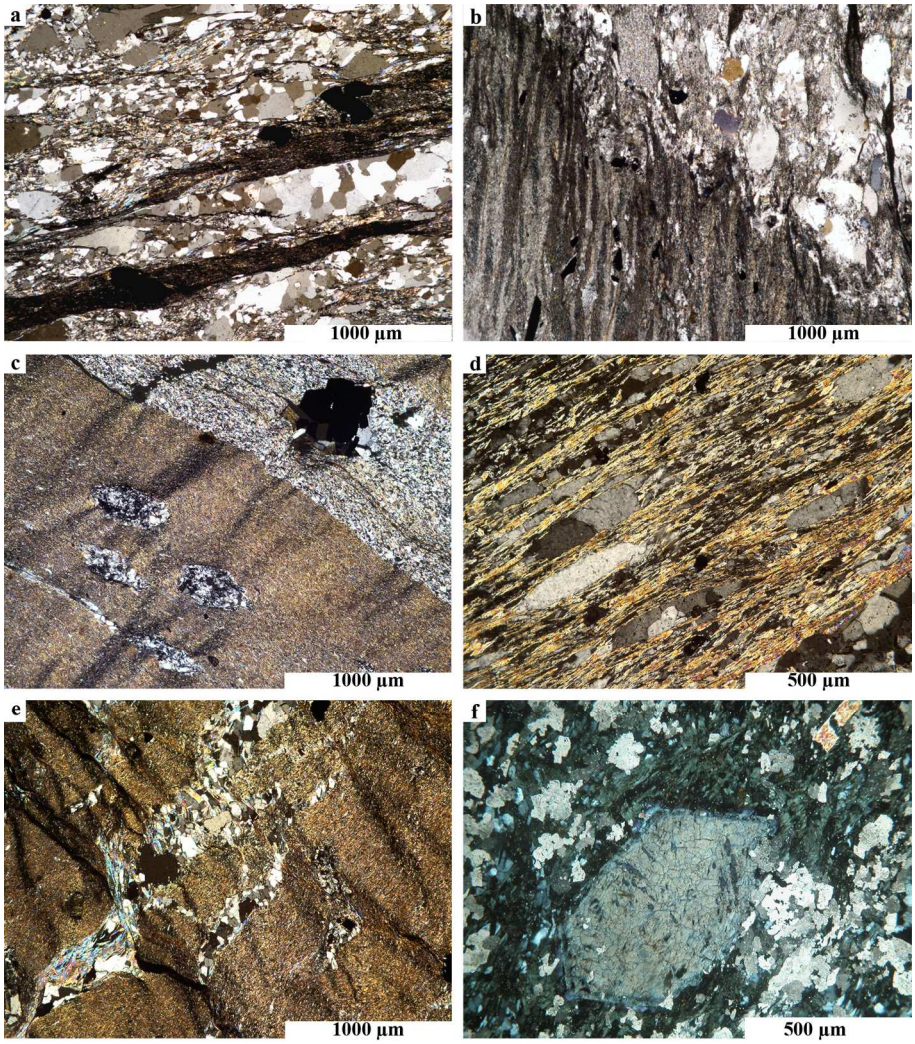

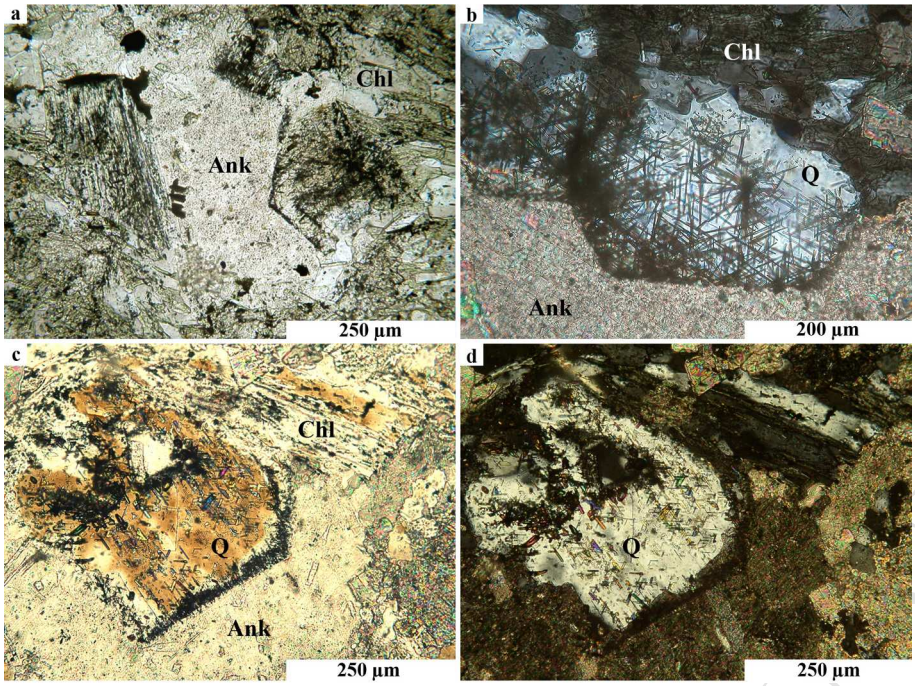

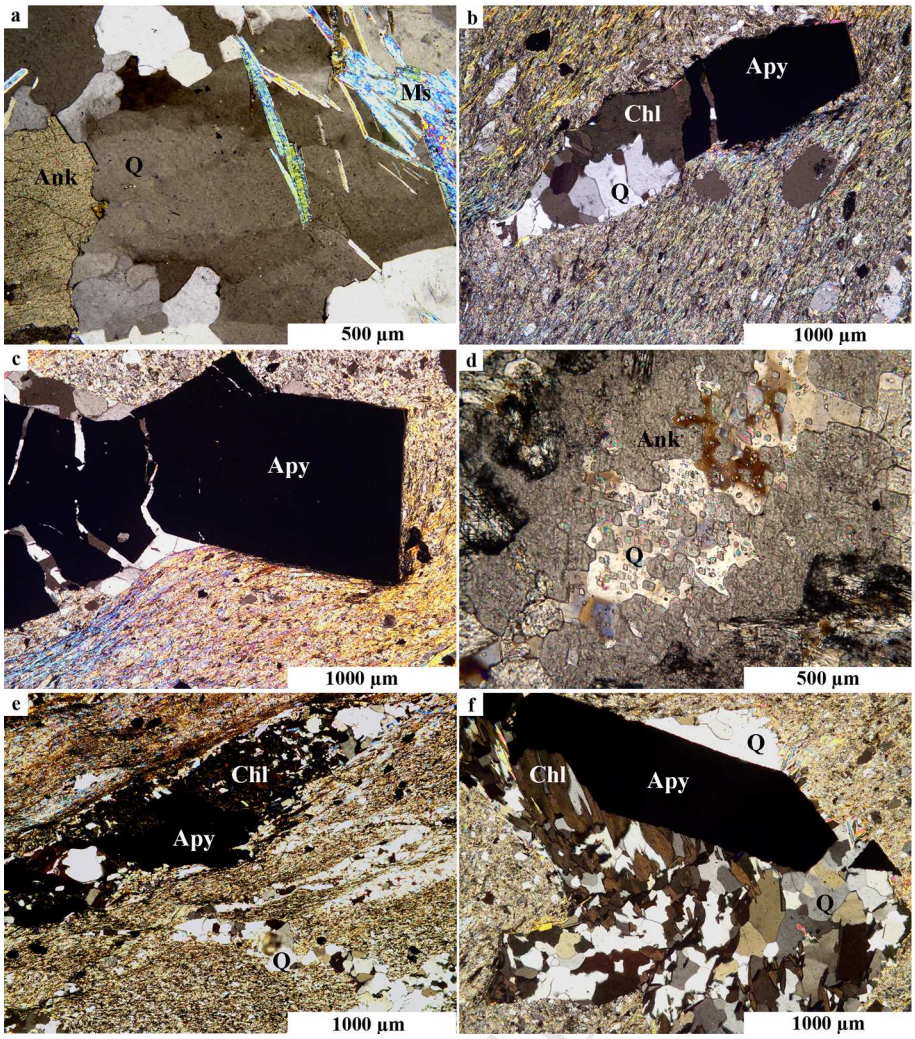

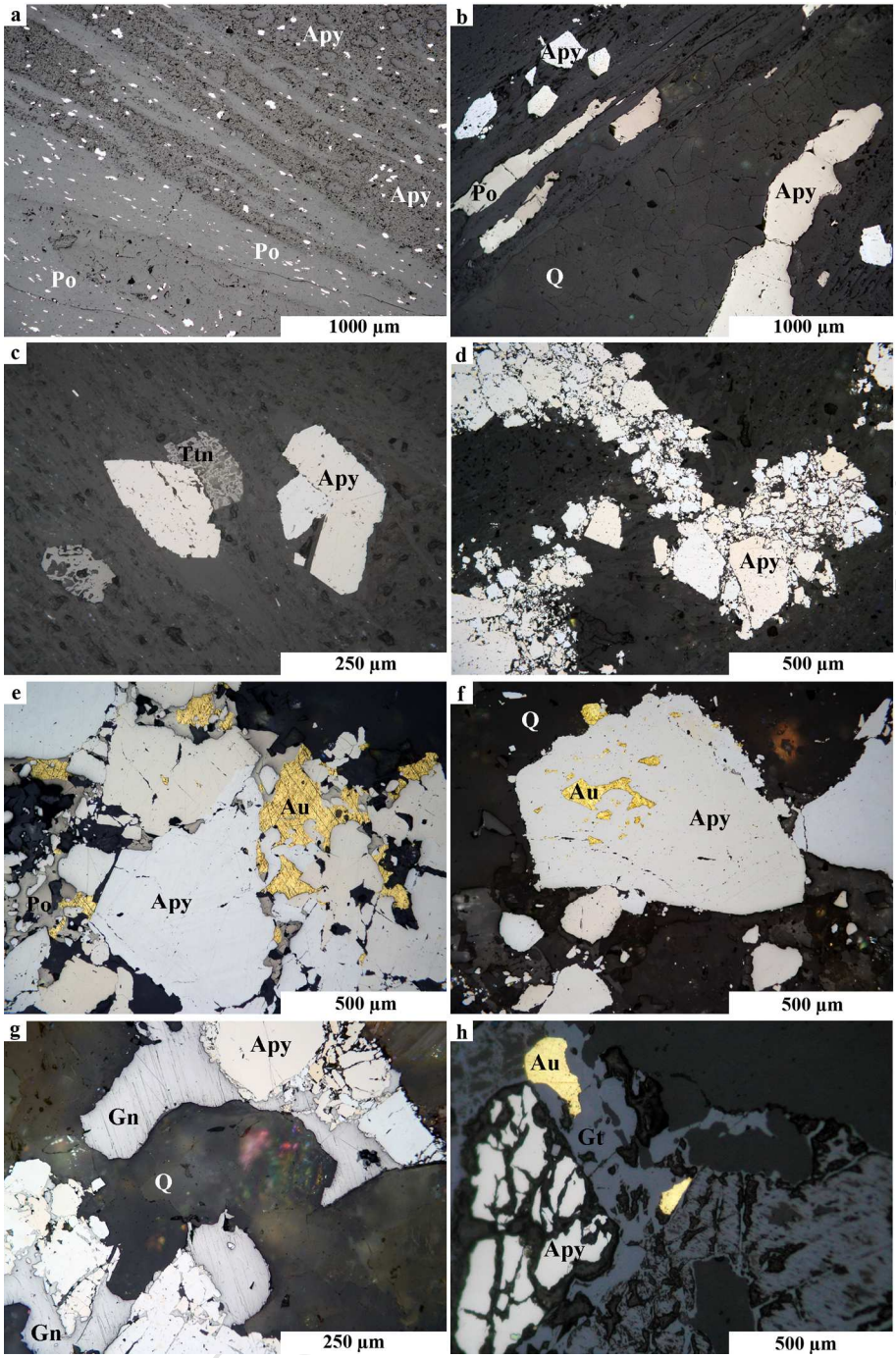
a
Apy
Apy
Po
Po
1000 µm
b
Apy
Po
Apy
Q
1000 µm
c
Ttn
Apy
250 µm
d
Apy
500 µm
e
Au
Po
Apy
500 µm
f
Q
Au
Apy
500 µm
g
Apy
Gn
Q
Gn
250 µm
h
Au
Gt
Apy
500 µm

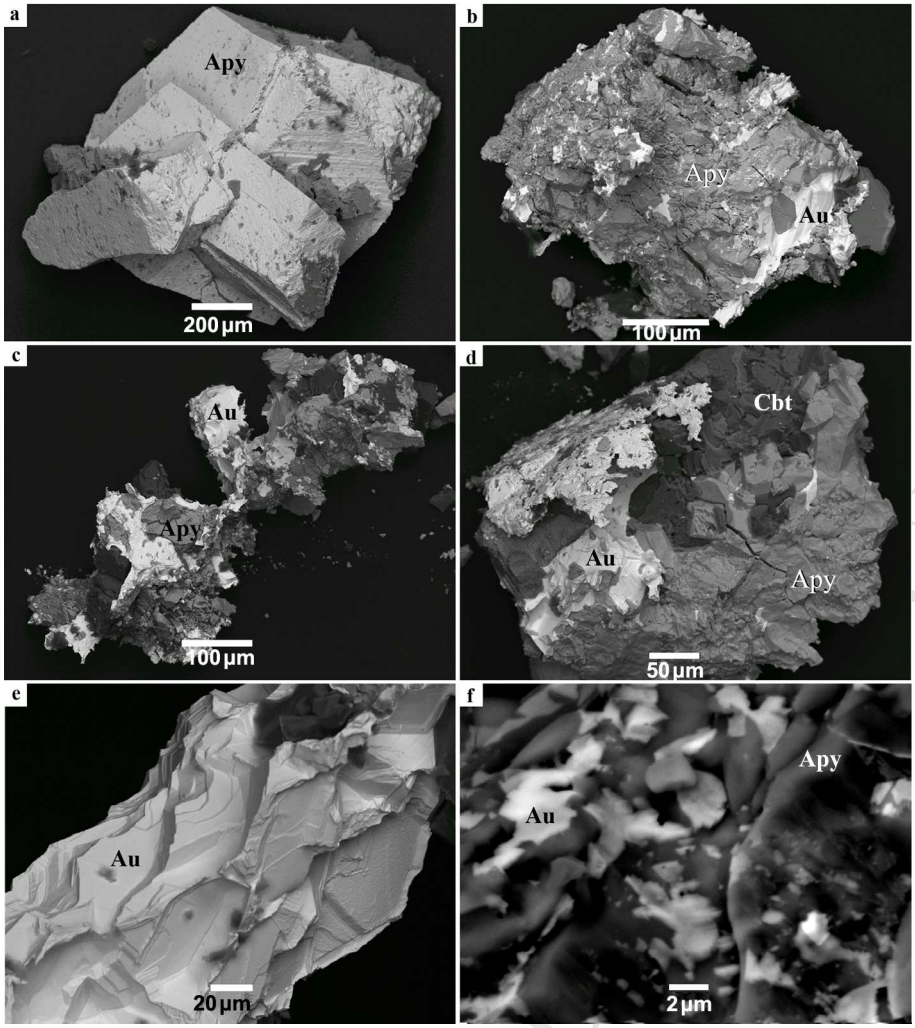

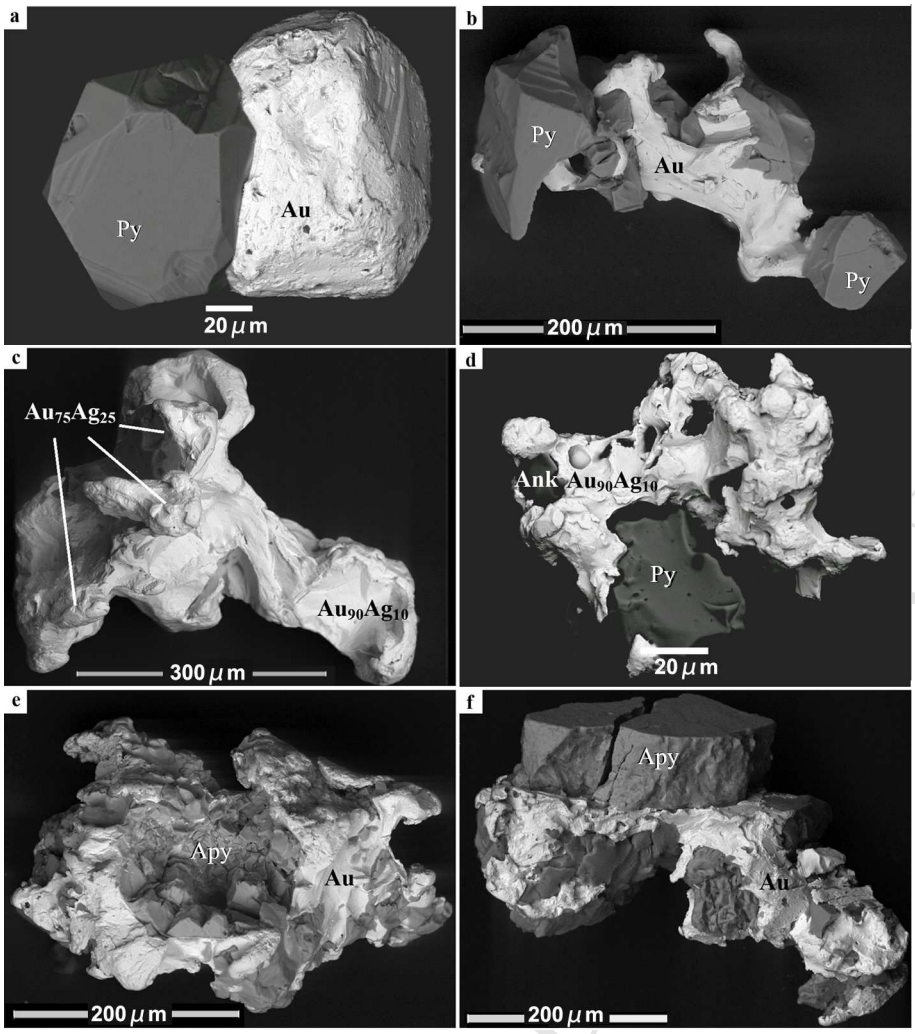

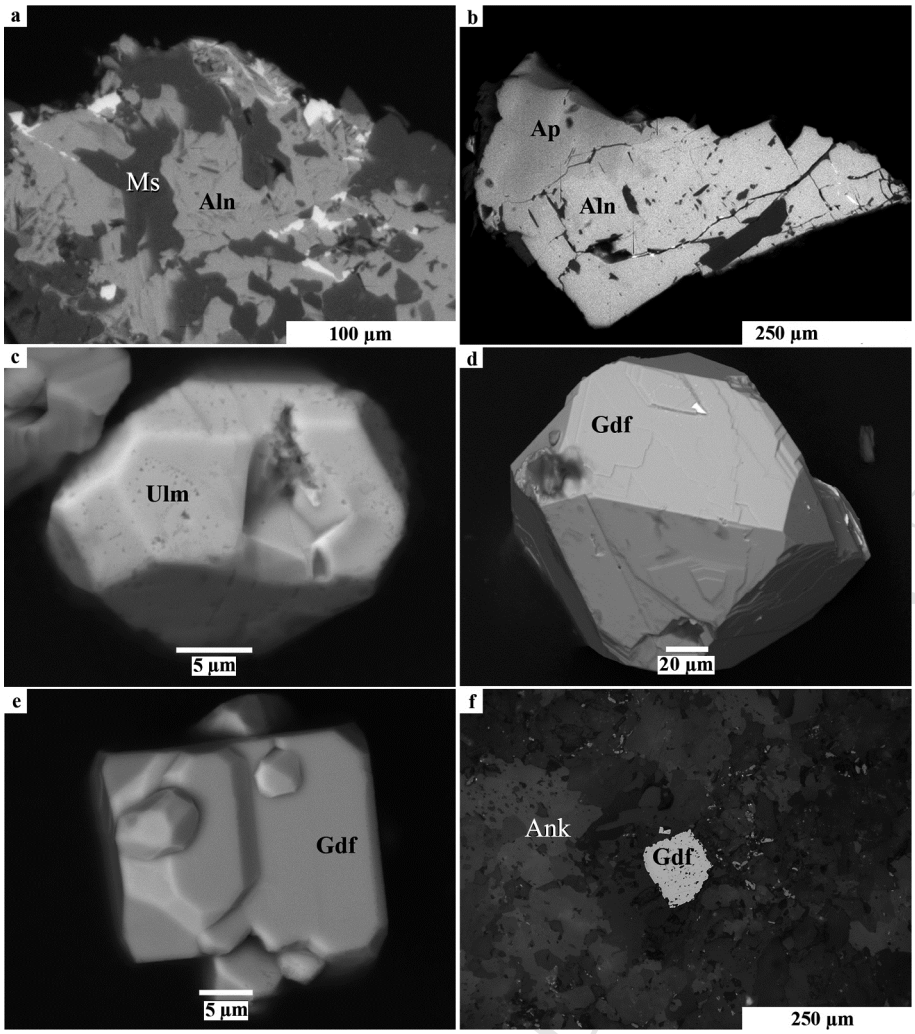

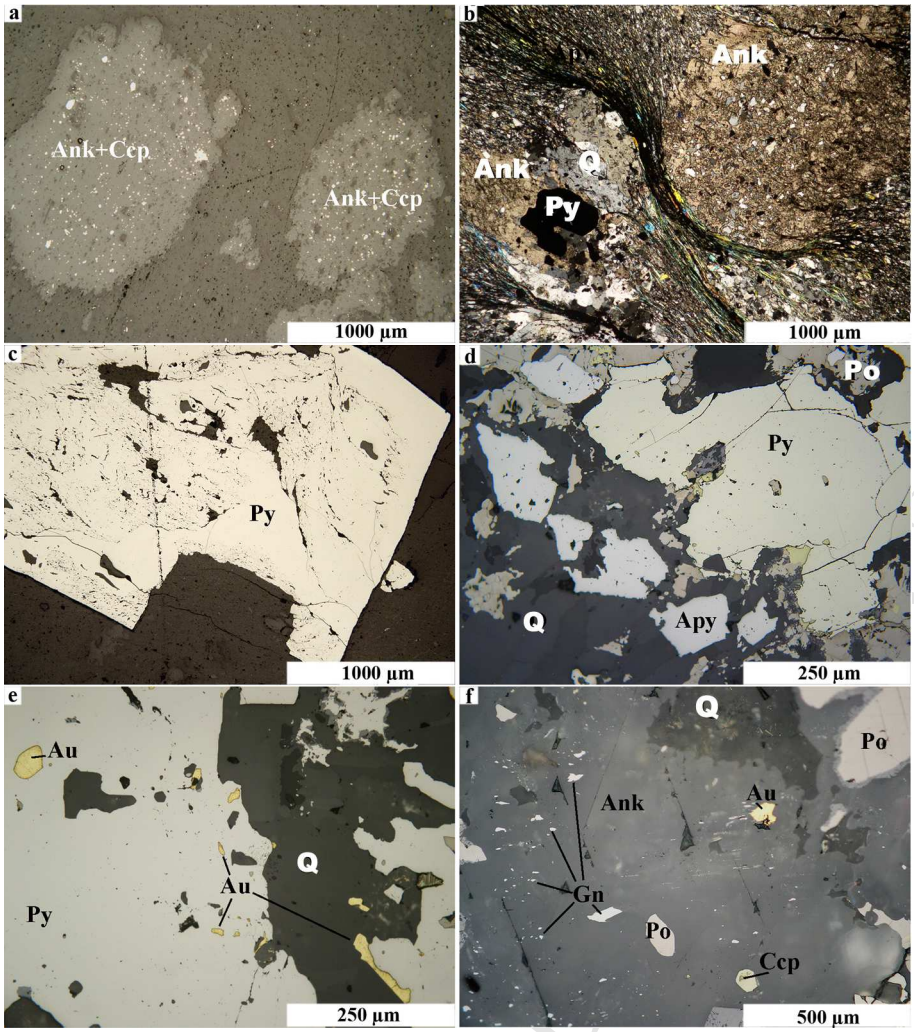

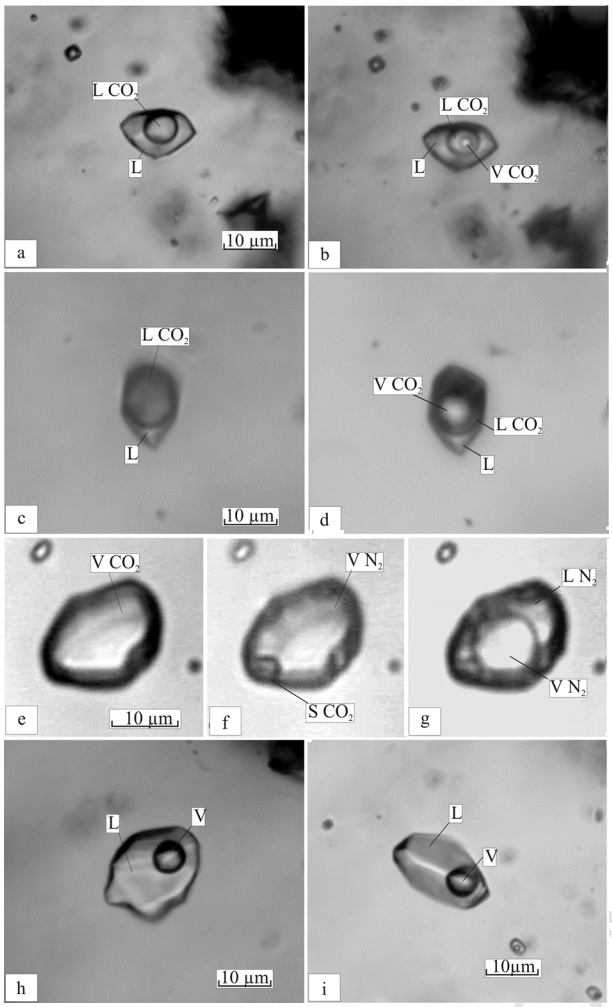

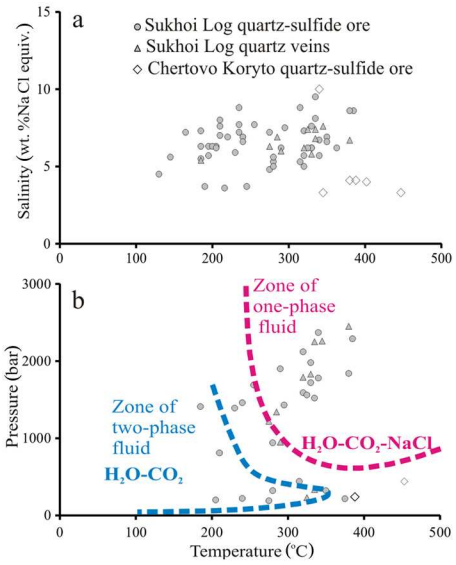

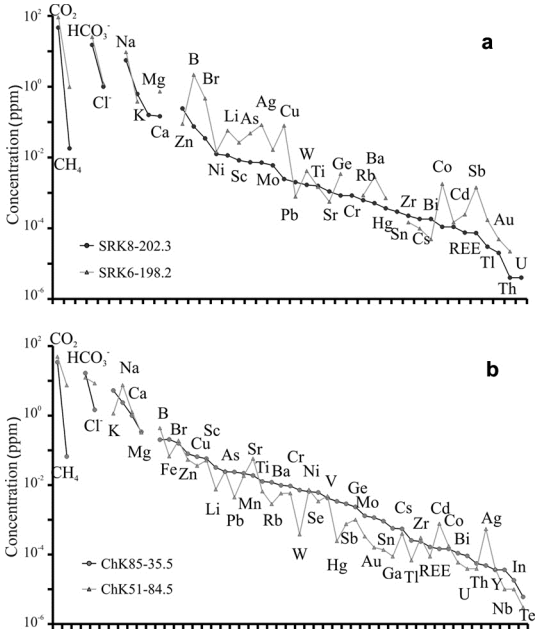

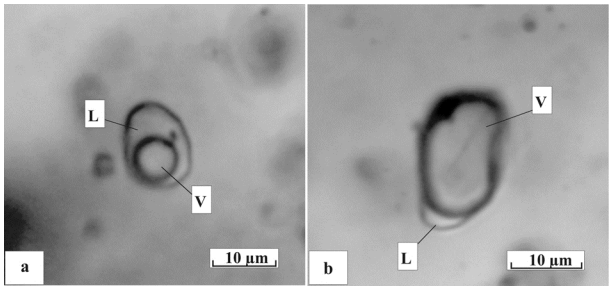

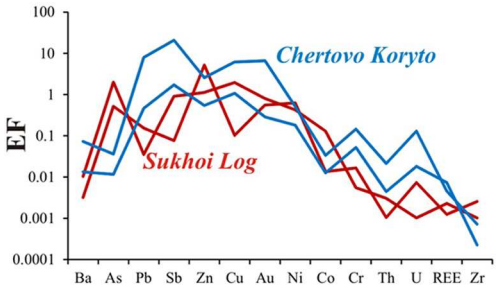

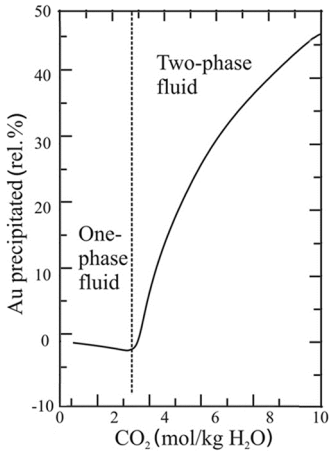

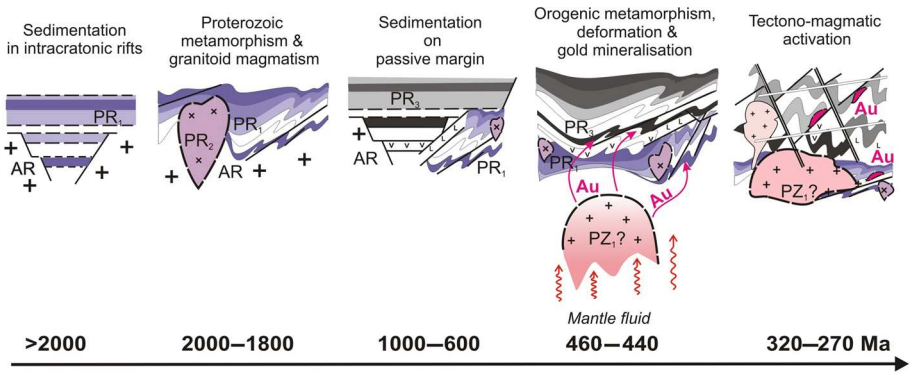

Gold mineralization and orogenic metamorphism in the Lena Province of Siberia as assessed from Chertovo Koryto and Sukhoi Log deposits

Marina A. Yudovskaya[a,b,*], Vadim V. Distler[a], Vsevolod Yu. Prokofiev[a], Nickolay N. Akinfiev[a]

[a] *Institute of Geology of Ore Deposits, Petrography, Mineralogy and Geochemistry RAS, 35 Staromonetny, Moscow 119017, Russia*

[b] *EGRI, University of the Witwatersrand, Private Bag 3, Wits 2050, South Africa*

* Corresponding author. E-mail address: marina.yudovskaya@wits.ac.za; maiya@igem.ru

- Gold mineralisation of Lena province is structurally controlled and hosted in various strata
- Black shale sequences are not anomalously enriched in metals except gold
- Gold deposits occur in rocks subjected to both prograde and retrograde metamorphism
- Gold precipitation is promoted by mixing between aqueous and carbonic gaseous fluids
- Mineralisation was broadly synchronous with early Paleozoic metamorphism and orogeny

Supplementary Table 1

Chemical composition of rocks of the Khomolkho formation at Sukhoi Log by INAA along SRK6 borehole

depth, m		Na2O	Sc	Cr	Fe2O3	Co	As	Rb	Sb	Cs	Ba	La	Ce	Nd	Sm	Eu	Tb	Yb	Lu	Hf	Ta	Au	Th	U	SREE
from	to	wt. %	ppm	ppm	wt. %	ppm	ppm	ppm	ppm	ppm	ppm	ppm	ppm	ppm	ppm	ppm	ppm	ppm	ppm	ppm	ppm	ppm	ppm	ppm	ppm
171	172	1.66	21.4	118	7.79	19.0	33.4	104	1.6	5.2	421	34.6	57.5	43.7	6.30	1.37	0.67	2.8	0.41	4.8	0.91	0.084	8.45	1.06	147
172	173	1.71	21.9	126	7.88	17.7	24.6	121	1.4	4.6	675	37.1	61.3	42.4	6.73	1.53	0.66	2.7	0.42	4.6	0.97	0.069	9.07	0.67	153
173	174	1.36	17.9	99	11.49	53.0	103.8	103	3.7	3.9	-75	37.7	63.1	40.3	6.78	1.49	0.75	2.4	0.38	4.2	0.69	2.87	6.95	0.81	153
174	175	1.57	21.1	121	7.43	20.5	35.8	114	0.1	4.6	561	24.5	39.9	30.4	5.27	1.29	0.81	2.8	0.42	5.2	0.90	0.035	7.16	0.74	105
175	176	1.52	19.4	100	6.14	12.2	8.1	109	0.1	4.0	359	25.8	43.0	31.6	4.51	1.16	0.47	2.0	0.25	4.1	0.69	0.014	6.03	0.93	109
176	177	1.50	19.5	100	5.67	13.6	30.2	114	1.7	4.6	413	21.2	33.1	24.6	4.11	1.04	0.80	2.6	0.37	4.8	0.81	0.160	6.81	1.18	88
177	178	1.57	19.4	102	5.91	10.6	23.4	101	1.8	4.0	527	25.0	44.9	29.4	5.13	1.20	0.63	2.3	0.34	4.5	0.68	0.546	7.04	0.92	109
178	179	1.58	19.3	117	6.64	16.1	23.6	102	4.2	4.4	415	23.5	41.9	36.7	4.72	1.14	0.67	2.6	0.38	4.4	0.89	6.06	7.70	1.38	112
180	181	1.56	19.6	121	7.12	12.3	23.9	128	1.6	3.6	337	23.4	40.6	29.5	5.05	1.09	0.79	2.5	0.36	4.3	0.76	0.330	7.50	1.07	103
181	182	1.39	18.4	128	8.18	15.5	23.0	98	3.0	3.6	318	28.0	44.9	35.6	5.48	1.25	0.62	2.2	0.35	4.4	0.72	0.089	6.50	0.92	118
182	183	1.60	19.5	109	6.48	12.4	21.9	118	0.1	4.1	340	30.6	52.3	39.7	6.08	1.34	0.61	2.5	0.33	4.4	0.74	0.134	7.68	0.73	133
183	184	1.43	18.3	104	7.58	15.9	41.9	110	1.6	3.4	340	27.6	47.0	46.6	5.29	1.17	0.66	2.2	0.32	4.5	0.76	1.32	6.79	0.83	131
184	185						23.6															6.62			
185	186						22.3															7.21			
186	187						45.0															16.90			
187	188						20.0															4.91			
188	189	1.05	20.8	103	6.03	14.7	20.6	121	4.3	5.6	634	26.4	43.6	33.8	4.84	1.14	0.69	2.2	0.33	3.6	0.62	0.114	5.93	1.05	113
189	190	1.04	19.8	112	7.53	14.2	29.8	118	0.8	4.3	459	24.2	37.8	29.3	4.49	1.03	0.43	2.1	0.34	4.1	0.64	1.58	4.85	1.05	100
190	191	0.98	21.2	111	7.18	18.9	37.1	139	0.6	5.2	448	29.2	49.7	37.4	5.26	1.14	0.50	2.0	0.27	3.6	0.53	1.52	6.31	1.42	125
191	192	0.95	19.4	99	6.51	11.4	16.9	120	6.7	5.4	272	21.6	37.4	29.5	3.88	0.90	0.47	2.0	0.27	3.4	0.54	0.248	5.19	0.84	96
192	193	0.85	20.0	104	7.44	20.0	51.2	119	1.1	4.4	287	30.0	53.6	36.0	5.77	1.41	0.52	2.1	0.28	3.5	0.55	12.06	7.23	0.66	130
193	194	0.82	18.2	89	7.26	18.1	51.8	106	-0.1	4.4	441	20.5	31.3	29.6	4.00	0.89	0.49	2.1	0.33	3.3	0.55	1.645	4.96	1.59	89
194	195	0.84	19.0	107	6.92	14.3	31.7	112	3.6	4.4	303	17.6	27.8	20.9	3.02	0.76	0.48	1.9	0.29	3.3	0.50	0.747	4.82	0.90	73
195	196	0.83	19.1	91	7.43	18.3	35.3	119	0.8	4.7	428	18.2	29.8	23.6	3.33	0.89	0.45	2.5	0.35	2.9	0.48	4.51	5.04	1.07	79
196	197	0.84	22.0	118	8.73	18.9	54.5	166	0.1	5.5	560	25.8	46.3	28.8	5.00	1.05	0.59	2.1	0.34	3.6	0.62	1.29	6.06	1.15	110
197	198	0.90	23.2	124	9.96	23.7	73.5	149	4.6	5.5	480	26.8	45.1	29.6	4.87	1.16	0.74	2.5	0.37	4.7	0.63	1.78	6.35	1.16	111
198.1	199.1	0.39	8.3	69	6.46	18.2	36.5	72	2.3	1.6	156	11.8	19.8	14.6	1.86	0.54	0.53	1.2	0.19	1.5	0.26	11.00	2.38	0.44	51
199	200	0.35	8.0	97	5.49	8.5	15.1	50	1.5	1.8	170	10.4	17.5	14.0	2.15	0.49	0.28	1.0	0.13	1.5	0.26	0.654	2.46	0.38	46
199.9	200.9	0.75	19.7	119	7.32	12.9	32.4	123	0.6	5.3	282	20.5	36.6	25.8	3.65	0.82	0.31	1.8	0.31	3.2	0.55	1.686	5.87	0.89	90
200.8	201.8	0.95	22.5	108	7.33	14.7	43.4	154	5.0	4.2	752	29.1	48.3	35.3	4.57	1.17	0.39	2.0	0.37	4.1	0.63	22.82	6.20	1.21	121
201.8	202.8	0.75	18.0	87	7.55	20.3	49.7	119	0.7	4.2	360	32.3	56.5	40.5	6.82	1.43	0.72	1.9	0.31	3.4	0.48	0.920	5.46	0.91	140
202.8	203.8	0.89	21.7	108	7.36	22.2	41.7	142	1.2	5.4	515	27.0	46.4	37.1	5.31	1.17	0.73	2.5	0.36	3.7	0.61	0.900	6.74	1.22	121
203.8	204.8	0.89	22.2	104	7.40	15.2	43.3	156	0.1	5.1	597	26.8	42.1	39.0	5.47	1.30	0.86	2.9	0.44	3.9	0.70	0.215	5.96	1.02	119
204.8	205.8	0.94	24.3	123	9.00	22.9	37.4	141	0.9	6.4	523	38.8	66.1	46.3	6.82	1.56	0.56	2.9	0.40	4.7	0.64	2.53	8.18	1.22	163
205.8	206.8	0.99	26.6	135	8.91	25.9	71.7	152	1.0	7.8	440	26.4	45.3	26.8	4.68	1.08	0.62	2.5	0.41	4.3	0.78	0.643	6.51	1.69	108
206.8	207.8	0.77	20.2	112	7.90	21.1	53.9	110	0.9	4.7	393	29.2	49.9	38.5	5.53	1.22	0.51	2.1	0.32	3.3	0.55	1.42	5.79	1.03	127
207.8	208.8	1.11	26.7	145	8.39	22.7	59.1	161	0.7	5.7	533	19.1	30.0	34.2	3.60	1.03	0.63	2.7	0.42	4.6	0.74	2.27	7.33	1.31	92
208.8	209.8	0.93	26.3	143	9.05	21.7	50.0	167	1.6	7.0	640	30.8	53.2	35.3	5.74	1.36	0.74	2.6	0.39	4.8	0.73	1.55	7.70	2.03	130
209.8	210.8	1.04	26.2	139	10.19	21.0	63.2	143	3.5	5.9	629	28.8	52.6	37.1	5.06	1.19	0.73	2.4	0.41	4.9	0.84	2.31	7.10	1.14	128
210.8	211.8	0.95	27.1	149	9.67	21.9	77.9	194	0.9	6.8	568	31.1	51.6	38.7	5.26	1.33	0.60	2.4	0.38	5.0	0.80	6.82	8.08	0.99	131
211.8	212.8	0.81	22.6	123	8.69	22.1	73.2	117	0.9	5.8	512	23.6	36.9	24.2	3.52	0.96	0.60	2.3	0.39	4.0	0.70	11.88	5.73	1.36	93
212.8	213.8	0.69	16.9	106	6.98	15.6	48.8	144	1.1	4.5	319	24.7	42.8	38.2	7.88	2.32	1.00	2.1	0.31	3.3	0.48	5.14	5.28	1.76	119
213.8	214.8	0.69	20.9	105	6.93	16.0	51.2	144	0.7	5.0	295	12.6	20.8	13.2	2.19	0.59	0.30	1.6	0.34	3.3	0.58	8.60	4.55	1.20	52
214.8	215.8	0.50	18.3	103	6.45	17.1	68.8	160	12.4	4.2	291	20.7	33.3	26.6	3.50	0.81	0.56	1.9	0.27	3.5	0.58	3.25	5.42	0.77	88
215.8	216.8	0.51	14.4	95	6.33	15.9	27.4	123	1.4	3.3	190	21.4	38.3	25.1	3.95	0.93	0.49	1.9	0.30	3.3	0.56	2.28	5.48	0.92	92
216.8	217.8	0.74	21.2	122	7.46	18.8	54.2	149	0.8	5.7	517	26.0	40.4	25.9	4.22	1.00	0.76	2.8	0.43	4.5	0.84	3.03	6.74	0.77	102
217.8	218.8	0.62	18.6	113	7.15	17.3	47.4	102	1.4	4.5	457	34.7	56.2	43.3	6.04	1.30	0.85	2.3	0.36	4.9	0.75	0.266	7.19	0.87	145
218.8	219.8	0.66	20.0	116	7.18	17.5	59.6	154	2.5	5.9	696	26.3	47.2	28.2	4.48	1.17	0.71	2.7	0.41	4.8	0.64	11.14	7.95	0.93	111
219.8	220.8	0.61	20.3	113	7.32	24.1	49.1	130	1.1	4.6	400	23.5	40.4	32.9	4.27	1.07	0.61	2.5	0.35	4.3	0.73	1.76	6.87	0.98	106
221	222	0.43	15.9	90	7.20	21.8	112.8	123	4.5	3.7	243	25.1	41.9	42.7	4.40	1.10	0.48	2.0	0.24	3.1	0.60	5.51	5.76	2.04	118
222.2	223.2	0.59	19.0	123	8.07	23.7	51.6	160	4.7	4.4	409	24.5	42.2	34.9	4.57	1.10	0.50	2.1	0.33	4.2	0.64	3.32	6.74	1.35	110
223.2	224.2	0.56	20.7	125	7.60	27.0	52.3	143	0.1	5.1	291	36.6	59.6	41.3	5.86	1.38	1.07	2.7	0.43	5.3	0.91	0.495	7.74	1.15	149
224.2	225.2	0.65	21.5	86	6.89	14.4	50.0	146	1.1	4.6	385	32.9	56.2	39.2	6.08	1.39	0.65	2.8	0.42	5.3	0.87	1.11	8.63	0.48	140
225.2	226.2	0.65	21.0	125	7.38	22.8	69.8	134	1.3	5.1	361	24.2	40.0	25.8	3.76	0.98	0.69	2.7	0.40	4.7	0.89	8.93	7.40	1.54	98
226.2	227.2	0.73	20.7	129	8.53	24.4	66.7	124	1.9	4.9	294	34.1	57.4	47.2	6.67	1.48	0.68	2.5	0.40	4.4	0.81	2.78	7.38	0.82	150

227.2	228.2	0.70	21.1	118	7.58	18.7	1.2	131	1.1	4.7	488	32.6	53.8	45.8	6.25	1.35	0.57	2.6	0.41	4.7	0.78	0.374	7.21	1.95	143
228.2	229.2	0.66	21.7	127	7.89	19.6	31.2	131	0.2	4.9	495	33.9	54.1	36.3	5.16	1.33	0.75	3.0	0.45	4.9	0.82	32.82	7.51	-0.26	135
229.2	230.2	0.72	20.1	111	8.33	34.8	74.9	124	1.2	5.1	417	24.5	41.1	25.4	3.82	1.02	0.63	2.8	0.48	4.7	0.79	7.32	7.39	1.06	100
230.2	231.2	0.66	20.3	120	7.33	17.5	20.5	144	1.9	4.3	462	27.7	44.7	34.3	5.02	1.14	0.72	2.9	0.43	5.2	0.87	0.678	7.16	1.04	117
231.2	232.2	0.73	20.4	112	7.78	19.4	17.1	140	0.9	5.1	475	32.5	58.4	45.5	5.92	1.48	0.64	2.4	0.37	4.7	0.89	10.36	8.15	1.61	147
232.2	233.2	0.91	20.8	125	7.47	17.8	15.2	150	2.6	4.3	357	33.3	54.5	41.3	5.83	1.32	0.69	2.7	0.39	5.1	0.82	0.371	7.88	0.60	140
233.2	234.2	0.78	20.8	116	6.88	15.4	35.9	114	0.8	5.1	664	31.8	54.9	37.2	5.58	1.39	0.94	2.5	0.33	4.8	0.80	0.139	7.66	0.89	135
234.2	235.2	0.87	20.8	120	8.34	29.0	22.2	119	1.1	4.6	590	32.0	54.2	35.5	5.93	1.37	0.68	2.7	0.42	4.8	0.81	4.48	7.42	0.91	133
234.2	235.2	1.02	21.0	122	8.41	26.8	20.6	119	0.8	5.0	335	28.3	50.7	29.7	5.03	1.36	0.67	2.7	0.40	5.0	0.73	0.555	7.44	0.91	119
235.2	236.2	0.90	21.6	115	8.10	21.6	32.3	133	1.3	5.2	479	44.3	72.6	59.3	7.49	1.66	0.91	2.7	0.39	4.8	0.80	0.444	9.34	0.99	189
235.2	236.2	0.94	21.9	138	8.30	22.2	43.8	117	1.1	4.7	431	30.3	52.5	34.6	4.96	1.26	1.02	2.8	0.31	5.4	0.78	0.363	7.56	0.90	128
236.2	237.2	1.23	21.0	118	7.91	20.6	22.7	123	0.8	5.0	332	32.2	51.7	34.9	5.06	1.39	0.62	2.9	0.42	5.2	0.84	0.076	8.01	0.84	129
237.4	238.4	0.14	2.6	50	2.97	3.5	5.6	15	1.4	0.4	39	3.9	7.2	4.3	0.68	0.24	0.06	0.3	0.04	0.6	0.08	1.01	0.97	0.07	17
238.4	239.4	0.03	0.8	52	2.34	2.8	1.6	2	0.7	0.3	9	2.1	3.9	1.8	0.24	0.07	0.05	0.1	0.02	0.2	0.04	0.006	0.51	-0.10	8
239.4	240.4	2.10	34.5	215	12.13	33.7	52.3	160	0.7	7.2	493	52.4	87.2	44.1	7.57	2.04	1.08	4.3	0.56	7.6	1.13	0.070	13.44	1.01	199
240.4	241.4	1.22	26.2	170	9.75	26.4	34.9	117	0.8	5.7	349	39.9	65.2	38.6	5.86	1.64	0.84	3.2	0.45	5.9	0.85	0.145	9.41	1.10	156
241.4	242.4	1.18	24.4	152	9.75	20.9	28.0	135	0.7	5.6	374	31.9	54.2	38.1	5.39	1.43	0.79	3.1	0.42	5.6	0.75	0.118	8.42	1.62	135
242.4	243.4	1.71	19.2	132	8.47	23.6	34.8	104	2.2	4.1	392	34.3	63.4	42.6	6.10	1.58	0.85	3.0	0.43	5.0	0.78	0.264	8.59	1.00	152
243.4	244.4	1.80	20.7	165	9.34	24.4	33.4	80	2.9	5.1	207	36.4	59.9	35.9	5.80	1.51	0.97	3.2	0.44	6.3	0.89	0.475	7.54	1.31	144
244.4	245.4	1.78	20.3	133	7.96	19.5	45.3	116	3.9	4.0	389	31.6	54.1	32.7	4.57	1.32	0.64	2.8	0.42	5.6	0.78	7.28	8.56	0.71	128
245.4	246.4	2.11	20.1	137	8.44	26.9	18.8	87	0.1	3.4	334	32.9	56.6	35.0	5.42	1.48	0.70	2.8	0.41	5.6	0.80	2.53	8.36	1.38	135
246.4	247.4	1.92	22.0	147	8.14	21.6	1.3	104	54.9	3.1	433	35.5	59.9	34.3	5.67	1.47	0.93	3.0	0.36	5.9	0.80	0.173	7.57	0.95	141
247.4	248.4	1.52	20.3	129	8.49	22.8	43.6	114	1.6	3.4	-75	39.6	62.6	50.1	5.56	1.53	0.94	2.8	0.51	5.3	0.83	12.94	7.96	0.68	164
248.4	249.4	1.97	22.1	135	8.52	27.5	53.7	97	2.1	4.1	329	39.6	68.8	39.0	6.13	1.50	0.87	3.2	0.45	6.7	0.84	0.473	10.04	1.44	160
249.4	250.4	2.07	21.4	145	8.34	24.6	29.9	147	0.8	4.1	289	35.2	58.8	34.7	5.41	1.42	0.83	2.8	0.42	5.6	0.88	1.46	8.50	1.37	140
250.4	251.4	1.99	22.9	165	9.33	22.0	26.1	120	1.2	5.1	240	36.2	58.9	34.5	6.27	1.50	0.86	3.1	0.51	6.2	0.84	2.05	8.50	1.39	142
251.4	252.4	2.25	22.8	148	8.75	25.4	38.1	146	1.2	3.6	292	40.1	66.5	36.1	6.51	1.60	1.07	3.0	0.43	5.7	0.75	0.552	8.56	1.31	155
252.4	253.4	2.12	22.8	141	8.33	15.8	1.3	94	1.7	4.3	372	45.4	81.2	49.7	6.94	1.66	0.83	3.0	0.42	6.4	0.96	0.106	9.34	1.08	189
254.4	255.4	1.21	17.3	126	7.25	19.8	32.7	88	0.6	3.7	249	32.1	57.8	32.5	5.06	1.21	0.52	2.7	0.35	4.4	0.64	0.107	6.20	0.99	132

Supplementary Table 2

Chemical composition of rocks of the Mikhailovsk formation at Chertovo Koryto by INAA along ChK85 borehole

depth, m		Na2O	CaO	Sc	Cr	Fe2O3	Co	As	Rb	Mo	Sb	Cs	Ba	La	Ce	Nd	Sm	Eu	Tb	Yb	Lu	Hf	Ta	Au	Th	U	REE
from	to	wt. %	wt. %	ppm	ppm	wt. %	ppm	ppm	ppm	ppm	ppm	ppm	ppm	ppm	ppm	ppm	ppm	ppm	ppm	ppm	ppm	ppm	ppm	ppm	ppm	ppm	ppm
5	6	0.53	1.76	21.3	134	7.11	6.7	419	200	6.51	2.23	10.28	885	17.5	32.9	11.3	2.86	0.81	0.32	1.74	0.25	3.24	0.81	0.43	12.3	3.17	68
7	8	0.91	0.73	21.3	144	7.16	21.5	463	198	4.00	0.19	8.38	698	29.3	58.2	22.5	4.17	0.83	0.32	1.45	0.27	2.82	0.78	0.01	13.4	3.37	117
9	10	1.07	0.50	19.7	130	7.05	24.5	804	146	4.30	0.20	7.51	573	25.0	55.3	23.7	4.20	0.90	0.32	1.66	0.21	3.19	0.75	0.01	12.5	2.76	111
10	11	1.17	0.98	17.1	109	6.99	16.6	3906	154	4.60	0.21	7.12	508	26.6	55.2	21.0	4.02	1.03	0.29	1.49	0.32	3.86	0.68	0.07	12.6	1.64	110
11	12	1.11	0.99	13.4	86	5.85	11.6	612	111	3.80	0.18	5.62	422	17.1	35.5	16.1	2.89	0.83	0.26	1.38	0.21	2.69	0.55	0.20	10.7	2.33	74
12	13	1.89	2.25	11.8	89	5.73	18.7	614	44	3.90	0.17	3.51	411	23.3	46.1	20.5	3.54	0.96	0.25	1.25	0.26	4.25	0.74	0.01	10.4	2.11	96
13	14	1.59	1.54	10.0	89	5.07	11.4	1781	79	4.20	0.60	3.82	236	20.9	46.0	16.4	3.48	0.96	0.14	1.34	0.23	4.61	0.59	0.91	10.5	2.54	90
14	15	1.93	0.50	11.9	97	5.78	15.0	580	77	3.90	0.18	3.24	360	22.4	44.7	19.0	3.39	0.89	0.25	1.26	0.20	5.04	0.64	0.50	12.5	2.63	92
16	17	1.56	0.84	12.5	93	6.12	18.6	849	104	3.90	0.19	4.77	508	30.6	60.0	22.3	4.28	1.05	0.26	1.50	0.17	4.13	0.61	0.91	13.3	2.73	120
17	18	1.05	0.72	18.0	123	7.17	20.1	1204	152	4.20	0.22	7.31	561	24.4	48.8	20.4	3.95	0.94	0.30	1.70	0.24	4.12	0.81	0.15	13.9	3.46	101
20	21	1.55	0.90	16.5	112	6.60	13.4	540	118	4.10	0.18	7.06	595	32.4	63.3	28.8	4.66	1.12	0.28	1.68	0.21	4.07	0.76	0.08	13.1	3.47	132
23	24	1.24	0.50	15.2	110	6.67	15.1	1986	117	4.50	0.74	7.71	481	25.7	55.1	24.3	4.02	1.09	0.28	1.40	0.26	3.50	0.70	0.24	12.2	3.16	112
24	25	1.71	1.08	22.4	141	8.30	17.0	260	185	3.80	0.18	7.32	649	41.4	78.6	32.3	6.06	1.30	0.33	1.80	0.28	4.07	0.85	0.24	16.4	3.91	162
28	29	1.53	1.16	14.2	103	6.32	11.6	1018	102	4.20	0.17	5.78	517	36.2	74.9	28.9	5.07	1.27	0.27	1.66	0.28	4.73	0.73	2.23	15.5	3.29	149
32	33	1.13	2.83	19.0	133	7.15	22.5	1395	168	4.40	0.20	6.56	807	37.0	66.8	28.0	4.97	1.11	0.31	1.33	0.21	3.13	0.75	1.96	12.1	3.49	140
33	34	1.33	1.14	11.5	95	5.84	19.9	5689	109	5.30	0.23	4.47	238	34.3	63.7	25.7	4.02	1.19	0.25	1.37	0.12	4.41	0.68	0.69	13.2	3.01	131
34	35	1.02	0.50	20.9	137	7.81	19.7	1565	173	4.60	0.21	9.29	786	35.8	69.6	30.4	5.40	1.33	0.32	1.62	0.23	3.65	0.83	0.57	14.1	3.29	145
35	36	1.15	1.26	18.8	125	7.68	19.2	1447	145	4.40	0.20	8.80	604	35.7	70.4	27.4	5.01	1.32	0.31	1.48	0.20	4.22	0.78	1.36	15.2	2.99	142
36	37	1.17	1.26	22.3	149	8.15	22.3	841	188	6.40	0.87	9.48	590	38.2	73.4	29.2	5.45	1.27	0.33	1.67	0.28	3.24	0.88	0.07	14.1	4.10	150
37	38	1.20	0.50	19.6	130	7.76	24.6	920	163	4.00	0.18	9.82	672	36.3	72.8	29.2	5.79	1.28	0.31	1.72	0.31	3.90	0.82	0.33	13.1	2.84	148
38	39	1.48	1.05	17.4	118	6.97	16.1	476	149	4.00	0.16	4.67	592	36.4	66.9	25.6	5.48	1.24	0.30	1.81	0.26	3.77	0.77	0.12	13.2	3.35	138
39	40	1.11	1.46	20.3	136	7.75	16.4	41	167	5.30	0.16	9.80	581	31.0	61.6	24.9	4.88	1.09	0.32	2.01	0.33	2.42	0.73	0.26	13.1	3.36	126
41	42	1.41	0.87	19.3	128	7.35	20.6	897	174	15.22	0.19	6.83	602	34.7	64.8	25.2	5.14	1.14	0.31	1.94	0.23	3.44	0.86	0.06	13.7	4.44	133
43	44	0.82	0.50	19.5	127	7.62	17.0	2451	181	4.90	1.07	7.58	517	31.5	61.2	24.7	4.70	0.99	0.31	1.51	0.21	3.06	0.63	0.09	11.8	2.31	125
44	45	1.40	1.07	13.0	112	5.80	12.9	1725	119	4.10	0.97	4.24	427	31.3	62.3	24.3	4.40	1.22	0.26	1.32	0.22	5.45	0.63	0.06	12.3	2.90	125
45	46	1.06	0.50	8.1	80	4.77	11.6	6130	66	5.00	1.89	2.99	331	26.1	55.0	19.0	3.42	0.92	0.14	1.18	0.16	4.94	0.53	0.82	10.2	1.42	106
47	48	1.99	0.71	10.2	99	5.30	10.6	1634	119	4.10	0.17	3.85	454	26.8	58.5	21.5	4.10	0.92	0.50	1.34	0.22	4.67	0.67	0.07	11.1	3.37	114
49	50	1.54	0.50	16.4	119	7.18	14.2	1080	132	4.20	0.19	5.63	722	34.3	65.2	22.3	5.02	1.06	0.28	1.79	0.31	3.83	0.75	0.30	12.3	2.63	130
50	51	1.47	0.50	16.4	112	6.78	24.7	2263	127	4.50	0.21	7.34	907	21.3	46.6	18.5	3.59	1.06	0.29	1.29	0.21	4.60	0.72	0.02	11.8	3.10	93
52	53	1.56	0.50	12.1	109	5.98	14.8	2942	97	4.10	0.18	3.95	414	29.7	57.4	23.2	4.47	1.13	0.25	1.38	0.21	6.32	0.74	0.88	11.1	2.33	118
54	55	1.32	0.20	12.1	90	5.42	12.6	3784	88	8.90	0.74	4.08	513	25.2	51.9	17.7	3.68	0.76	0.24	1.18	0.18	3.47	0.60	0.36	9.1	1.68	101
57	58	1.23	1.44	20.8	132	8.19	24.3	2640	135	5.00	1.34	7.46	643	19.1	43.8	18.5	3.91	0.99	0.32	1.46	0.31	3.50	0.73	0.27	12.0	3.14	88
58	59	1.62	0.20	16.3	109	6.94	19.6	1267	190	4.00	0.19	6.19	741	18.8	40.6	16.9	3.45	0.94	0.28	1.29	0.27	3.50	0.68	0.03	10.9	2.69	83
60	61	1.25	1.05	9.5	97	5.00	11.6	2501	82	4.50	0.17	4.21	425	22.6	49.7	22.5	3.66	0.90	0.14	1.32	0.22	5.42	0.63	0.16	11.0	2.27	101
61	62	1.62	1.10	11.8	103	5.71	11.3	566	113	3.90	0.17	5.50	576	32.7	62.0	25.7	4.64	1.17	1.02	1.62	0.25	4.91	0.77	0.03	12.2	3.53	129
62	63	1.16	0.97	17.5	126	7.73	16.5	487	152	10.41	0.16	7.49	880	31.7	66.3	27.2	4.91	1.22	0.29	1.87	0.28	4.44	0.79	0.07	13.2	3.84	134
64	65	1.14	1.39	19.8	136	7.71	16.5	318	107	3.90	0.16	8.27	1060	35.2	67.6	28.3	5.27	1.10	0.30	1.73	0.30	3.38	0.84	0.05	13.5	3.69	140
66	67	1.16	1.50	18.6	116	7.49	17.7	932	101	4.10	0.18	7.95	609	34.0	70.7	25.2	4.81	1.04	0.29	1.65	0.29	3.13	0.68	3.56	12.8	3.18	138
67	68	1.38	1.49	18.6	131	7.32	12.6	199	97	3.70	0.17	7.43	853	30.3	60.9	30.7	4.57	0.99	0.29	1.83	0.30	3.68	0.86	0.38	11.3	3.70	130
68	69	0.16	8.95	17.3	154	9.85	33.0	100	86	4.40	0.16	6.23	1070	85.3	186.0	85.0	14.73	4.67	0.31	1.88	0.22	12.09	2.97	0.57	6.0	1.19	378
69	70	1.31	0.20	19.1	123	7.90	23.5	1274	114	4.10	0.19	6.57	867	30.3	61.4	26.7	4.76	1.20	0.30	1.45	0.18	3.46	0.76	0.01	11.0	2.75	126
71	72	1.87	1.06	19.4	127	7.71	17.6	7	138	3.40	0.15	7.09	853	36.9	72.7	30.9	5.73	1.33	0.30	1.50	0.26	3.58	0.85	0.00	13.7	3.61	150
74	75	0.00	11.86	19.7	175	11.65	38.3	76	-12	4.80	0.17	6.80	1024	115.2	248.4	121.0	20.17	5.82	2.02	2.15	0.17	14.67	3.97	0.03	5.9	1.87	515
75	76	0.97	1.57	19.2	131	7.61	17.7	3598	151	4.80	1.22	6.75	1018	39.6	82.3	36.3	5.56	1.67	0.30	1.35	0.17	4.33	0.79	6.11	12.4	4.01	167
76	77	1.70	0.20	13.6	101	6.24	13.4	1383	87	3.80	0.17	5.92	658	32.4	64.2	25.9	4.80	1.22	0.26	1.37	0.28	3.48	0.71	0.20	12.0	2.84	130
78	79	2.09	1.73	12.2	102	5.91	17.6	1111	69	4.00	0.17	5.56	558	32.8	65.4	25.2	4.50	1.17	0.25	1.36	0.25	5.37	0.70	0.01	12.0	3.43	131
80	81	0.69	0.20	16.3	120	8.02	17.5	4388	115	4.80	1.49	9.19	1178	29.5	59.7	24.3	4.66	1.08	0.28	1.61	0.25	4.19	0.77	0.60	12.8	4.61	121
82	83	0.47	5.09	14.8	130	8.87	33.1	6103	-10	5.20	0.22	5.22	869	75.7	165.9	74.2	12.02	3.55	0.29	1.54	0.14	10.55	2.43	3.38	6.7	2.10	333
85	86	0.43	0.20	7.1	64	4.38	12.4	21950	97	9.20	4.40	3.29	311	14.2	30.7	9.7	2.01	0.56	0.13	0.72	0.06	1.81	0.44	3.76	5.2	0.56	58
87	88	0.70	0.20	14.7	105	7.11	17.2	6585	88	5.40	1.57	7.25	702	25.2	54.3	22.8	3.69	0.97	0.27	1.46	0.24	3.31	0.68	1.27	10.5	3.44	109
88	89	2.22	0.20	12.8	110	6.10	12.5	1034	106	3.90	0.17	5.55	468	28.9	59.6	22.0	4.32	1.05	0.26	1.45	0.21	4.99	0.75	0.24	12.3	2.58	118
89	90	1.43	1.23	17.0	127	7.09	20.1	4677	87	4.80	0.22	8.57	735	34.8	71.8	25.5	4.88	1.32	0.28	1.35	0.30	4.05	0.74	1.20	11.9	2.32	140
90	91	0.82	0.83	15.3	121	7.80	22.7	3251	108	4.30	0.19	7.13	727	40.0	83.9	32.9	5.63	1.42	0.28	1.50	0.26	3.35	0.85	0.19	9.5	2.19	166
91	92	0.46	4.41	14.0	185	6.87	23.0	404	61	4.00	0.78	5.20	567	62.4	125.6	55.2	7.92	2.41	0.28	1.49	0.22	7.55	2.24	0.00	9.0	1.53	256
92	93	1.30	0.20	10.2	83	4.27	11.2	2586	97	4.50	0.40	4.61	291	20.5	41.5	20.1	3.18	0.73	0.15	1.03	0.19	3.49	0.56	0.09	8.8	1.84	87
93	94	1.19	0.20	5.5	65	2.59	4.7	1221	70	4.30	0.12	2.09	153	17.6	33.8	13.3	2.40	0.57	0.11	0.78	0.11	3.32	0.34	0.36	6.5	1.53	69
94	95	1.33	0.20	21.1	139	8.75	34.5	5894	131	9.99	1.31	9.05	818	37.8	75.7	29.1	5.13	1.24	0.32	1.72	0.33	3.87	0.75	0.11	13.3	3.58	151

95	96	1.15	0.20	13.3	91	7.66	13.1	3433	90	12.78	0.99	6.02	719	30.8	63.9	25.6	4.28	1.15	0.26	1.28	0.16	3.67	0.69	0.17	10.5	2.65	127
97	98	1.59	0.85	10.6	89	5.52	13.9	5487	96	4.70	0.17	3.99	207	24.8	50.1	24.4	3.62	0.84	0.15	1.22	0.28	3.39	0.58	0.24	10.0	2.39	105
98	99	1.29	4.55	19.6	124	8.37	24.6	15980	138	8.50	3.21	7.95	839	32.1	71.4	29.7	4.80	1.32	0.31	1.55	0.06	3.54	0.73	2.81	12.6	2.32	141
99	100	1.25	0.20	19.6	138	8.16	16.8	14130	152	7.80	2.08	7.95	563	32.1	70.3	28.8	4.42	1.27	0.30	1.57	0.14	3.49	0.72	0.90	12.5	2.86	139
100	101	1.14	0.20	14.3	111	6.14	15.3	19457	123	10.10	2.72	6.19	920	23.6	51.6	21.3	3.31	0.90	0.35	1.52	0.04	2.85	0.65	0.56	10.4	3.56	103
101	102	2.32	0.20	8.3	83	4.60	11.3	959	27	4.20	0.21	2.69	333	26.3	47.8	18.0	3.30	0.88	0.28	1.16	0.15	4.01	0.50	0.00	8.5	2.18	98
102	103	2.45	2.83	8.8	88	4.51	13.2	852	48	4.10	0.20	3.10	79	25.4	49.8	18.3	3.60	0.94	0.28	1.35	0.23	5.21	0.54	0.00	9.6	2.40	100
103	104	1.86	0.20	9.1	85	4.82	9.2	890	57	3.60	0.21	3.28	79	29.5	55.0	21.1	3.73	0.90	0.29	1.37	0.20	4.78	0.62	0.24	9.9	2.20	112
104	105	0.74	0.20	10.7	98	5.33	11.5	2605	65	4.60	0.25	3.59	440	25.8	53.1	24.1	4.14	1.11	0.31	1.42	0.17	4.18	0.66	0.05	8.7	2.38	110
106	107	0.81	0.40	13.4	98	7.17	19.4	5516	95	5.10	0.29	7.44	757	29.8	58.3	27.2	4.37	0.97	0.35	1.67	0.19	3.28	0.65	0.07	11.1	2.86	123
108	109	1.99	0.35	11.6	95	5.87	13.7	558	57	3.90	0.23	3.08	88	22.5	48.6	21.4	3.69	0.90	0.32	1.38	0.16	3.17	0.60	0.00	9.1	2.61	99
110	111	1.07	0.85	15.1	113	7.39	18.8	26793	118	44.07	2.11	7.05	372	26.5	56.4	22.7	2.88	0.89	0.36	1.60	0.27	2.87	0.71	0.23	11.1	0.74	112
112	113	1.11	0.47	16.4	113	7.35	13.3	9516	133	5.70	0.31	9.17	104	28.8	55.0	24.1	4.12	1.00	0.37	1.69	0.18	2.90	0.66	0.43	11.1	2.63	115
114	115	2.00	0.39	16.2	114	7.31	14.6	933	84	3.90	0.28	6.94	104	27.9	55.9	22.6	4.20	1.01	0.37	1.67	0.20	3.03	0.69	0.01	10.3	3.06	114
116	117	0.17	0.41	4.3	40	4.35	5.3	7066	19	5.00	0.17	1.94	59	12.0	18.1	6.5	1.12	0.35	0.22	0.72	0.08	0.83	0.22	3.54	3.1	0.96	39
118	119	1.72	0.42	9.4	88	5.61	9.9	5063	62	12.30	0.22	4.74	81	26.8	52.6	19.8	3.73	1.11	0.30	1.23	0.15	4.39	0.59	0.01	9.5	2.57	106
119	120	1.57	0.50	10.9	98	5.61	10.6	11154	82	6.10	0.24	5.08	87	27.5	55.3	22.2	3.68	0.92	0.31	1.46	0.17	5.04	0.65	3.41	11.7	1.89	111
120	121	0.98	2.52	13.3	99	6.40	12.0	4945	119	5.30	0.27	5.64	480	22.9	43.1	19.2	3.61	0.85	0.35	1.33	0.19	2.46	0.58	0.07	8.4	1.67	91
121	122	1.28	2.10	15.5	110	7.17	12.3	4570	111	4.60	0.28	7.72	102	24.7	51.0	24.1	4.32	1.02	0.37	1.51	0.18	3.08	0.70	0.14	10.2	2.12	107
122	123	0.45	0.51	20.5	130	7.16	10.8	12664	188	6.40	0.37	11.03	682	37.0	71.1	29.0	5.04	1.24	0.61	2.03	0.24	2.68	0.77	0.08	11.7	2.95	146
124	125	0.00	8.00	18.1	247	10.77	35.8	189	8	4.40	1.08	6.64	118	91.0	179.2	81.7	13.78	4.27	0.64	2.04	0.25	6.37	2.49	0.00	10.0	3.94	373
126	127	1.57	0.35	11.1	95	5.30	8.7	1948	102	6.15	0.24	5.86	551	24.6	51.6	23.5	3.86	0.94	0.31	1.50	0.17	3.81	0.65	0.00	13.8	3.42	107
128	129	0.94	0.37	17.1	127	7.34	11.0	2907	203	4.80	0.27	9.12	829	34.2	64.5	24.5	4.67	1.08	0.38	1.85	0.25	3.62	0.72	0.13	12.5	3.14	132
130	131	1.63	0.35	9.1	85	5.10	17.7	3923	50	4.80	0.22	5.14	237	27.3	51.0	17.7	3.69	0.96	0.29	1.15	0.18	4.22	0.52	0.14	10.3	1.83	102
132	133	1.33	0.41	10.9	85	5.27	9.5	1768	73	11.77	0.25	6.21	85	29.3	57.0	24.2	3.77	1.00	0.31	1.23	0.15	2.95	0.60	0.44	9.8	2.12	117
134	135	1.30	0.34	13.5	101	5.68	13.2	287	130	7.02	0.23	6.85	533	25.8	50.6	21.4	4.01	0.87	0.34	1.68	0.22	3.56	0.65	0.06	10.6	2.51	105
136	137	1.15	0.33	14.6	105	6.49	13.2	53	103	15.21	0.68	7.28	412	25.5	50.1	23.1	4.17	0.88	0.35	1.63	0.27	3.17	0.75	0.00	11.2	3.08	106
138	139	1.58	2.20	15.0	112	6.19	14.4	140	133	4.57	0.23	5.39	394	32.3	58.0	23.9	4.16	0.87	0.35	1.63	0.23	3.39	0.71	0.03	10.7	3.20	121
142	143	1.91	1.61	10.1	89	5.16	10.2	39	78	12.58	0.19	4.12	454	28.2	56.6	20.8	4.00	1.02	0.30	1.49	0.16	3.98	0.62	0.06	10.6	2.03	113
144	145	1.16	2.91	16.3	113	6.40	13.6	381	150	5.67	0.83	7.78	893	35.8	66.9	29.9	5.16	1.14	0.36	1.88	0.31	3.69	0.80	0.04	12.1	3.57	141
145	146	1.32	2.69	21.4	138	8.36	22.4	1361	141	4.40	0.25	11.39	602	39.8	72.6	32.6	5.72	1.38	0.65	2.00	0.26	3.34	0.87	0.00	13.9	3.51	155
146	147	1.99	0.37	15.4	120	6.98	17.7	261	117	3.70	0.25	7.87	314	40.1	72.1	28.8	5.74	1.35	0.36	2.02	0.29	4.44	0.93	0.02	13.9	3.43	151
149	150	2.07	8.80	7.4	80	5.10	13.6	3486	89	6.70	0.21	4.44	75	28.8	55.3	21.3	3.24	1.03	0.27	1.24	0.15	5.48	0.59	29.48	13.2	3.15	111
150	151	1.09	2.16	19.0	128	7.55	18.9	3714	133	11.70	1.98	8.67	841	40.0	79.3	35.0	5.89	1.44	0.60	2.11	0.22	3.92	0.86	0.01	14.3	3.86	165